Development, characterization and control of E. coli communities on an automated experimental platform

Maaike Fonsine Sangster

THÈSE

Pour obtenir le grade de

DOCTEUR DE L'UNIVERSITÉ GRENOBLE ALPES

École doctorale : CSV- Chimie et Sciences du Vivant
Spécialité : Biologie cellulaire
Unité de recherche : Laboratoire Interdisciplinaire de Physique

Développement, caractérisation et contrôle de communautés d'E. coli dans une plateforme expérimentale automatisée

Development, characterization and control of E.coli communities on an automated experimental platform

Présentée par :

Maaike Fonsine SANGSTER

Direction de thèse :

Hans GEISELMANN PROFESSEUR DES UNIVERSITES, Université Grenoble Alpes	Directeur de thèse
Eugenio CINQUEMANI Inria	Co-directeur de thèse

Rapporteurs :

Fabien LETISSE
PROFESSEUR DES UNIVERSITES, Université Toulouse 3 - Paul Sabatier
Steffen KLAMT
SENIOR SCIENTIST, Max Planck Institute

Thèse soutenue publiquement le **11 mai 2023**, devant le jury composé de :

Johannes GEISELMANN PROFESSEUR DES UNIVERSITES, Université Grenoble Alpes	Directeur de thèse
Fabien LETISSE PROFESSEUR DES UNIVERSITES, Université Toulouse 3 - Paul Sabatier	Rapporteur
Steffen KLAMT SENIOR SCIENTIST, Max Planck Institute	Rapporteur
Madalena CHAVES DIRECTRICE DE RECHERCHE, INRIA centre Sophia Antipolis - Mediterranée	Examinatrice
Franz BRUCKERT PROFESSEUR DES UNIVERSITES, Grenoble INP	Président
Eugenio CINQUEMANI CHARGE DE RECHERCHE HDR, INRIA centre Grenoble - Rhône-Alpes	Co-directeur de thèse

Invités :

Hidde de Jong
DIRECTEUR DE RECHERCHE, Inria Grenoble Rhône-Alpes

Acknowledgements

First of all, I would like to thank the members of the jury for their involvement and interesting questions: Madalena Chaves as examinator and Franz Bruckert as the president of the jury, and of course Fabien Létisse and Steffen Klamt as reporters for reading the thesis, valuing my work, and suggesting some rightful changes.

This PhD project could of course not have been completed without supervision. Thank you Eugenio for your enthusiasm and help when it came to all questions control, bioreactor software, and Kalman filters, and of course for being present weekly to support me with the general process of doing a PhD in France. Thanks to Hans for being an always optimist and practical help with everything wet-lab. Thanks to Hidde for being an essential part of the thesis project, especially when it came to thinking about and rethinking the mathematical model. In the lab I also had essential help from Célia Boyat, Corinne Pinel and Noel Scaramozzino.

I could have never completed the PhD work without a great network of PhD students at LIPhy. I think we really had something special going as a group that started just before the pandemic. The list is too long, but I want to particularly thank Antrea Pavlou and Laila Blomer for organizing many many get-togethers and being such an active part of the lab community. Thank you Saranath for complaining, smoke/tea breaks, and occasional runs to refresh the mind. Thank you Thibault Clavier for chats and laughs in between failed experiments and transformations. Thank you Wanda for an eventful time full of runs, climbs, manifs and side-quests.

Grenoble is full of special people that helped me from going insane by just doing a bunch of fun stuff (and I'd like to believe that I returned the favour). A special thanks to Laura, Suzanne, Flora and Mads! Lorenzo, I know this is too cheesy for your taste, but thank you for being the chill to my stressed; these years would not have been the same without your calming presence.

Beter een goede buur dan een verre vriend, maar ik ben oneindig dankbaar voor vriendschappen die de afstand hebben overleefd. Bedankt Marijn voor zoom-sessies met The Great British Bake-off, eindeloze gesprekken, en al je bezoekjes aan Gren. Bedankt Imme voor je enthousiasme over van alles en nogwat, voor heerlijke thee en eten en voor het feit dat je er altijd bent wanneer het telt. Bedankt Thao voor goede tijden in Vietnam, Frankrijk, en Nederland!

Natuurlijk wil ik ook mijn familie bedanken. Bedankt opa en oma; niet veel kleinkinderen kunnen zeggen dat ze regelmatig contact hebben met hun grootouders via WhatsApp! Papa en mama, bedankt voor jullie onvoorwaardelijke steun, wat voor geks ik ook bedenk. Bedankt Reiny, dat je me altijd bent komen opzoeken op mijn rare avonturen.

Summary

The study of microorganisms in communities is important for the understanding of their metabolism and their association with human disease, but also for a range of biotechnological applications, since microbial consortia can be used to increase the production of relevant compounds. Our group previously developed a coarse-grained mathematical model of a promising consortium. In this PhD project, we construct this consortium of two *E. coli* strains, a glucose specialist and an acetate specialist, with the aim of improving our quantitative understanding of the conditions for co-existence and the possible accompanying trade-offs. To study the growth of this consortium, we use an automated experimental platform that we developed in-house, which allows us to vary and measure the growth conditions dynamically. We show that the growth of the individual strains can be explained well with the existing mathematical model. However, our results also suggest that acetate cycling should be modeled in more detail in order to explain the growth of the consortium at low growth rates where co-existence occurs. With this study, we provide insight into the community dynamics and emergent properties of a prototypical synthetic microbial consortium. It highlights the importance of studying co-cultures as opposed to mono-cultures and provides an improved understanding of overflow metabolism in *E. coli*.

Résumé

L'étude des micro-organismes dans les communautés est importante pour la compréhension de leur métabolisme et de leur association avec les maladies humaines, mais aussi dans les biotechnologies, où les consortiums microbiens peuvent être utilisés pour augmenter la production de composés pertinents. Notre groupe a précédemment développé un modèle mathématique simple d'un consortium prometteur. Dans ce projet de doctorat, nous construisons ce consortium de deux souches d'*E. coli*, une souche spécialiste du glucose et une souche spécialiste de l'acétate, dans le but d'améliorer notre compréhension quantitative des conditions de coexistence et des compromis possibles. Pour étudier la croissance de ce consortium, nous utilisons une plateforme expérimentale automatisée que nous avons développée en interne et qui nous permet de varier et de mesurer les conditions de croissance de manière dynamique. Nous montrons que la croissance des souches individuelles peut être bien expliquée par le modèle mathématique existant. Cependant, nos résultats suggèrent également que le cycle de l'acétate devrait être modélisé plus en détail afin d'expliquer la croissance du consortium à de faibles taux de croissance où la coexistence se produit. Avec cette étude, nous fournissons un aperçu de la dynamique de la communauté et des propriétés émergentes d'un consortium microbien synthétique prototypique. Elle souligne l'importance d'étudier les co-cultures par opposition aux monocultures et permet de mieux comprendre le métabolisme de l'overflow chez *E. coli*.

Contents

1 Introduction

> To awaken quite alone in a strange town is one of the pleasantest sensations in the world. You are surrounded by adventure. You have no idea of what is in store for you, but you will, if you are wise and know the art of travel, let yourself go on the stream of the unknown.
>
> Freya Stark

1.1 The study of microbial communities

To understand the microbial world around us, scientist have tended to study the physiology of microorganisms in isolation. In nature however, microbes live in complex communities with characteristics that are not always predictable from the properties of the individual strains. For example, in lake sediments, methanogens live in synthropy with fermenters; they reduce the concentration of hydrogen in the anaerobic environment, allowing the otherwise thermodynamically infeasible fermentation of organic carbon [1, 2]. Another complex microbial community that has been the subject of numerous studies in the last years is the human gut. It is populated by more than a 1000 microbial species [3], and the composition of this microbial community differs from person to person but is remarkably stable over time [4].

One way to understand the factors that give rise to this specificity and stability in microbiomes, is to study them as a whole, in a top-down approach [5]. In order to understand which species are present in a microbiome and what their function is, different techniques can be used. First of all, to measure the species that are present in the microbiome, amplicon sequencing of 16S ribosomal RNA (16S rRNA) is used [6]. The 16S rRNA gene is present in all prokaryotes and is highly conserved. By sequencing specific conserved and more variable regions within this gene, researchers can get information about the phylogeny of the microbiome. When the sequenced 16S rRNA genes are similar enough (the threshold of 97% is commonly used), they are considered to belong to the same operational taxonomic unit (OTU). Secondly, to understand which function the microbes in a microbiome are fulfilling, metagenomics or metatranscriptomics can be used to understand which genes are present in the population and which genes are transcribed [6].

By combining these techniques with modeling (modeling approaches are described in detail in the next section), researchers can study the dynamics and interactions in microbiomes with impressive detail. For example, by determining the absolute abundances of species in the human infant microbiome over time, it was found that the assembly of the microbiome in the infant gut is the result of positive and negative interactions between species; not only bacteria, but also fungi and archaea [7]. By measuring OTUs in the mouse gut following antibiotic treatment, it was demonstrated that antibiotics can induce infection by

Clostridium difficile, presumably because they weaken important commensal microbes that could negatively interact with this infectious microbe [8]. A third interesting result from a combination of omics techniques and modeling is the demonstration that cooperation takes place in kefir communities: the dominant species in kefir, *L. kefiranofaciens*, could only grow when the community members were present, but not individually in pure milk. The results of metabolomics indicated that this was thanks to cross-feeding of amino-acids and lactic acid [9].

Although these top-down approaches provide valuable information about important microbial communities, they also have number of drawbacks. First of all, interactions between species in large communities are often measured in terms of correlation between species, but a mechanistic understanding is usually lacking [6]. Secondly, the post-processing of the wealth of data coming from top-down approaches is complex, and it is not simple to assign a functionality to all measured species, gene expression data and protein concentrations [10]. Thirdly, natural communities live in complex, uncontrolled environments. It is therefore often hard to disentangle the impact of the environment on the community from the interactions between species. For these reasons, to understand more about the interactions in microbiomes, it is important to culture and characterize their members [3].

One way to simplify the study of large microbial communities, is to use subsets from real communities, but grow them in a laboratory setting. We could call these communities top-down synthetic communities, in the sense that one starts from a large community and selects its key players [11]. These top-down synthetic communities solve some of the drawbacks from studying communities as a whole in their natural environments; the complexity is considerably reduced and the environment is more controlled. For example, Dos Santos et al. [12] selected four species found in industrial machine oils. They made a model of the interactions in this small community by growing the species one by one in spent medium (medium in which they previously grew one of the other species) and measuring the effect of this medium on growth. Using this approach, they found a surprising positive interaction of two species with another one. It turned out that the lab medium that they used was toxic to this one species, and that the other two species could alleviate the toxicity. This result illustrates that, even within a seemingly simple four-species community, the nature of interactions is not always straightforward. Although positive interactions are easily measurable at the population level, it is important to elucidate the mechanism of these interactions, because this might change the predictions of long-term dynamics of the consortium; the researchers argued that in this consortium, the positive interaction is likely quite stable because it did not seem to involve a cost [12].

Another interesting study using subsets from natural communities was the study of bacterial communities from rainwater-filled tree holes under controlled environmental conditions [13]. The researchers could show that negative interactions between abundant species drove broad functional measures such as respiration, metabolic potential and cell yield, whereas positive interactions between rare species influenced more specific functionalities such as the capacity to degrade certain substrates.

Although, in the two examples above, the complexity of large communities was substantially reduced and the environment was controlled, one drawback remains: the mechanistic understanding of interactions is still largely lacking, mainly because the species in these top-down chosen communities are not model species, so the understanding of their metabolism

and genome is limited [11]. To overcome this drawback, an alternative approach is to use bottom-up synthetic communities. These are communities in which the expected interaction between the species is engineered, so that it can be studied in a controlled setting [5, 14]. It is important to stress that the approach of bottom-up synthetic communities is not a replacement of the top-down approaches above, but rather both are necessary to understand the various aspects of microbial communities. Bottom-up synthetic communities are further removed from the natural world, which makes it harder to apply the results of their study to relevant settings such as the human gut. On the other hand, their decreased complexity and increased controllability and reproducibility make them appropriate model systems to gain mechanistic insights in community interactions [10].

For instance, to understand the conditions for cross-feeding in microbial communities, Wintermute et al. [15] grew 46 auxotrophic *E.coli* strains in a pairwise manner. They then measured the growth and the relative abundance of each strain in each pairing, and determined how much each strain could profit from the co-culture with each other strain. Overall, their results suggested that cross-feeding mostly happened with metabolites of little value to the secreting strain. This seems in accordance with the results by Dos Santos et al. [12] reported earlier, in the sense that positive interactions are more likely to occur when they require no active investment of one partner in the other. This study illustrates the value of bottom-up synthetic communities. It was done on the well-known model species *E.coli*, which made it relatively easy to make the strains auxotrophic and tag them with fluorescence proteins. As a result, the study could measure a large range of pairwise interactions in a reproducible way. Also, the influence of the medium on the cells was already well-characterized, making the study environmentally well controlled.

Another interesting study on a synthetic *E.coli* community was done to address the importance of spatial separation for cross-feeding: Dal Co et al. [16] grew two auxotrophic *E.coli* strains in a microfluidic device and found that the interaction range of the two cell types was in the order of a few cell lengths and depended on uptake, leakage, and diffusion of the exchanged amino acids, as well as on the density of cells in the device. This study illustrates the value of bottom-up synthetic communities for answering fundamental ecological questions: the interaction ranges could only be measured because the cells were grown and tracked in the very well controlled environment of the microfluidic device.

Besides their usage to gain fundamental knowledge on the operation of microbial communities, synthetic communities have also been identified as a promising tool for biotechnological application, because they could be used to perform complex tasks through division of labour [14]. In fact, undefined microbial communities have been used for years in fields such as wastewater treatment and biodegredation [11], and synthetic communities could improve their functionality because they could be scaled down to only the essential species to perform a specific task. This would leave more energy and carbon for the functionality of the consortium, as opposed to being used by undefined species that might not be necessary for the performance of the consortium [11]. Another promising aspect of synthetic communities is the potential to control them; one can design and engineer microbial consortia so that their dynamics can in principle be externally controlled (e.g. via optogenetics or chemical inducers), for instance to online-stabilize the community or optimize performance in real time [17–19].

As a proof of concept of the value of synthetic microbial consortia, Bernstein et al. [20]

investigated a synthetic cross-feeding consortium of *E.coli*, consisting of a glucose-consuming *E.coli* strain and a metabolically engineered glucose-negative strain consuming the first strain's by-products. They could improve the net biomass production of the consortium as compared to a monoculture, presumably because the glucose-negative strain reduced inhibitory byproduct levels and utilized substrate carbon that would otherwise be wasted [20].

A topic of interest that comes back in many studies on microbial communities, is the topic of cooperation in microbial communities, and to what extent a cooperative interaction is stable in the long term. A type of cooperation that is found in anaerobic marine and freshwater sediments and in environments of extreme pH and temperature is obligate syntrophy [5]: in these environments, fermentation of organic carbon is only possible thanks to methanogens reducing the hydrogen concentration in the environment. This cooperation is mutually obligate, because the fermentors cannot grow without the methanogens and vice versa: due to the lack of electron acceptors in the environment, the strains are thermodynamically interdependent [21].

In aerobic environments, cross-feeding also occurs but is not always mutually dependent. We have already seen some examples of this kind of non-obligate cross-feeding in this section. We mentioned that microbes isolated from machine oils cooperated to alleviate medium toxicity and that this interaction seemed be stable because it did not involve a high cost for the cooperators [12]. Similarly, in the large cross-feeding study by Wintermute et al. [15], the researchers found that cross-feeding happened mostly with metabolites of little value to the secreting strain.

A cross-feeding interaction that has been repeatedly found in *E.coli* populations is a spontaneous polymorphism that arises when a monoclonal population of cells is grown for multiple generations [22, 23]. This laboratory evolution leads to two distinct subpopulations of cells, one which has improved growth on glucose (glucose specialist), and one which shows improved growth on acetate (acetate specialist). It seems that the acetate specialist is cross-feeding on the by-product acetate excreted by the glucose specialist. The cross-feeding interaction seems to be stable over time, but it is not obligate, as both specialists can also grow independently on glucose as well as acetate.

This evolved cross-feeding interaction in *E.coli* previously inspired research into synthetic microbial communities. As described above, Bernstein et al. [20] studied a synthetic *E.coli* consortium capable of cross-feeding acetate and showed that it was a promising object for biotechnological purposes because the consortium showed increased biomass production as compared to the monocultures. Inspired by these results, our group previously studied a similar synthetic consortium using a course-grained mathematical model (described below in Section 1.4) and made predictions about the conditions for its coexistence [24]. Given the promising results by Bernstein et al. [20] and the model [24], as well as the prevalence of cross-feeding in natural interactions, in this thesis we aimed to study a synthetic consortium of *E.coli* glucose and acetate specialists to answer some fundamental ecological questions. Can acetate cross-feeding stabilize the growth of the consortium? How does the acetate specialist affect the growth of the glucose specialist and vice versa? And in what conditions can this consortium stably coexist?

1.2 Modeling microbial communities

One way to study microbial communities is by using computational models. Different kinds of models have been used to study various aspects of microbial communities. In this section, we outline some of these methods and we explain the choice of model for this thesis.

To describe the interactions between populations in an ecosystem, researchers have long been using Lotka-Volterra (L-V) models [25, 26]. L-V models model the dynamics of species as differential equations, assuming that the fitness of an individual is the sum of its basal fitness, i.e. its growth rate in isolation, and fitness influences from pairwise interactions with other individuals and the environment [27]. This allows researchers to identify microbe-microbe or environment-microbe interactions that shape the community dynamics [7]. They can be used to make sense of time-varying abundances of OTUs that are found from 16S rRNA sequencing. As described in the section above, by measuring OTUs in the mouse gut following antibiotic treatment, it was demonstrated with an L-V model that antibiotics can weaken important commensal microbes that could negatively interact with the infectious microbe *Clostridium difficile* [8]. Likewise, Rao et al. [7] looked at positive and negative interactions between species during the assembly of the human microbiome.

Importantly, L-V models only incorporate positive and negative interactions between species and external perturbations [8] but they are agnostic about the mechanisms of these interactions. This is useful when one wants to get an idea about interactions in an ecosystem without having access to mechanistic information. However, L-V models might conceal interesting communities properties, because they group all interactions between two species into one interaction describing the fitness effect and therefore lack a mechanistic description [27]. This was demonstrated well in a study by Momeni et al. [27] in which the researchers compared mechanistic two-species models, that considered the interaction mediators specifically as state variables, with L-V models, which only modeled interactions between species, see Figure 1 . They showed that the type of L-V model that most accurately described the results of the mechanistic model depended on whether the mediator was reusable or consumable, on how the fitness of the two species compared, as well as on initial species densities; Choosing the wrong L-V model would lead to flawed predictions. The study therefore highlighted the need for more mechanistic models (i.e. models that consider interaction mediators explicitly) to describe community dynamics [27].

Indeed, explicit modeling of resources in so-called consumer-resource models [28] has led to some interesting model predictions that would not have been found using only L-V models. For example, Niehaus et al. [29] looked at big *in silico* communities and found that in communities where more members provided resources for other species and inhibited their own growth, more species could coexist. Importantly, they also showed that coexistence was supported more by depletable mediators (i.e. resources consumed or degraded by the receiving cell) than by reusable mediators (e.g. signalling molecules), illustrating the importance of the explicit modeling of these mediators. Other consumer-resource models [30, 31] managed to describe communities in energy-limited environments such as those in anaerobic marine and freshwater sediments [1, 5] and make predictions on their dynamics and the impact of energy-limitation. In these kind of energy-limited environments, explicit modeling of resources was helpful to understand both the impact of depletion of metabolic substrates as well as the effect of accumulation of products on microbial growth and community struc-

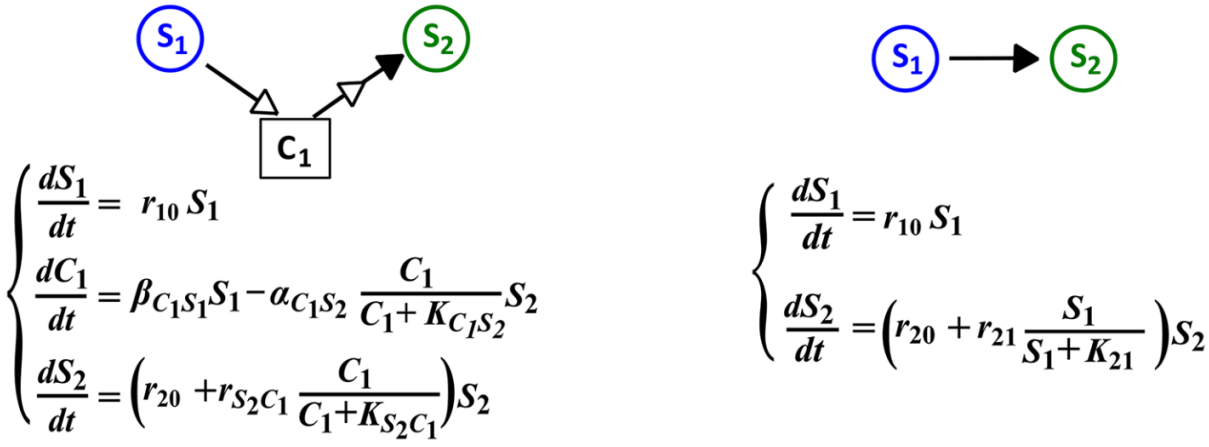

Figure 1: The difference between Lotka-Volterra models (right) and models with explicit resources (left). Adapted from [27]. Species S_1 releases chemical C_1. C_1 is consumed by species S_2 and promotes S_2's fitness. Both species have a basal growth rate (r_{10} and r_{20}). In the mechanistic model, the growth rate of S_2 is positively impacted by the chemical C_1, whereas in the L-V model, S_2 is directly influenced by S_1.

.

ture[30].

Whereas the models described above are systems of differential equations simulating the dynamic behaviour of the modeled networks [32], another type of models that have been recently used to describe microbial communities are constraint-based models, see Figure 2. Constraint-based models are metabolic models in which the possible flux distributions in the cell are investigated at steady-state (i.e. the change in metabolite concentrations is zero) [32]. Specifically, in Flux Balance Analysis (FBA), the optimal flux distribution is calculated given physical and chemical constrains as well as an objective function such as fast growth of microbial cells [32]. FBA can be combined with dynamic models (dFBA [33]) or resource allocation models in which the costs of enzymes are taken into account [34, 35].

Given the abundance of data on microbial communities, these kind of genome-scale metabolic models are starting to be used not only to understand individual species but also to model communities; they can provide insight into the strength of metabolic interactions that cannot be measured directly [37]. For example, Koch et al. [38] built stoichiometric community models from single species FBA models by reducing single species models to suitable net conversions; this approach resulted in insights on interdependencies and feasible community compositions for anaerobic digestion in biogas plants.

In a sense, constraint-based models are more comprehensive than L-V or consumer-resource models because they take into account much more information on the reactions taking place in a community. One drawback, however, is that these models are purely metabolic models; they assume that all community interactions are driven by metabolism. This might often be realistic, but not always, since other social traits such as toxin production, quorum sensing and cell-to-cell interactions have also been shown to play a role in community dynamics [36].

Other difficulties of constraint-based modeling for communities mostly have to do with

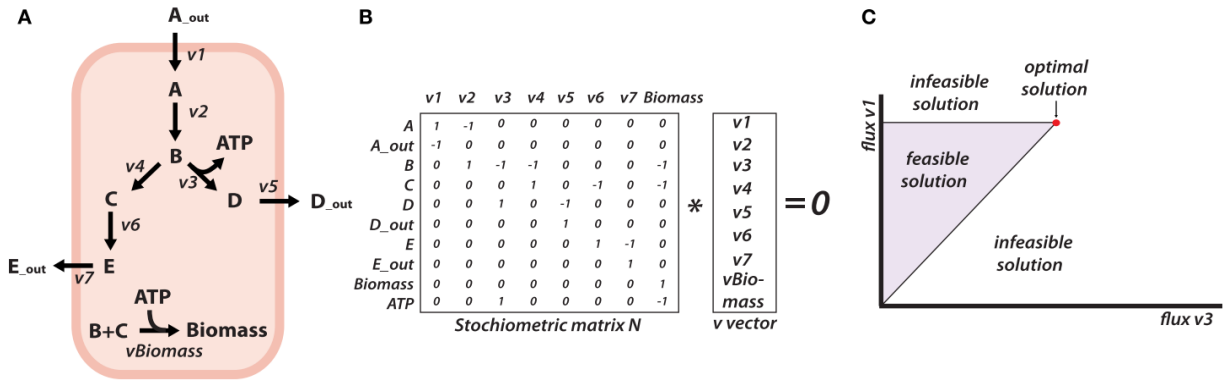

Figure 2: Taken from [36]. Constraint-based modeling of a micro-organism. (A) The microorganism takes up metabolite A and produces biomass, and products D and E. (B) The stoichiometric matrix N representing the network depicted in A, with rows corresponding to metabolites and columns to fluxes. The stoichiometric matrix multiplied with the flux vector is in steady-state. (C) The biomass flux is optimized to find the optimal flux distribution.

.

the fact that a lot of information is needed to build them reliably, that might not always be readily available. For example, in single-species models, one can obtains uptake rates of resources ('exchange rates') from the environment relatively easily, which allows to put bounds on these fluxes. This is much more complicated in communities, since multiple species might be competing for the same resource [36]. Furthermore, the biomass composition of species in the community might not be available if the community consists of non-model species [37]. Lastly, it is unclear what the objective function in a community is. Is it the community growth rate, or do species rather individually optimize their growth?

In general, all of the models described above shine light on different important aspects of microbial metabolism and microbial communities. L-V models and consumer-resource models give information specifically about which species in a community may be interacting and what is the direction of the interaction. On the other hand, genome-scale models can give detailed predictions on the impact of metabolism on community dynamics.

As for this thesis, we chose a middle ground between phenomenological L-V models and genome-scale, constraint-based models to study a synthetic consortium of *E.coli* glucose and acetate specialists: we base our study on a course-grained kinetic model describing the dynamics of a limited amount of variables [24]. Details about the model in [24] can be found below in Section 1.4. Since we are specifically interested in the effect of acetate cross-feeding on the behaviour of our consortium, and want to uncover the mechanisms behind this interaction, we do not need the level of detail of a genome-scale model [39], but we do need some detail about the main mechanisms behind the exchange of metabolites. By explicitly modelling the most relevant metabolic parts, we hope that we can use the model to understand the impact of these parts on the consortium dynamics. However, since the model structure in [24] is based mostly on observations done on individual *E.coli* strains, we shall see in the main part of the thesis that parts of the model might need to be adapted or extended in order to describe the growth of the community.

1.3 *E.coli* glucose and acetate metabolism

Since we will study an *E.coli* consortium growing on glucose and cross-feeding on acetate, we will describe the relevant aspects of *E.coli* glucose and acetate metabolism in this section. For a schematic overview, see Figure 3.

To take up glucose, *E.coli* mainly uses the phosphotransferase system (PTS) [40]. The PTS both transports glucose across the membrane and phosphorylates it [41]. *E.coli* possesses two PTS systems, PtsG and PtsM that can transport glucose with different affinities [42]: PtsG has a high affinity for glucose, whereas PtsM is the only transport system for mannose, but can also be used to scavenge glucose with lower affinity in some conditions [43, 44]. The two PTS systems share some enzymes, whereas others are specific for each carbon source. In both PTS, EIICB is responsible for the phosphorylation of glucose [45]. The phosphate group is derived from phosphoenolpyruvate and is transferred via a cascade of PTS proteins [45]. The gene *ptsG* codes for the enzyme EIICB^{Glc}, whereas *manXYZ* codes for EIICB^{Man}.

Besides the PTS systems, *E.coli* has several other uptake systems that are specific to other sugars, but can take up glucose as well, usually with lower affinities. In batch however, it was shown that a double knock-out of *ptsG* and *manXYZ* was sufficient to block growth on glucose completely [45], suggesting that those are the only two transport systems essential in batch conditions.

A transporter that has been shown to be overexpressed in glucose-limited conditions (i.e. in a chemostat) and to have a high affinity for glucose is the galactose transport system Mgl, encoded by *mglBAC* [42]. Indeed, part of the glucose uptake in these conditions seems to be done by Mgl [42, 46]. However, a knock-out of *ptsG* and *manXYZ* could not sustain growth in a chemostat at D=0.28 h^{-1} [42], indicating that transport by Mgl alone is not enough for *E.coli* to grow on glucose in a chemostat.

It has long been observed that fast-growing cells have an increased glycolysis-to-respiration ratio, leading to fermentation under aerobic conditions [47]. This happens in fast-growing tissue, like cancer cells, where it is called the Warburg effect [48, 49], as well as in yeast cells [50], where it is usually called the Crabtree effect. In bacteria, this effect is called the bacterial Crabtree effect, or more commonly overflow metabolism, and it results in the excretion of acetate during fast growth on glucose. The practical mechanisms behind overflow metabolism differ between eukaryotic and prokaryotic cells (in eukaryotes, mitochondria are implicated [49]), but the fundamental causes might well be similar. Multiple explanations for the occurrence of overflow metabolism have been proposed.

Basan et al. [51] suggested that overflow metabolism is the result of resource allocation: it is used by cells to balance the proteomic demands of energy biogenesis and biomass production. At higher growth rates, cells need to produce more biomass. Cells need proteins to produce biomass, in particular ribosomes, but also to generate energy. Given that more proteins are needed for respiration than for fermentation, it can be advantageous for fast-growing cells to use fermentation instead of respiration for energy biogenesis. This way, more proteins can be allocated to biomass production.

Likely, proteome allocation in cells evolved as a result of a thermodynamic limitation: an FBA model with an upper limit on Gibbs free energy dissipation could predict overflow metabolism in yeast and *E.coli* cells correctly [50], suggesting that overflow metabolism is

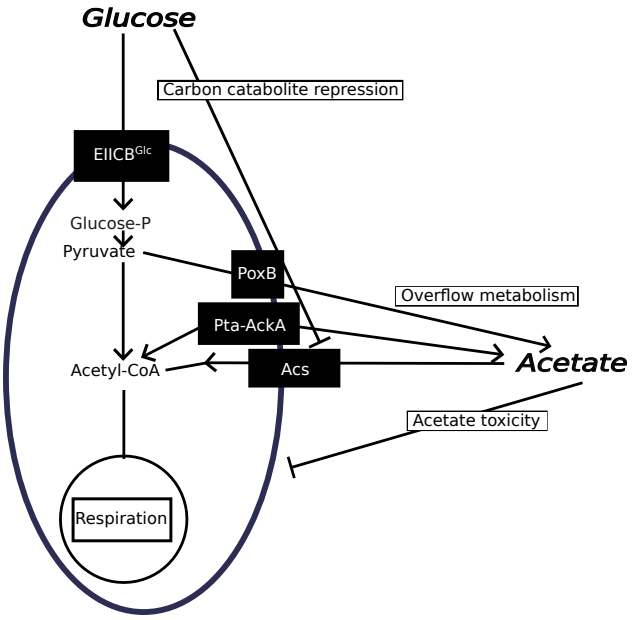

Figure 3: Schematic of *E.coli* glucose and acetate metabolism. Glucose is taken up and phosphorylated by EIICB^{Glc}. It can be used to generate energy in respiration, but it can also be excreted as acetate (to generate less energy) by PoxB or Pta-AckA. Under aerobic conditions, this is called overflow metabolism. Acetate is toxic to cells, especially at low pH. Acetate can be taken up by Pta-AckA and Acs. However, Acs is repressed at high glucose uptake rates due to carbon catabolite repression.

fundamentally caused by thermodynamic constraints.

In *E.coli*, overflow metabolism results in a threshold for acetate excretion, see Figure 4: below a certain growth rate, no acetate is excreted. Above the threshold, acetate excretion steadily increases. In batch culture on glucose, overflow metabolism leads to excretion of acetate during exponential growth, followed by a phase of acetate uptake, see Figure 5.

The enzymes involved in acetate metabolism in *E.coli* are poxB, Pta, AckA and Acs. PoxB only excretes acetate [55], the Pta-AckA pathway is reversible [56, 57], and Acs only takes up acetate [58]. It seems that acetate is continuously secreted by Pta-AckA and taken up by Acs [52, 53, 59]. At high glucose uptake rates, however, Acs is subject to carbon catabolite repression. High glucose uptake rates result in dephosphorylation of EIIA in the PTS. The dephosphorylated EIIA inhibits adenylyl cylase, which results in low cAMP levels and inactive CRP, the transcriptional activator of *acs* [54]. On top of this transcriptional control, Acs is also the subject of post-transcriptional modifications: exponential growth on glucose leads to the acetylation of Acs, rendering it inactive [60]. As a result of this carbon catabolite repression, no acetate is taken up by Acs at high glucose uptake rates, leading to a net overflow of acetate. Indeed, a coarse-grained dynamic model with implemented carbon catabolite repression could be fitted well to fed-batch data of *E.coli* growing on glucose and excreting acetate [61].

One mechanism that this model did not describe, however, is the reversibility of the Pta-AckA pathway: it was shown that this pathway can switch from production to consumption of acetate depending on the external concentration of acetate and the internal concentration of acetyl-CoA [56]. At high grow rates, the internal concentration of acetyl-CoA is high, resulting in acetate overflow. At low growth rates, this internal concentration is low, which favours acetate uptake by Pta-AckA [62]. Therefore, acetate uptake at low growth rates is likely to be done both by Pta-AckA and by Acs.

An important reason for the study of overflow metabolism is its impact on biotechnology. Since *E.coli* is often used to produce valuable products [63, 64], the excretion of acetate is an unwanted sink of carbon [65]. Besides that, acetate disrupts recombinant protein production [66], acidifies the medium, and is overall toxic to *E.coli* growth. The mechanism of its toxicity is not entirely clear. It might be disrupting the proton motive force [22, 67], or disturbing the balance of homo-cystein and acetate phosphate in the cells [68]. Either way, acetate toxicity depends on the pH, and is worse at lower pH. At pH 6.4, 128 mM acetate decreases the growth rate by a factor of 7 [68].

In this thesis, we will study a consortium growing on glucose and acetate. Studying this consortium will give us insights into the impact of the above described phenomena of overflow metabolism, carbon catabolite repression and acetate toxicity on a consortium.

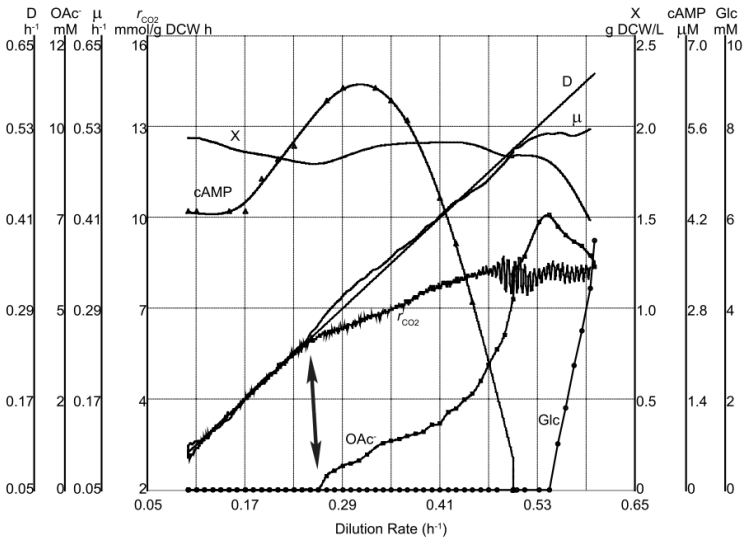

(a)

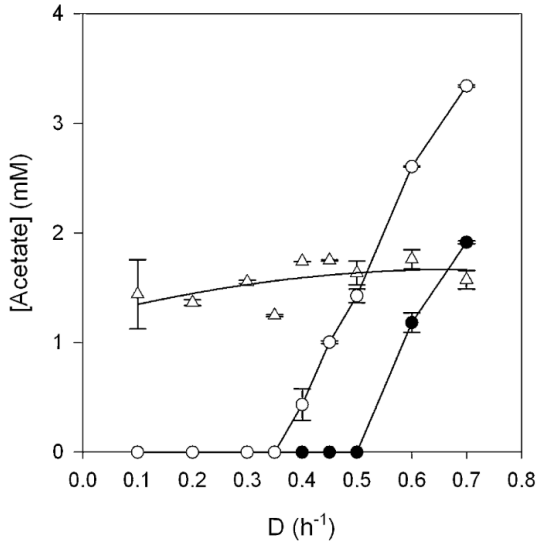

(b)

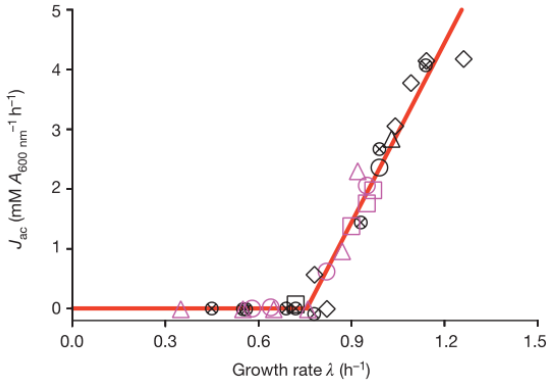

(c)

Figure 4: The threshold of acetate overflow differs between different strains and labs. (a) Data generated by Valgepea et al. [52]. Strain *E. coli* K12 MG1655 D, dilution rate (h^{-1}); X, biomass concentration (gDW/L); μ, specific growth rate (h^{-1}); rCO2, specific CO_2 production rate (mmol/gDW/h); OAc-, acetate concentration (mM); Glc, glucose concentration (mM); cAMP, cyclic AMP concentration (μM). Arrow indicates the start of overflow metabolism. (b) Data generated by Renilla et al. [53]. Strain used: *E.coli* BW25113. The black dots show the acetate overflow for the WT. Open triangles: Δ*acs*. Open circles: Δ*aceA*. (c) Data generated by Basan et al. [51]. Strain *E.coli* K12. Black symbols: growth on various carbon sources. Purple symbols: growth of cells with titratable or mutant uptake systems. Black diamonds: growth on various carbon sources supplemented with seven non-degradable amino acids (AA). Red line: the best-fit of all the data to a threshold equation for acetate excretion.

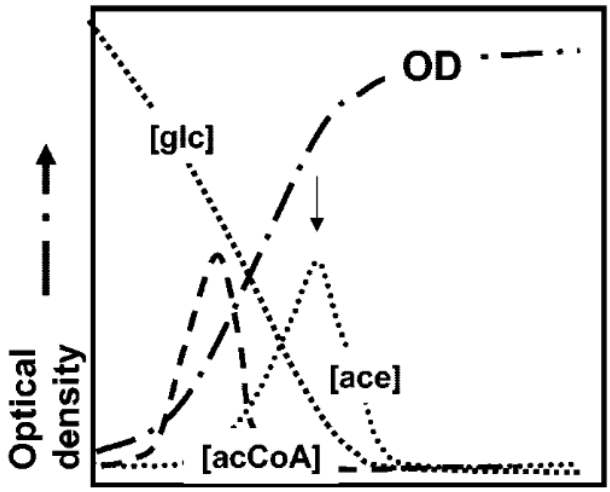

Figure 5: Figure from [54]. During exponential growth on glucose (glc), *E.coli* builds up intracellular acetyl-CoA (acCoA) that is excreted as acetate (ace). This acetate is taken up after glucose is exhausted. X-axis indicates time.

.

1.4 Model of a synthetic microbial community

Previously, our group published a course-grained mathematical model of a synthetic microbial community consisting of a protein producer strain and an acetate cleaner strain [24]. We chose this specific consortium to study, because previous research showed that a similar consortium could evolve spontaneously in laboratory settings by growing *E.coli* for a big number of generations, both in batch ([23]) and in chemostat ([22]). Moreover, it was suggested that coexistence of this consortium could lead to higher biomass concentrations than the protein producer strain alone [20].

The goal of the model study was to investigate the conditions for increased productivity of a heterologous protein by the consortium, compared to a single species. We asked whether a consortium could enhance the productivity, and how the coexistence of the two strains is influenced by the metabolic load due to heterologous protein expression. The model describes a consortium of a producer (glucose specialist) and a cleaner (acetate specialist) species, see Figure 6. The producer takes up glucose to produce heterologous protein (H) and biomass (B_P). This heterologous protein is undefined in the model but represents any protein of industrial interest, for example a medicine or a lipase as used in detergents. As a result of overflow metabolism [54, 65], the producer does not only produce the protein, but also excretes acetate, which, in high concentrations, is toxic for the cells. Acetate is not only toxic but also a carbon source. However, to our current understanding, acetate cannot be taken up at the same time as glucose, due to carbon catabolite repression [54]; it is taken up only after the glucose in the medium is exhausted. Instead, in the consortium, acetate is taken up immediately by the cleaner. The cleaner's acetate uptake is enhanced such that the cleaner removes the toxicity for the producer, while also being able to grow itself. The cleaner's glucose uptake is diminished, so most of the glucose is left for the producer. In this section, we explain the model's structure and equations, as well as the main predictions.

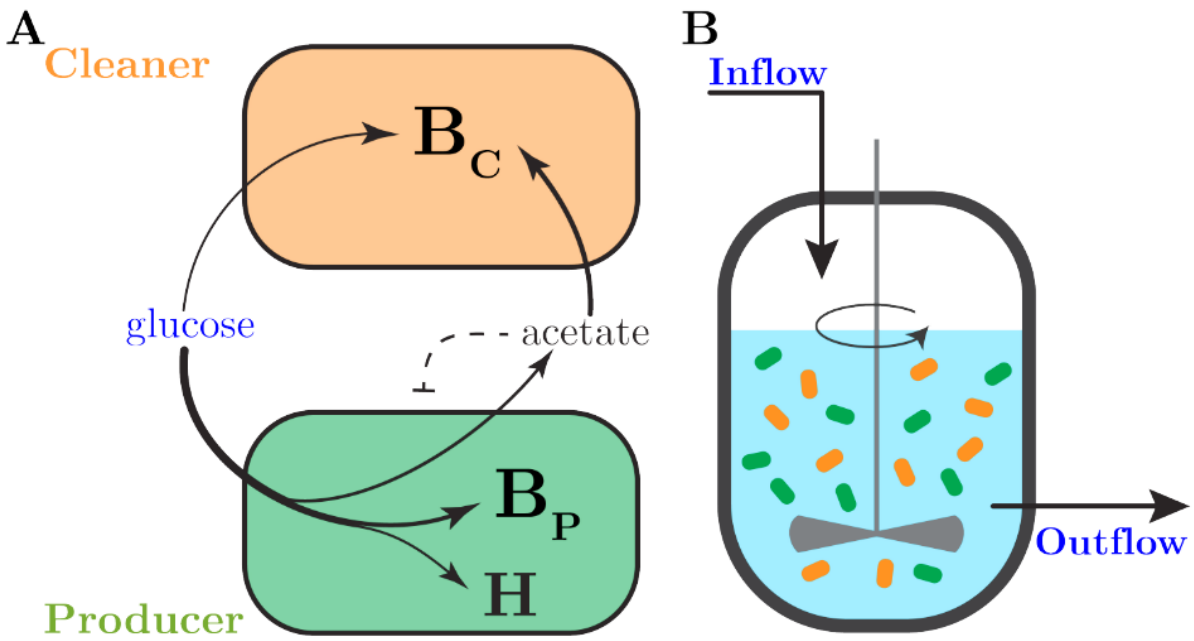

Figure 6: A: Strains in the consortium modeled by [24]. B_P and B_C denote the biomass concentrations of the producer and cleaner species, respectively. H is the concentration of the heterologous protein. All concentrations are relative to the bioreactor volume (as opposed to cell volume). B: The two strains are grown in a chemostat, with equal inflow and outflow rates resulting in a constant reactor volume.

.

A schematic of the model is given in Figure 7. The change of the variables over time, representing the evolution of concentrations in a constant reactor volume with dilution rate D (see also Figure 6), is given by the differential equations below. We use the subscript P for the producer and the subscript C for the cleaner.

$$\frac{dB_P}{dt} = (1 - Y_H)(Y_g r^g_{upP} + Y_a(r^a_{upP} - r^a_{overP}))B_P - k_{deg}B_P - DB_P, \tag{1}$$

$$\frac{dB_C}{dt} = (Y_g r^g_{upC} + Y_a(r^a_{upC} - r^a_{overC}))B_C - k_{deg}B_C - DB_C, \tag{2}$$

$$\frac{dG}{dt} = -r^g_{upP}B_P - r^g_{upC}B_C + D(G_{in} - G), \tag{3}$$

$$\frac{dA}{dt} = (r^a_{overP} - r^a_{upP})B_P + (r^a_{overC} - r^a_{upC})B_C - DA. \tag{4}$$

$$\frac{dH}{dt} = Y_H(Y_g r^g_{upP} + Y_a(r^a_{upP} - r^a_{overP}))B_P - k_{deg}B_P - DB_P, \tag{5}$$

The meaning of the variables are given in Table 1. The meanings and values of the parameters are given in Table 2. In Equation (1) and (2), the specific rate of biomass production per unit of biomass is given by $Y_g r^g_{upP} + Y_a(r^a_{upP} - r^a_{overP})$. When the cells are producing a heterologous protein, $Y_H > 0$, indicating that part of the biomass produced is assigned to the synthesis of a heterologous protein. Figure 7 shows the situation in which $Y_H = 0$ for both strains, so all biomass produced is assigned to the autocatalytic biomass, i.e. the biomass actively involved in cellular growth and maintenance.

The rate equations in this model are Michaelis-Menten functions of the metabolite concentrations, plus some regulatory mechanisms. The rate equations are expressed as follows.

$$r^g_{upP} = k_g \frac{G}{G + K_g} \frac{\theta_a^n}{A^n + \theta_a^n}, \tag{6}$$

$$r^g_{upC} = k_{\Delta PTS} \frac{G}{G + K_g} \frac{\theta_a^n}{A^n + \theta_a^n}, \tag{7}$$

$$r^a_{overP} = k_{over} \max(0, r^g_{upP} - l), \tag{8}$$

$$r^a_{overC} = k_{over} \max(0, r^g_{upC} - l), \tag{9}$$

$$r^a_{upP} = k_a \frac{A}{A + K_a} \frac{\theta_g^m}{r^g_{upP} + \theta_g^m}, \tag{10}$$

$$r^a_{upC} = k_a \frac{A}{A + K_a} \frac{\theta_g^m}{r^g_{upC} + \theta_g^m} + k_{Acs} \frac{A}{A + K_{Acs}}. \tag{11}$$

In Equation (6) and (7), the glucose uptake rate (r^g_{up}) is regulated by acetate toxicity. θ_a represents the acetate concentration at which the glucose uptake is reduced by half due to

the toxic effect of acetate on the cells. The acetate overflow (r^a_{over}, Equation (8) and (9)) is modeled such that acetate is excreted when the glucose uptake rate exceeds the threshold l. Above the threshold, the acetate secretion rate is proportional to the excess glucose uptake rate. The acetate uptake rate (r^a_{up}) in Equation (10) and (11) is regulated by carbon catabolite repression. θ_g represents the glucose uptake rate at which the acetate uptake is reduced by half due to carbon catabolite repression. The cleaner has an increased acetate uptake modeled by $k_{Acs}A/(A + K_{Acs})$.

Table 1: Meaning of the variables in [24].

Variable	Meaning	Units
B	concentration of cells in the reactor	$\mathrm{gDW^{-1}\,L^{-1}}$
G	glucose concentration in the reactor	$\mathrm{g\,L^{-1}}$
A	acetate concentration in the reactor	$\mathrm{g\,L^{-1}}$
G_{in}	glucose concentration in the inflow	$\mathrm{g\,L^{-1}}$
H	concentration of heterologous protein in the reactor	$\mathrm{gDW^{-1}\,L^{-1}}$

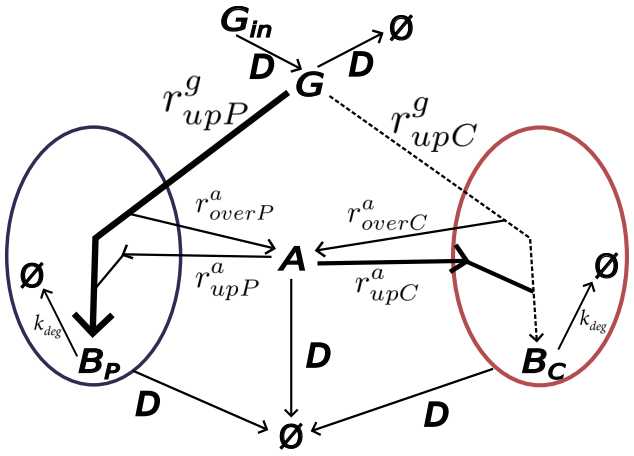

Figure 7: A schematic of the model in [24] of glucose and acetate metabolism for a glucose specialist (subscript $_P$) and an acetate specialist (subscript $_C$). During glucose-fueled growth, glucose (G) is taken up and transformed into biomass (B) through r^g_{up}. In the case of overflow metabolism, the glucose can be excreted as acetate (A) through r^a_{over}. Acetate can be taken up from the medium through r^a_{up}. In a chemostat, glucose is supplied from the inflow (G_{in}) and flushed out with dilution rate D. The cells are flushed out at the same rate. Biomass is degraded for maintenance metabolism through k_{deg}. For clarity of the figure, the negative impact of acetate inhibition and carbon catabolite repression are not indicated here.

Table 2: Values of the model parameters in [24].

Parameter	**Value**	**Units**	**Meaning**
k_g	1.53	$\mathrm{g\,gDW^{-1}\,L^{-1}}$	maximal glucose uptake rate of the glucose specialist
K_g	0.09	$\mathrm{g\,L^{-1}}$	half maximal rate constant for glucose uptake
θ_a	0.52	$\mathrm{g\,L^{-1}}$	inhibition constant of acetate on the glucose uptake rate
n	1	NA	exponent shaping the non-linear effect of acetate toxicity
k_{over}	0.17	NA	proportionality constant for acetate excretion
l	0.7	$\mathrm{g\,gDW^{-1}\,h^{-1}}$	threshold for acetate excretion
k_a	0.97	$\mathrm{g\,gDW^{-1}\,h^{-1}}$	maximal acetate uptake rate
K_a	0.5	$\mathrm{g\,L^{-1}}$	half maximal rate constant for acetate uptake
θ_g	0.25	$\mathrm{g\,gDW^{-1}\,h^{-1}}$	inhibition constant of acetate uptake
m	1	NA	exponent shaping the non-linear effect of carbon catabolite expression
Y_g	0.44	$\mathrm{gDW\,g^{-1}}$	biomass yield for growth on glucose
Y_a	0.298	$\mathrm{gDW\,g^{-1}}$	biomass yield for growth on acetate
Y_H	0	NA	heterologous protein yield
k_{deg}	0.004	$\mathrm{h^{-1}}$	degradation rate constant
$k_{\Delta PTS}$	0.38	$\mathrm{g\,gDW^{-1}\,h^{-1}}$	maximal glucose uptake rate of the acetate specialist
k_{Acs}	1.46	$\mathrm{g\,gDW^{-1}\,h^{-1}}$	maximal acetate uptake rate of Acs
K_{Acs}	0.012	$\mathrm{g\,L^{-1}}$	half maximal rate constant of Acs
D	-	$\mathrm{h^{-1}}$	dilution rate, depends on experiment

The analysis of the model indicated first of all that coexistence of the protein producer and acetate cleaner is possible in a chemostat over a range of dilution rates (see Figure 8), and that it can lead to productivity gain as compared to a single species, in chemostat as well as in fed-batch conditions [24]. Secondly, it was found that coexistence is also possible with a 20% metabolic load, meaning that 20% of the producer cells' resources are used for protein production. Given the promising findings of the model, in this PhD project, we aimed to construct the modeled consortium *in vivo* in order to further advance and scrutinize the findings of the existing model, and analyze the conditions for coexistence of the acetate specialist and the glucose specialist.

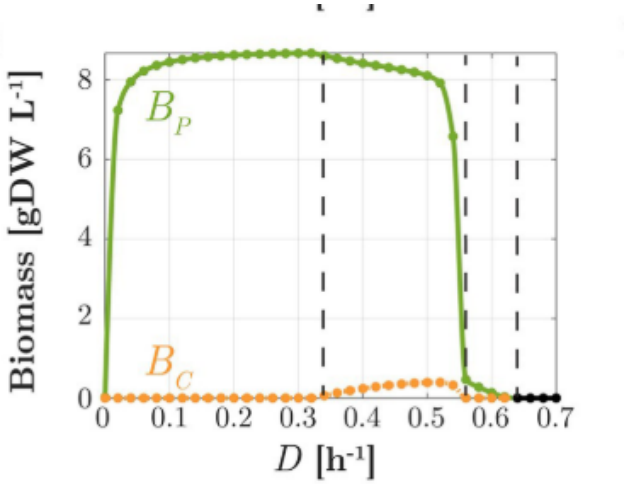

Figure 8: Prediction by the model in [24] for the concentration of producer (B_P) and cleaner (B_C) in steady-state as function of the dilution rate D. The model predicts that the cleaner and the producer can coexist at high dilution rates between 0.35 and 0.55 h^{-1}.

1.5 Experimental methods to study *E.coli*

In this section, we describe the methods that can be used to modify and study the growth of microbes, and specifically *E.coli*, *in vivo*. More details of the exact protocols used in this study are given in the Materials and Methods.

1.5.1 Modifying *E.coli*

To modify the genome of *E.coli*, recombineering can be used [69], which makes use of 50 base pair (bp) homologies to insert a sequence into the genome [70].

First, a pSIM plasmid [71] containing a recombination system is inserted into the cells. This plasmid contains the bacteriophage λ Red system necessary for recombineering and a chloramphenicol resistance gene for selection. It has a temperature-sensitive replicon so that it can be removed when recombineering is completed.

Next, the sequence of interest is inserted in a two step selection process, using a selection cassette (see Figure 9). The selection cassette contains a constitutively expressed kanamycin resistance gene and the gene *ccdB* coding for the toxin CcdB that is inducible by arabinose.

In the first, positive selection step, the cassette (flanked by 50 bp sequences homologous to the desired region in the chromosome) is inserted at the target locus and the cells that have recombined are selected on plates containing kanamycin: cells not containing the cassette will not grow on these plates. In the second, negative selection step, the sequence of interest (again flanked by 50 bp regions) is inserted at the same location, replacing the cassette, and the cells that no longer contain the cassette are selected by plating on arabinose: cells still containing the cassette will not grow on these plates.

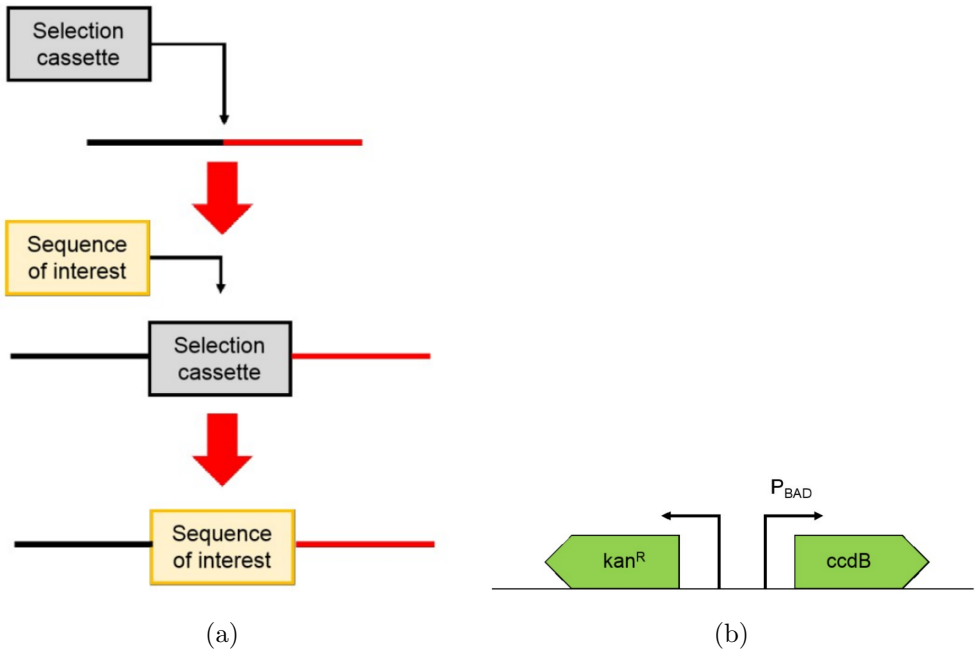

(a) (b)

Figure 9: Modification of the genome by recombineering. (a) Modification takes place in two steps. First, we insert a selection cassette, and select the cells that contain the cassette (positive selection) by growing them on kanamycin. Then, we insert the sequence of interest, and select the cells that no longer contain the cassette (negative selection) by growing them on arabinose. (b) For the positive selection step, the selection cassette contains a constitutively expressed kanamycin resistance gene. For the negative selection step, the selection cassette contains the *ccdB* gene coding for the toxin CcdB that is inducible by arabinose.

To create deletions in the cells, the Keio collection can be used [72], see Figure 10. The Keio collection is a large collection of *E.coli* K-12 single-gene deletion mutants that contain a kanamycin selection cassette flanked by FLP recognition target (FRT) sites in place of the deleted gene. FLP recombinase recognizes these FRT sites [73] and can be used to loop out the kanamycin cassette, leaving behind an in-frame 102 bp scar.

To create plasmids expressing a gene of interest, Gibson assembly is a widespread method [74]. First, a linear vector and the desired insert with overlapping ends are created by PCR with the appropriate primers. Then, the insert and the vector are assembled *in vitro* using a kit containing a 5' exonuclease, a DNA polymerase and a DNA ligase. The resulting plasmid can then be inserted in the bacteria, e.g. using electroporation.

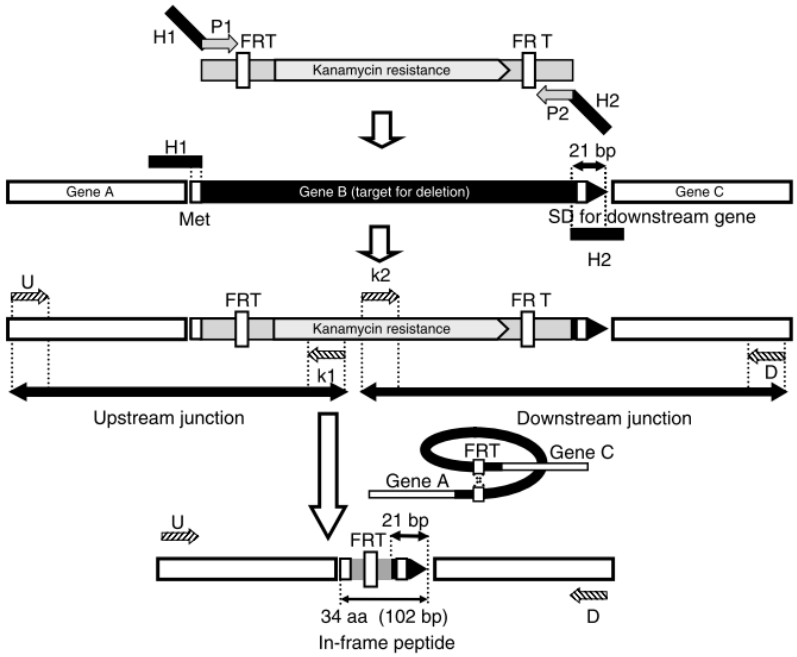

Figure 10: Figure from Baba et al. [72]. In the first step, the gene to be deleted is replaced with a kanamycin resistance gene flanked by two FRT sites. Novel junctions created between the resistance cassette and neighboring upstream (gene A) and downstream (gene C) sequences can be verified by PCR with kanamycin (k1 or k2) and locus-specific (U or D) primers. In a second step, the cassette can be removed using FLP recombinase. This leaves a 102 bp scar sequence.

1.5.2 Growing and monitoring bacteria

To monitor the growth of bacteria, the optical density (OD) is commonly used [75]. It is assumed that the absorbance of the culture at 600 nm is proportional to the the concentration of cells. However, at high cell concentrations, we may observe multiple scattering events. Therefore, a calibration curve has to be constructed to properly relate OD to cell concentration [76]. The calibration curve used in this thesis is given in the Materials and Methods.

On the one hand, the optical density and fluorescence of the bacterial population as a whole can be monitored. On the other hand, it can be useful to quantify the light scattering and fluorescence of individuals in a population of bacterial cells. For this, flow cytometry can be used [77], see Figure 11. This technique allows for the determination of heterogeneity in a population of cells [78]: It allows to see variations in fluorescence and size between cells, as opposed to only giving the total population fluorescence and density.

Moreover, flow cytometry permits the quantification of gene expression of individual cells by tagging the desired the gene with a fluorescent protein. Flow cytometry can also be used to distinguish between different strains in a microbial community [79], provided that the strains are different enough. For example, strains tagged with different fluorescence proteins can be distinguished and counted to determine their abundance in the population [17].

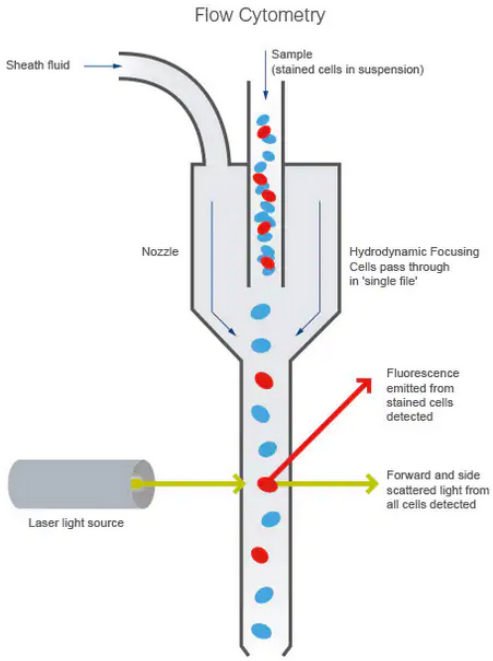

Figure 11: Image from https://www.abcam.com/protocols/introduction-to-flow-cytometry [80]. In flow cytometry, cells are passed through a thin capillary in a single file so that fluorescence and light scattering of individual cells can be measured.

One way to grow bacteria is in a batch culture: a small amount of cells is inoculated in a reactor with a given medium. The growth of the cells is then monitored until it comes

to a halt. This can be done, for example, in Erlenmeyer flasks that are incubated at the appropriate temperature and agitated. A way to grow bacteria in batch in a high-throughput manner is by growing them in microplates. Each well contains a batch experiment, so that multiple biological and technical replicates can be done at once. If one wants to evaluate growth on a given carbon source, it is important that this specific carbon source is the only limiting factor in the culture and that the other nutrients, as well as oxygen, are supplied in excess [81]. To supply enough oxygen in a microplate well, beads should be added to the wells, so that stirring of the culture is improved [82].

In a batch culture, the limiting nutrient is usually supplied in excess, so the cells grow at their maximal growth rate on that nutrient. Besides, the nutrients are being taken up so their concentrations are continuously changing. On the other hand, if one wants to maintain a bacterial population at a lower growth rate for a long period of time, this can be done by keeping the concentration of the limiting nutrient at a close-to-zero concentration, while supplying the other nutrients in excess [83]. This kind of growth is called a chemostat, because the concentrations of the chemicals are kept constant over time. The practical aspects of putting in place a chemostat are discussed further below.

1.5.3 Growing bacteria in a chemostat

Mathematically, chemostat growth is simpler to analyze than batch growth because steady-state can be assumed: the concentrations of nutrients and cells do not change. However, even when assuming a simple Monod growth law for growth of a single-strain bacterial population [84], some outcomes of chemostat culture are not entirely intuitive. Therefore, we will explain some of these outcomes briefly in this section.

At steady-state, the concentration of the limiting nutrient is called the residual nutrient concentration. It is this low nutrient concentration that determines the growth rate of the cells according to Monod's equation [84]:

$$\mu = \mu_{max} \frac{S}{S + K_s}, \tag{12}$$

where μ is the growth rate, S is the residual nutrient concentration, and K_s is the half-saturation constant. It follows that, in a chemostat with cells growing at a growth rate well below the μ_{max}, the residual nutrient concentration is in the order of the half-saturation constant.

The rate at which nutrients are supplied to and removed from the reactor is called the dilution rate (D). The dilution rate equals the flow rate divided by the reactor volume. In steady-state, the concentration of cells does not change. This means that, in steady-state, the dilution rate must equal the growth rate of the cells:

$$D = \mu \tag{13}$$

From Equations (12) and (13), it follows that in a chemostat, the dilution rate determines the residual nutrient concentration. The nutrient concentration in the inflow, on the other hand, counter-intuitively has no impact on the residual glucose concentration, but determines the steady-state concentration of cells [85], according to:

$$B = (S_{in} - \frac{K_s D}{\mu_{max} - D})Y_s, \tag{14}$$

where B is the steady-state biomass concentration, S_{in} the nutrient concentration in the inflow, and Y_s is the biomass yield of the limiting nutrient. Essentially, the steady-state concentration equals the nutrient concentration in the inflow multiplied by the biomass yield $S_{in}Y_s$, minus the small residual nutrient concentration $K_sD/(\mu_{max} - D)$.

Technically, chemostats are more complicated to operate than batch cultures because they are not a closed system: nutrients need to be pumped in and biomass and nutrients are pumped out continuously. This requires more software and hardware as compared to batch experiments that can be run with just a flask and an incubator. Moreover, the long run times and the continuous nutrient supply of chemostats require higher amounts of medium for each experiment. To limit the amount of medium needed and facilitate affordable chemostat experiments, several mini-bioreactor systems have been developed in the past years [86–91]. This thesis took inspiration from these developments to develop a mini-bioreactor system that has the additional possibility of online monitoring of the culture, as will be detailed in Section 2.2.

1.6 Problem statement and thesis outline

In this PhD project, we construct the consortium of two *E.coli* strains in Figure 7, a glucose specialist strain and an acetate specialist strain, with the aim of improving our quantitative understanding of the conditions for coexistence and the possible accompanying trade-offs. We grow the consortium in a chemostat and ask whether there is a dilution rate at which both strains can coexist stably. We are specifically interested in studying the impact of acetate cross-feeding on the coexistence of the consortium: can acetate cross-feeding stabilize the growth of the consortium? How does the acetate specialist affect the growth of the glucose specialist and vice versa? Furthermore, we scrutinize the findings of the model presented above; can it represent the growth of the individual strains as well as the consortium?

To answer these questions, first, in Section 2.1 we show how we constructed a glucose and an acetate specialist and explain our reasoning for the design of the consortium. We explain the choice of fluorescence proteins for tracking the individual strains in the consortium; we explain how we knocked out the glucose uptake rate system *ptsG* of the acetate specialist; we describe how we increased the acetate uptake rate of the acetate specialist by overexpressing the acetate uptake systems Pta-AckA and Acs, and we describe how we made the strains resistant to phage infections by removing *fhuA*.

Then, in Section 2.2, we describe the development and usage of a custom made, automated platform of mini-bioreactors used to grow the consortium and experimentally characterize its interaction dynamics. We describe the platform's hardware and software; we explain the development of an appropriate bioreactor setup and measurement routine; we develop calibration and processing procedures to interpret the raw data, and we establish a series of experimental choices to avoid culture instability and experimental artifacts.

We continue in Section 2.3 to experimentally characterize the individual strains. We compare the growth rate of the glucose specialist and the acetate specialist during individual batch growth on glucose and show that the glucose specialist grows faster than the acetate

specialist and that the glucose specialist excretes acetate in these conditions. We compare the growth rate of the glucose specialist and the acetate specialist in batch on acetate and show that the acetate specialist grows faster. We also look at the growth of the glucose specialist in a chemostat and show that it excretes acetate in this set-up as well.

After the experimental characterization, in Section 2.4, we ask whether the model described above can represent the growth of the individual strains. We fit the model to individual batch growth on glucose of the glucose specialist as well as the acetate specialist. Then, we fit the growth of the glucose and acetate specialist on acetate.

In Section 2.5, we investigate the potential for a stable coexistence of the consortium, both experimentally and numerically. We show that the model, calibrated with the data of the individual strains, does not predict coexistence of the consortium. However, the data of the consortium growing in the chemostat indicate that coexistence might be happening at low dilution rates. Given the discrepancy between the consortium data and the model predictions, in Section 2.6, we propose a new model (that we call the 'cycling model') for glucose and acetate metabolism that allows for coexistence of the consortium at low dilution rates. We calibrate this model with data from the literature, show that it can reproduce the data generated in our lab, and explore the possibilities of coexistence according to this new model.

As the cycling model makes some falsifiable predictions of the consortium dynamics, we assess these predictions in Section 2.7. Finally, in Section 2.8, we establish that we can further improve the stability of the individual acetate specialist as well as the consortium by adding antibiotics, and show that the acetate specialist seems to adapt to growth in the consortium by improving its glucose uptake rate.

2 Results

> Under normal conditions the research scientist is not an innovator but a solver of puzzles, and the puzzles upon which he concentrates are just those which he believes can be both stated and solved within the existing scientific tradition.
>
> Thomas Kuhn

2.1 Strain constructions

The main goal of this thesis was to analyze the behaviour of a cross-feeding synthetic consortium consisting of a glucose and an acetate specialist. To this end, we genetically modified the *E.coli* BW25113 strain already present in our lab to display the desired characteristics. The constructions are summarized in Table 3 and Figure 12. In this section, we give an overview of these constructions and explain our reasoning for the design of the consortium. We explain our choice of fluorescence proteins mCerulean-ME and mScarlet-I for tracking of the strains in Section 2.1.1. Section 2.1.2 explains how we knocked out the glucose uptake rate system PtsG of the acetate specialist. Section 2.1.3 describes how we increased the acetate uptake rate of the acetate specialist by overexpressing the acetate uptake systems Pta-AckA and Acs. Finally, Section 2.1.4 describes how we made the strains resistant to phage infections by removing *fhuA*.

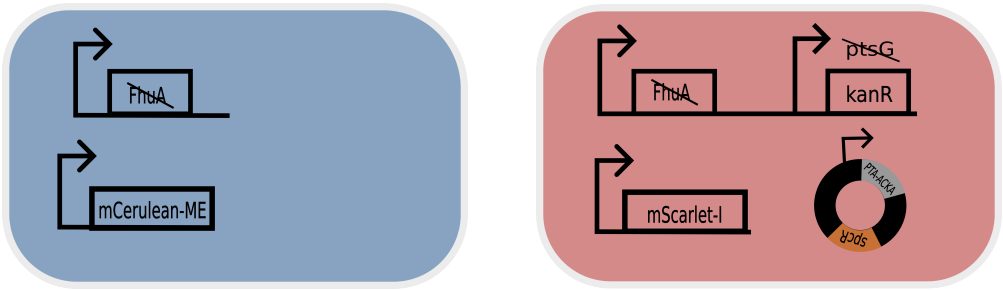

Figure 12: Schematic of the two constructed strains. The glucose specialist (blue, left) has the gene *fhuA* knocked out. It expresses blue fluorescent protein mCerulean-ME on the chromosome. The acetate specialist (red, right) also has a knock-out of *fhuA*. *ptsG* is removed and replaced by a cassette that conveys kanamycin resistance. It expresses the red fluorescent protein mScarlet-I on the chromosome. Lastly, the acetate specialist contains a plasmid with a spectinomycin resistance that overexpresses either *pta-ackA* (shown in this schematic) or *acs*.

2.1.1 Fluorescent proteins

In order to keep track of the fractions of the two strains in the bioreactor, we decided to insert a gene expressing a fluorescent protein in their genome. We chose the proteins mCerulean-ME and mScarlet-I controlled by the constitutive promoter *proC* [92], which were previously used and characterized in our lab by PhD student Antrea Pavlou [93]. Since we wanted the fluorescence to be a measure of cell number, we aimed for the red fluorescence expression to be as constant as possible. Therefore we used a constitutive promoter and inserted the genes into the chromosome by homologous recombination [69] to avoid copy number variation. The fluorescent proteins could be used to determine cell number both by measuring the total fluorescence of the culture using spectrometry and by measuring the fluorescence of individual cells using flow cytometry. We could detect both the mCerulean-ME and the mScarlet-I by spectrometry (see Figure S9 and S8), even though the mCerulean-ME has a significant background spectrum from the cells that needs to be taken into account. Initial flow cytometry experiments showed that mCerulean-ME was not identifiable in our flow cytometer, but mScarlet-I was. Since we expected our acetate specialist to be present in smaller amounts than the glucose specialist, we decided to mark the acetate specialist with mScarlet-I and the glucose specialist with mCerulean-ME, so that we could identify the small amounts of acetate specialist in the flow cytometer.

2.1.2 Reduction of glucose uptake

In order to reduce the glucose uptake rate of the acetate specialist, we knocked out *ptsG*, a gene coding for EIICB^{Glc} which is an essential part of the phosphotransferase system responsible for most of the glucose uptake in *E.coli* [45]. Knocking out this system does not completely inhibit the use of glucose by the cells, because the cell can resort to other, non-specific carbon uptake systems [45]; this is convenient for our consortium, since it will allow the acetate specialist to coexist with the glucose specialist at higher dilution rates than it otherwise could. As explained in the introduction, the model predicts that only when the two species grow at the same rate (equal to the dilution rate of the chemostat) can they stably coexist.

The glucose specialist's growth rate is mostly determined by its glucose uptake rate. The acetate specialist's growth rate would be determined only by its rate of acetate uptake if we forced it to grow by using only acetate and no glucose. However, leaving some capacity for glucose uptake allows the acetate specialist to take up glucose and acetate simultaneously. Since it has an enhanced acetate uptake rate, this could allow the acetate specialist to achieve the same growth rate as the glucose specialist in a chemostat (a growth rate equal to the dilution rate). Knocking out glucose uptake entirely and thereby limiting the acetate specialist to only take up acetate would likely narrow the range of coexistence in a chemostat too much.

We removed *ptsG* using the Keio collection [72]. We took the collection's strain with the *ptsG* knock-out, and amplified the region containing the knock-out and a Kanamycin resistance marker (for primers, see Section 4). We then transformed the product into a strain carrying mScarlet-I on the chromosome and selected the Kanamycin-resistant recombinants. Theoretically, this resistance could be removed using FLP recombination, but we did not

manage to make this recombination work and decided to leave the resistance instead. In fact, the kanamycin resistance was useful since it provided us with a complementary method to select for the acetate specialist by adding kanamycin to the medium.

2.1.3 Increase of acetate uptake

In order to increase the acetate uptake of the acetate specialist, we had the choice between overexpressing two acetate uptake systems: the Pta-AckA pathway or Acs [54]. We decided to construct both options in parallel so that we could test which one worked best for our purpose. In order to increase the expressions strength, we decided to overexpress the genes using plasmids. We used a pQE80 plasmid with a pSC101 origin of replication, which has a copy number of around 6-7 [94]. We put the genes under the control of an IPTG inducible promoter; this way we could control whether acetate uptake is increased or not by adding or removing IPTG. The plasmids were constructed by Gibson assembly [74] and carried a spectinomycin resistance to be able to select for them.

2.1.4 Resistance to phage infection

As described in Section 2.2.4, we knocked out *fhuA* in both strains to make them immune to infection by T1-like viruses [95]. We did this by replacing *fhuA* by a selection cassette and subsequently replacing the cassette by ssDNA, using homologous recombination [69], leading to a clean deletion of the open reading frame.

Table 3: Constructions executed for this study and their function

Construction	**Function**
proC:mCerulean-ME on chromosome	Distinguishing the glucose specialist in the consortium
proC:mScarlet-I on chromosome	Distinguishing acetate specialist
ptsG knockout in the acetate specialist	Decreasing glucose uptake in the acetate specialist
Overexpression of *acs* or *pta-ackA*	Increasing acetate uptake acetate specialist
fhuA knockout in both strains	Preventing infection by T1-like phages

2.2 Continuous-flow experiments on an automated mini-bioreactor platform

In order to grow the consortium, experimentally characterize its interaction dynamics, and eventually enable real-time control experiments, this thesis relied on a custom made, automated platform of mini-bioreactors, whose development started before the thesis and is still ongoing. Centered around a thermostated chamber hosting several 25 mL flasks for the growth of the bacterial cultures, the system enables chemostat as well as batch growth experiments, with periodic measurements for the monitoring of bacterial growth, and (feedback) control actions for the (real-time) adjustment of the growth conditions. The physical platform development joins the efforts of Inria project-team MicroCosme and team BIOP at LIPhy, whereas the operation software is jointly developed by MicroCosme and Inria project-team BIOCORE at Inria Sophia-Antipolis. Platform hardware and software are described in Section 2.2.1.

The typical usage of the platform in this thesis was the execution of experimental campaigns consisting of parallel chemostat experiments in several mini-bioreactors, with different experimental conditions (culture and substrate composition, dilution rate) explored in different experimental campaigns, each running over up to one week. Effective utilization of the platform required the development of an appropriate bioreactor setup and measurement routine, described in Section 2.2.2. In the course of my thesis, I was key contributor in these developments, in addition to contributing to the platform software development in terms of the sharing of user experience and suggestions.

To obtain biologically meaningful data, raw measurements need to be appropriately calibrated and processed (Section 2.2.3). Moreover, we established a series of experimental choices to avoid culture instability and experimental artifacts (Section 2.2.4).

Finally, in Section 2.2.5, we provide a protocol for a typical bioreactor experiment.

2.2.1 Platform description

Physical platform architecture

A picture of the mini-bioreactor platform is shown in Figure 13. In addition to the thermostated chamber hosting up to ten 25 mL bioreactors, the platform is arranged around a measurement cuvette, where liquid samples from the bioreactors are transferred via microfluidic tubes and peristaltic pumps, and where light sources and spectrometers are connected via optical fibers to measure absorbance and fluorescence spectra of the sample in the cuvette. Optical paths include filter wheels to select appropriate wavelenght bands. A main selection valve and additional microfluidic valves allow one to select which bioreactor sample is routed to the measurement cuvette, and to transfer the sample from the cuvette to waste after spectrometry measurements have been taken. Optionally, the sample can be transferred from the cuvette to a cytometer for single-cell measurements, before being pumped to waste. This typically requires to appropriately set up an additional system of liquid buffers for the dilution of the sample at a density suitable for cytometry.

Air and water inflows are used to empty and rinse tubes and cuvette before/after measurements. Based on this backbone, the specific setup of bioreactors (including subtrate and air input, excess volume outputs etc.) and other fluidic arrangements (e.g. sample dilution

system for cytometry) are customizable and depend on the experiment to be performed. For the experiments of this thesis, this is the object of Section 2.2.2. All platform devices are connected to a desktop computer that operates the platform. The computer software for platform operation is called ODIN+, shortened to ODIN from now on, described next.

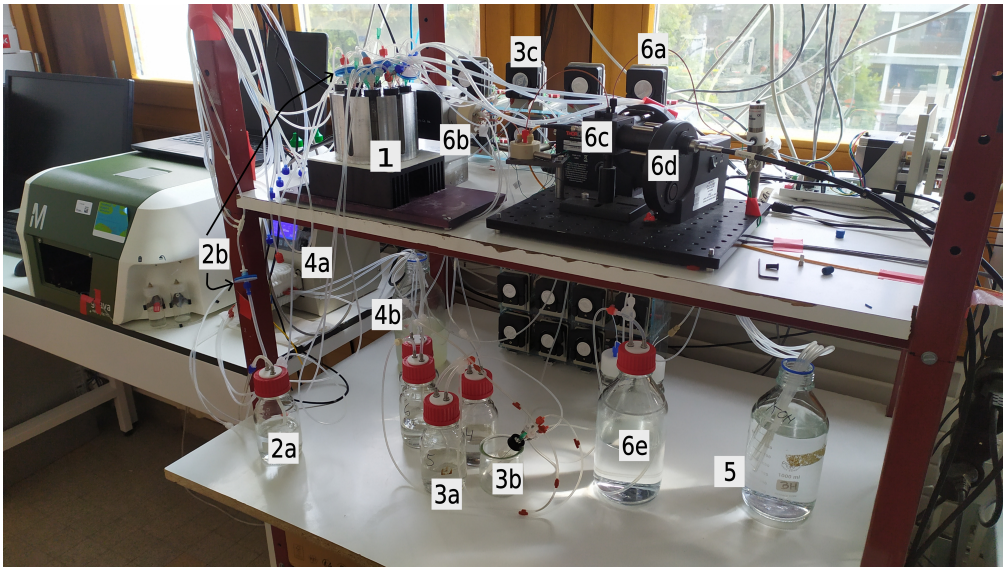

Figure 13: Picture of the mini-bioreactor platform. 1) Bioreactors 2a) KOH solution to sterilize the incoming air 2b) 0.22 μm filter to sterilize the incoming air 3a) Medium storage bottle 3b) KOH to sterilize air entering the medium storage bottles 3c) Pumps transporting medium to the bioreactors 4a) Pump removing culture from the bioreactors 4b) Waste container 5) KOH sterilizing the air leaving the bioreactors 6a) Pumps transporting samples 6b) Selection valve selecting the chosen bioreactor to be sampled 6c) Measurement cuvette 6d) Filter wheel to select input and output wavelength for the fluorescence measurements 6e) Water container for water samples

.

Automated platform operation: ODIN

Full refactoring of a former version developed by the BIOCORE project-team, ODIN is a web-based, modular software for the operation of bioreactor-like platforms and the automated execution of monitoring cultures as well as real-time (feedback) control experiments. Displayed in a browser, the ODIN graphical user interface (GUI) includes a dashboard for the manual operation of the platform and the visual inspection (plotting) of measurement and control results, and additional web pages to access the further functionalities of the software. These functionalities are architectured around the following elements (see Figure 14):

- ODIN Sequences: A sequence is a list of commands to platform devices (pump activation, positioning of a valve, activation of spectrometry etc.) written in a dedicated language and executed one after the other when the sequence is launched

- ODIN Algorithms: Python-based routines that can be launched periodically or in response to events (e.g. arrival of a measurement from a device). They can execute sequences and/or implement estimation (e.g. real-time calibration of spectrometer measurements) and control logics (e.g. decide for a change in pump speed to adjust dilution rate given absorbance measurements and an OD target)
- ODIN Campaigns: A container of algorithms that are proper to an experimental campaign.

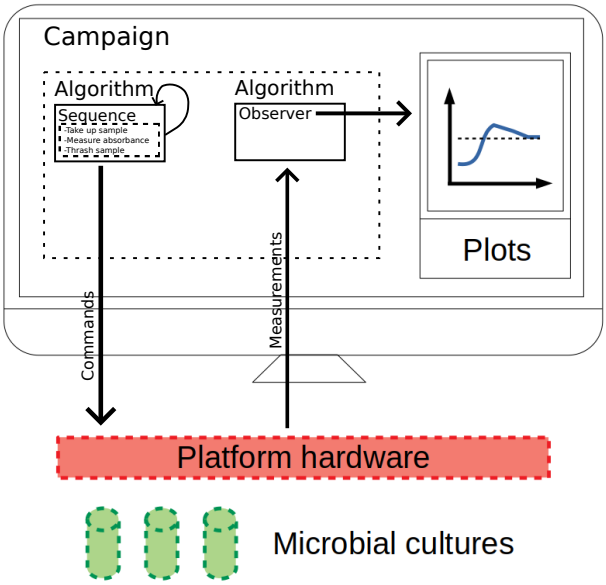

Figure 14: Schematic lay-out of an ODIN campaign. A measurement algorithm is defined for every bioreactor in the experiment such that, periodically, the algorithm is activated and launches the corresponding measurement sequence for the corresponding bioreactor. Additional observer algorithms are defined that wait for the arrival of measurements. Measurements calibrated by the observer are used for the absolute quantification of the experiment in real-time.

.

In the usage of this thesis, a measurement sequence, parameterized by a bioreactor number, is defined such that, when launched, all actions on the platform devices that are needed to correctly transfer a sample from the specified bioreactor to the measurement cuvette and to take the requested measurements, are performed automatically (including cleaning and emptying). A measurement algorithm is defined for every bioreactor in the experiment such that, periodically in time, the algorithm is activated and launches the corresponding measurement sequence for the corresponding bioreactor. An additional observer algorithm is defined that waits for the arrival of spectrometry measurements, calculates and returns OD measurements calibrated based on additional reference spectra of water and the dark current of the spectrometer. A similar algorithm calculating calibrated fluorescence measurements is used. The measurements calibrated by the observer are used for the absolute quantification

of the experiment in real-time. All algorithms for an experimental campaign are defined as part of an ODIN campaign.

Clearly, the structure of the measurement sequence (appropriate positioning of valves, pumps to activate, etc.) is directly related with the physical layout of the platform backbone described above. Details of the measurement sequence (pumping time needed to fill the cuvette, etc.) have been fixed based on calibration experiments. More sequence details will be discussed in Section 2.2.2. Additional sequences were defined for complete platform cleaning, on-demand extraction of bioreactor samples (e.g. for manual cytometry measurements), etc.

Crucially, the software embeds a scheduler, i.e. a system that automatically arbitrates when the (measurement) sequences can be executed depending on the current state of the platform. This is crucial to avoid that different samples are routed through the shared fluidic paths in conflict with each other, without the user explicitly handling these potential conflicts.

All data transiting in the software from/to the platform are automatically stored in a database. Export of the database information from one campaign comprises the data-set that is used for further data analysis. Additional software functionalities (platform configuration, feedback control features etc.) are not relevant to the thesis and are not described here.

2.2.2 Setup of a chemostat experiment

A typical experiment (campaign) consists of several bioreactors operated in parallel, plus additional liquid sources and buffers (water, M9 with carbon source, KOH etc.), that are set up to make a chemostat experiment. Each bioreactor is measured periodically, in a way that is described in this section.

Setup of one bioreactor

A schematic of the bioreactor is shown in Figure 15. A picture is shown in Figure 13. The same parts are numbered the same in both figures. The bioreactors (1) are 25 mL flasks of which 15 mL is filled with culture. They are placed in a metal incubator that is kept at 37°C. The caps of the reactors are made of silicone and allow for the insertion of needles that allow us to keep the culture sterile while inserting and removing medium and air. Air is pumped in via an adjustable pressure regulator (2). Air is used both to provide oxygen to the culture, as well as to stir it. In order to guarantee the air's sterility and partially saturate the air with water, it is pumped through a bottle filled with 1M KOH (2a). Additionally, it passes through two 0.22 μm filters (2b). To allow air to enter the reactor, there is also an air output: a small needle at the top of the reactor, whose tubing goes into a bottle of KOH (5) to prevent contact with the non-sterile environment.

The medium is stored separately for each bioreactor in a 250 mL bottle with a Duran 2-port connector cap (3a). One of the cap's connectors is used to pump out medium to the reactor. The other one is used to let air in to the bottle. It is connected to a small tube filled with KOH (3b) to prevent the entrance of non-sterile air. The pumps (3c) are calibrated before each experiment to determine the pump speed necessary for a certain dilution rate.

To ensure that input flow equals output flow, we insert a needle at the level of the liquid connected to a tubing that is inserted in a big pump (4a) and goes directly to waste (4b).

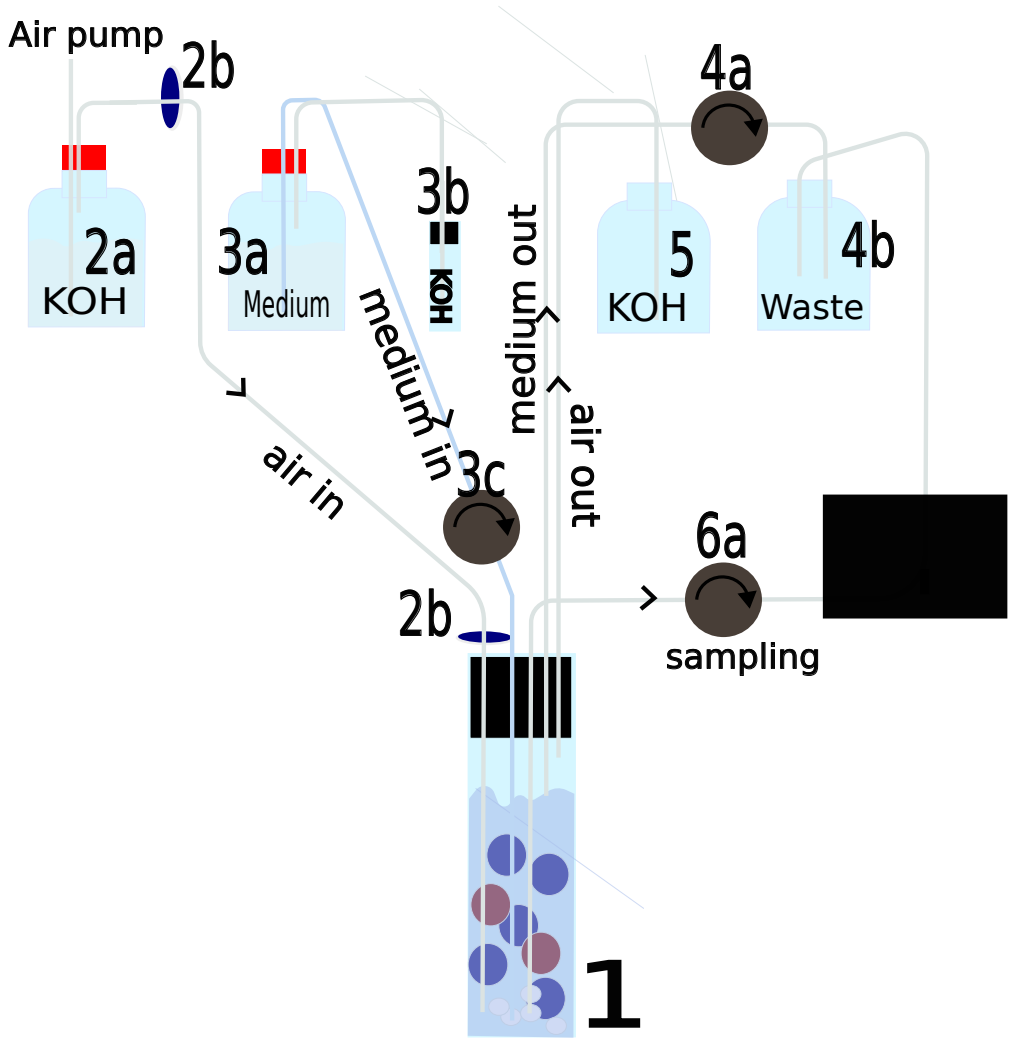

Figure 15: Schematic of the connection of one bioreactor. 1) Bioreactor 2a) KOH solution to sterilize the incoming air 2b) 0.22 μm filter to sterilize the incoming air 3a) Medium storage bottle 3b) KOH to sterilize entering the medium storage bottles 3c) Pump transporting medium to the bioreactors 4a) Pump removing culture from the bioreactors 4b) Waste container 5) KOH sterilizing the air leaving the bioreactors 6a) Pump transporting samples

.

In this way, culture medium is removed as soon as the liquid reaches the desired volume.

The samples are pumped (6a) to a selection valve (6b) that determines from which reactor the sample is drawn. From there, the sample goes to a measurement cuvette (6c) in which the absorbance and fluorescence are determined. A filter wheel (6d) is used to select the input and output wavelength for the fluorescence measurements. For each measurement, a sample of water (6e) is also taken, so that the absorbance can be calculated with respect to the blank. After the measurement, the sample is pumped to waste (4b).

2.2.3 Measurements of the culture and calibrations

Absorbance

For each absorbance measurement, three measurements are needed: the light intensity spectrum of water, the dark current of spectrometer, and the intensity spectrum of the sample. The value for the absorbance can then be calculated by taking the median intensity value of the measurements between 595 and 605 nm int and applying $abs_{sample} = \log_{10}((int_{water} - int_{dark})/(int_{sample} - int_{dark}))$.

Since we know that the measurement cuvette of the bioreactor has a path length of about 3 mm, its absorbance values will be different from that of a classic spectrophotometer with a path length of 1 cm. To check that the absorbance measurements taken by the platform are reliable and linearly related to absorbance measurements in OD600 as determined by a spectrometer, we diluted a dense culture of our WT several times and made a dilution-absorbance curve of the absorbance from both the bioreactor cuvette and the spectrometer, see Figure 16. We used a Ljung-Box test [96] to determine up to what absorbance value a line fit applied. Above this absorbance, the amount of cells does not scale linearly with absorbance. For the bioreactor, measurements were linear up to an absorbance of 0.55, whereas for the spectrometer the cut-off was determined to be at 2.3. The ratio of the slopes of the line fits was 3.6: i.e, for the same dilution, the spectrometer gave an absorbance that was 3.6 times higher than the absorbance in the bioreactor. Therefore, to convert bioreactor absorbance measurements below an absorbance of 0.55 to OD600, we have to multiply by 3.6.

Fluorescence

Since the species in our consortium contain fluorescent markers, we measure the fluorescence of the population to quantify the amount of the two species in our consortium. From the total amount of blue and red fluorescence, we can derive the abundances of the two species. For blue fluorescence measurements, we excite at 400 nm, with a bandwidth of 40 nm. Since the light that we use to excite is of much higher intensity than the light emitted by the fluorescent proteins, we could not observe the emitted light if the excitation light would end up in the sensors due to scattering. Therefore, to prevent that excitation light ends up in the emission spectrum, we use a highpass filter to filter out light below 450 nm from the emission spectrum. For red fluorescence measurements, the excitation wavelength is 580 nm, with a bandwidth of 40 nm. Light below 600 nm is filtered from the emission spectrum.

In order to determine whether variations in red fluorescence are due to variations in cell number or to variations in the measurement set-up, we developed a standard for red

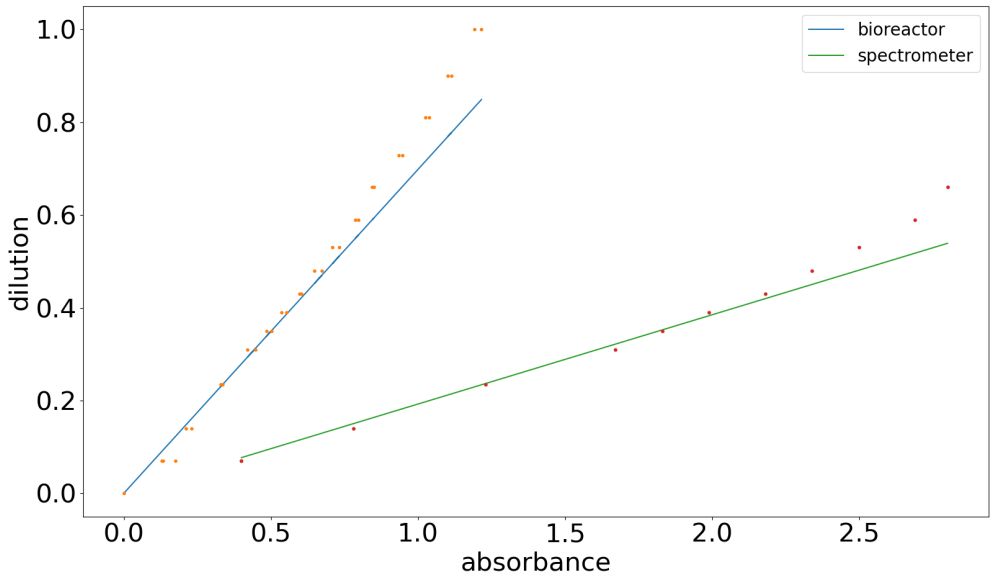

Figure 16: Dilution of the same cell sample in both the bioreactor cuvette and the spectrometer as a function of absorbance. The dots indicate the measurements, the lines indicate the line fit. We used a Ljung-Box test [96] to determine up to what absorbance the data could be considered to be linear.

.

fluorescence. We made a solution of Rhodamine B in ethanol of which we measure the spectrum before and after each experiment. The spectrum is shown in Figure 17. The figure shows 4 measurements before and 4 measurements after the experiment, using the two different emission filters. It can be observed that the fluorescence is stable at both wavelength ranges. We made aliquots of 2 mL of this rhodamine solution and stored them at -20 °C, so that we can determine the amount of variation in red fluorescence attributable to the experimental set-up before and after each experiment

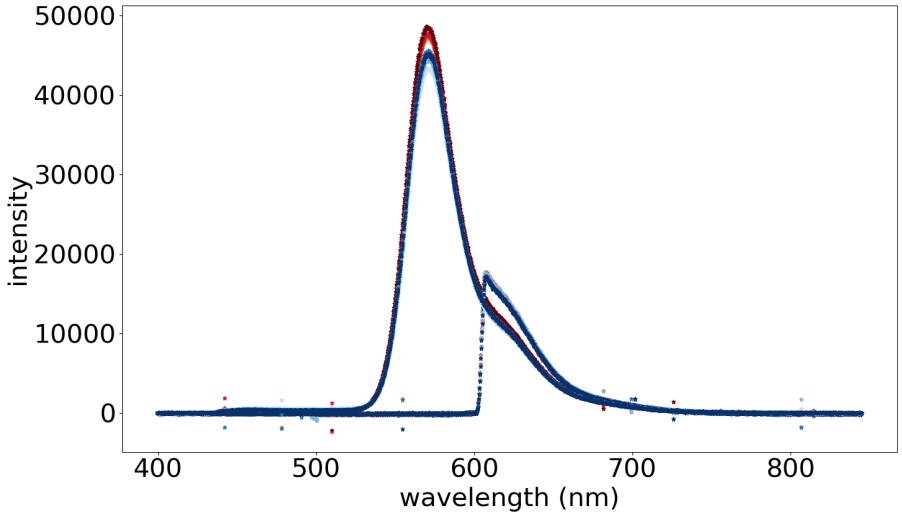

Figure 17: Spectrum of rhodamine B measured before and after a bioreactor experiment, excited at 400 nm (left spectra) and 580 nm (right spectra).

Flow cytometry

A second way to quantify the amount of the two species in our consortium is by using flow cytometry. With this method, we can distinguish individual cells that are expressing different fluorescent markers, based on the intensity of the different fluorescence wavelengths. This allows us to determine the relative species abundance in the consortium.

Figure 18 shows the result of such a measurement on five different samples containing WT cells and different amounts of the strain carrying the gene for the red fluorescent protein mScarlet-I on its chromosome. Here we plot the orange fluorescence at 620 nm against the forward scattering at 488 nm (FSC), the latter being a proxy for cell size [77]. Each dot represents a single measurement, and therefore shows the amount of FSC and Orange fluorescence of a single cell. To determine the fraction of each cell type in the mixture, the dots were clustered and colored based on k-means clustering (see Materials and Methods). This way, we can distinguish two clusters of cells: one that contains cells expressing a red fluorescent protein (red cloud; they have a higher Orange fluorescence intensity) and one with cells that do not express this protein (blue cloud). By counting the dots, we can therefore find out how much of each cell type is present in our consortium.

As shown in Figure 18, there are also some blue dots counted in the sample called M9, which contained only medium. Those cannot be distinguished from non-red cells: each blue cloud of a non-medium sample contains in fact two overlapping clouds: cells and undefined (dust) particles in the medium. To know how many of these dust particles are present in the sample and to correct for them, we decided to run an only-medium sample for each measurement, and to subtract the number of dust particles counted in this sample from the bacterial samples. The same volume of only-medium and bacterial samples was supplied to the flow cytometer, so it could be reasonably assumed that the number of dust particles in each sample was approximately the same.

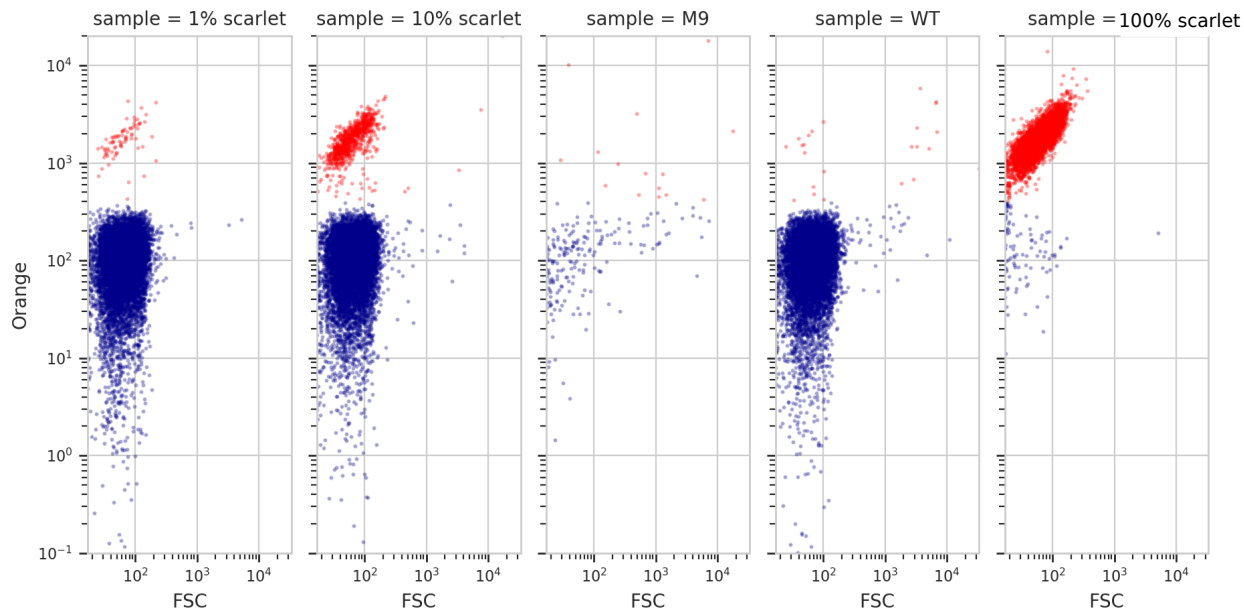

Figure 18: Scatter plots of five flow cytometry samples containing the WT and different amounts of the strain carrying the gene for the red fluorescent protein mScarlet-I on its chromosome. We plot orange fluorescence versus forward scattering.

.

To verify how well we can determine the amounts of cell types present in our consortium, we prepared samples with known amount of cells carrying the mScarlet-I gene. Then, we compared the amount of red cells counted by our flow cytometry procedure to the known amount. The result is shown in Figure 19. This figure shows that the fraction as calculated by our method turns out to be slightly larger than the expected fraction (the dots are a bit above the orange line with slope=1). However, we can conclude from this calibration that we can detect small amounts of red cells (around 1%) in a reasonably precise way. We therefore proceeded to use mScarlet-I protein as a marker for the acetate specialists in our consortium, and used flow cytometry to determine their relative amount.

To be able to take flow cytometry measurements during a bioreactor experiment, we automated the procedure. The set-up is shown in Figure 20. After determination of its absorbance and fluorescence, the bioreactor sample is taken to the mixing tube. There, it is diluted with buffer around a 1000 times in two steps. The sample is then pumped to the flow cytometer. After the flow cytometry measurement, which can be automatically launched with ODIN, the sample is pumped back to the mixing tube. The tube and tubing are cleaned with buffer and the contents are pumped to waste.

To verify that we can accurately determine the fraction of red cells in a mixture using this automated procedure, we compared the fraction of red cells measured by this automatic procedure to the known amount, as shown in Figure 21. In this figure, we also compare the fraction calculated using k-means clustering to the fraction calculated by setting a threshold at a fluorescence value at 700, as well as two replicate buffer samples measured used to determine the amount of dust in the buffer. From this calibration, the threshold method

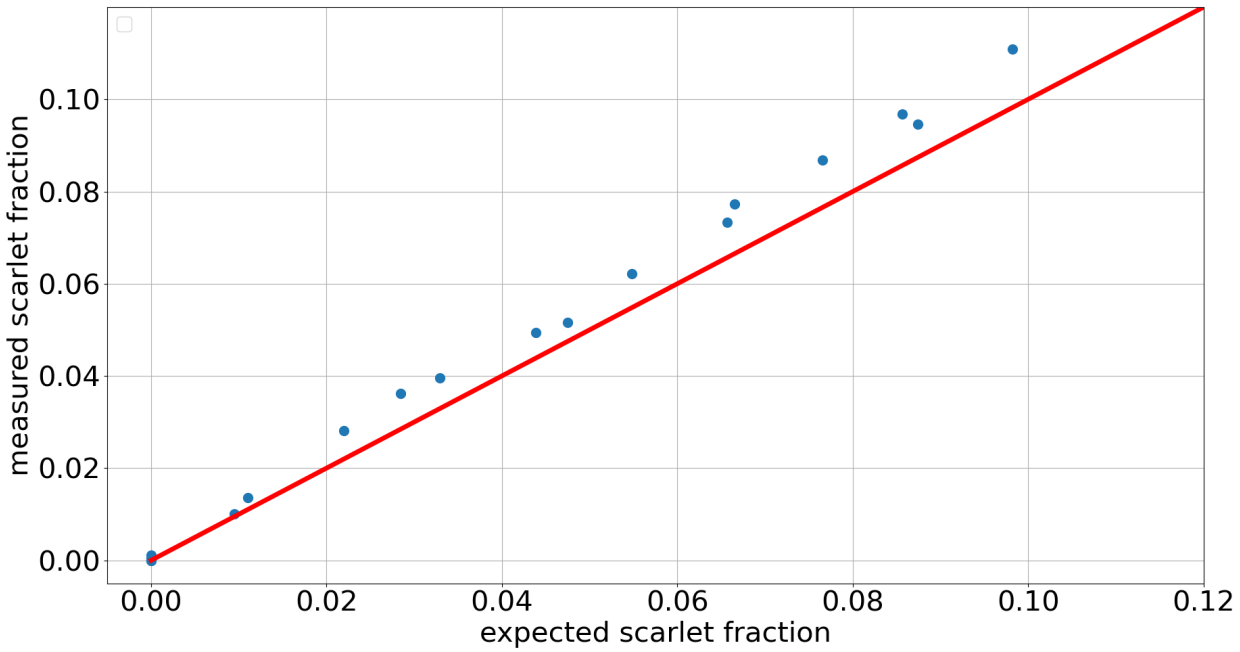

Figure 19: The fraction of red cells (mScarlet-I) counted as described above vs. the expected fraction of scarlet based on the volume of cells that we put in the sample. The red line indicates the line with slope=1

.

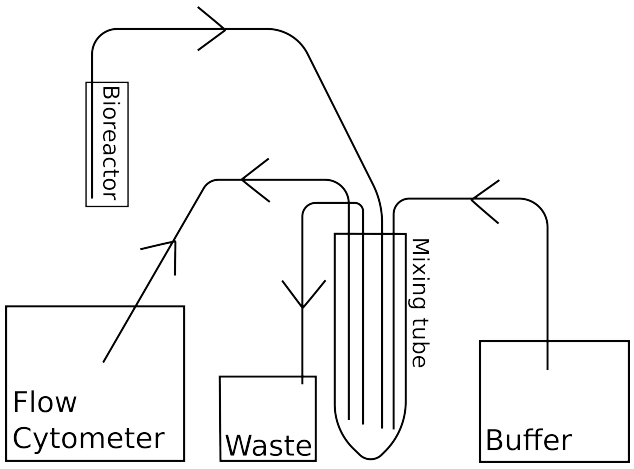

Figure 20: Schematic of the automatized set-up for flow cytometry measurements. After determination of its absorbance and fluorescence, the bioreactor sample is taken to the mixing tube. There, it is diluted with buffer. The sample is then pumped to the flow cytometer. After the flow cytometry measurement, the sample is pumped back to the mixing tube. The tube and tubing are cleaned with buffer and the contents are pumped to waste.

seems slightly more accurate than k-means clustering, independent of the buffer sample used. We conclude that with the automated procedure, we can detect small amounts of red cells in a reasonably precise way and that setting a threshold for red fluorescence is more accurate than k-means clustering. Therefore, we proceeded to use these automated measurements in combination with a red fluorescence threshold to determine the amount of red fluorescence cells in our consortium.

The biggest difficulty with automatized flow cytometry measurement remained however the sensitivity of the instrument to tiny particles (dust) other than cells present in the set-up. Even when the tubes were flushed carefully before and after each measurement, this did not always lead to satisfactory results. Therefore, for most of the experiments mentioned in this manuscript, the samples were taken manually and supplied to the cytometer by hand.

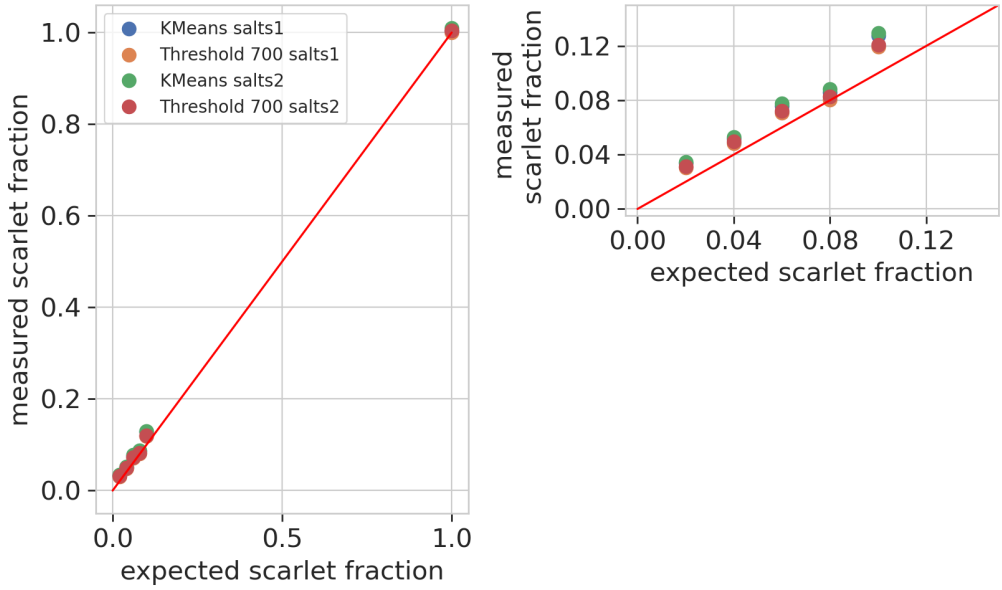

Figure 21: The fraction of red cells (mScarlet-I) counted as described above vs. the expected fraction of scarlet based on the volume of cells that we put in the sample. The red line indicates the line with slope=1. The different colors indicate two different buffer samples used to calculate the amount of dust and two different methods to calculate the fraction. We calculated the fraction calculated using k-means clustering to the fraction calculated by setting a fluorescence threshold of 700, and used two different buffer samples ('salts1' and 'salts2').

2.2.4 Achieving long-term stability in the chemostat

One of the goals of this PhD project was to observe the composition of the designed consortium in steady-state. However, it proved to be a challenge to reach steady-state (i.e. no change in the concentrations of cells and metabolite concentrations) and have the cells grow stably for extended periods of time. There might be biological reasons for an unstable culture, such as an overshoot [85] or changes in gene expression [97], but we also experienced some technical causes of culture collapse. Events that threatened the stability of culture

in our experiments were: contamination, clogging, viral infections, and a decreasing culture volume. In this section, we describe how we dealt with those problems during this PhD.

Sterility

Contamination of the culture is a problem because it could lead to an unknown microbe taking over the population, preventing us from investigating the culture that we are interested in. In order to prevent contamination during the experiments, we isolated the platform as much as possibly from the non-sterile environment. As describe in Section 2.2.1, air was always first filtered and passed through KOH before entering the reactor or the medium bottles. Medium was stored in well-sealed bottles and the reactors were only accessed by the needles going through the silicon septum but never opened during experiment. To clean the platform, 70% ethanol was run through all tubing before the experiment. All needles were replaced by new sterile ones at the start of each experiment.

Clogging

A major problem that prevented experiments from being biologically relevant, was clogging of tubing and needles. Clogging prevented air and medium from both entering and exiting the reactors, leading to spilling, emptying of the reactors, or a lack of oxygen and bubbling. To resolve this issue, we used tubing and needles that were as big as possible for the required task. The air input needles that we used at first had a diameter of 0.60 mm; They clogged during multiple experiments. Replacing them by needles with a diameter of 0.80 mm fixed the issue. For the medium input reservoir, we were using a 25.4 cm long needle with an inner diameter of 0.51 mm inserted in a bottle with a silicone cap. Since this long thin needle tended to clog, probably due to precipitation of some of the salts present in the medium, we replaced it by a 2-port connector cap connected to 3 mm wide tubing. Needles were also avoided in the medium and air output; the air output tubing was inserted directly in a 1M solution of KOH, whereas the medium output was hanging in an open waste bottle whose contents were sterilized by means of bleach. All in all, by using needles with a maximal diameter and by replacing needles by tubing where possible, we were able to mostly eliminate clogging events during our chemostat experiments.

Phage infections

Before growing the community in chemostat on the platform, we first tried to grow the glucose specialist individually and encountered troubles in growing these cells for more than 10 hours. The cells would grow nicely, but after some time, the culture would collapse: the density of the cells would rapidly go down, see Figure 22.

We hypothesized that this instability was the result of a phage (a virus that infects bacteria) infection in the culture. Therefore, we attempted to solve the problem by keeping the platform as clean as possible. When this did not result in a more stable culture, however, we tried to grow a strain in which the gene coding for the protein FhuA had been knocked out. FhuA is a transport protein that can serve as a receptor for phages [98] and that our lab had previously knocked out to protect against them. Figure 23 shows the result of an experiment in which we grew the wild-type (WT) and an *fhuA* knock-out strain already

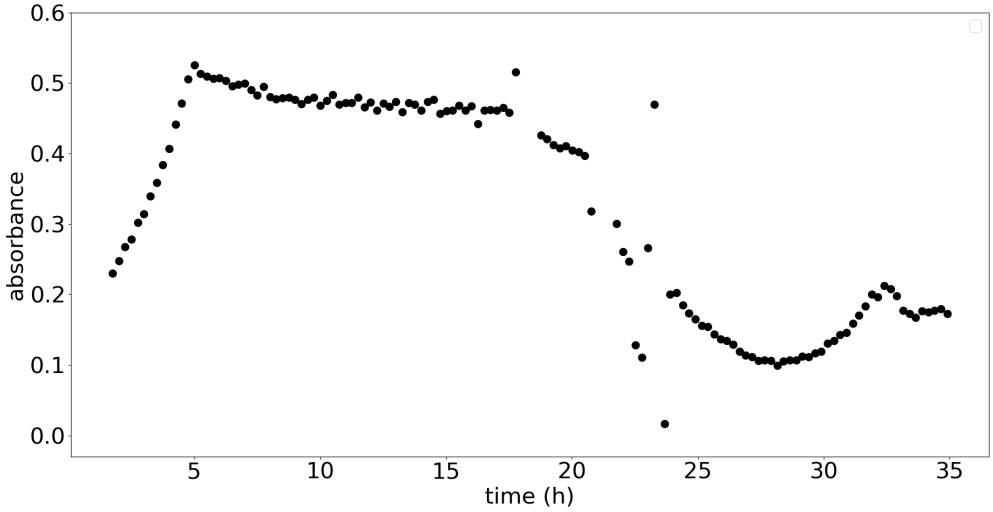

Figure 22: Absorbance dynamics for the glucose specialist in chemostat. The culture is in steady-state (no change in absorbance) from 7 to 17 hours. After this, the absorbance decreases, probably because of a phage infection.

present in the lab in two different bioreactors. It is clear that the knock-out performed much better: we managed to keep it in steady-state for about 19 hours. This experiment therefore indicated that knocking out *fhuA* in our strain could protect against a phage infection and result in a more stable culture in the bioreactor. We proceeded to do this knock-out in our already constructed strains. Indeed, in the experiments that were performed subsequently, we no longer encountered phage infection events.

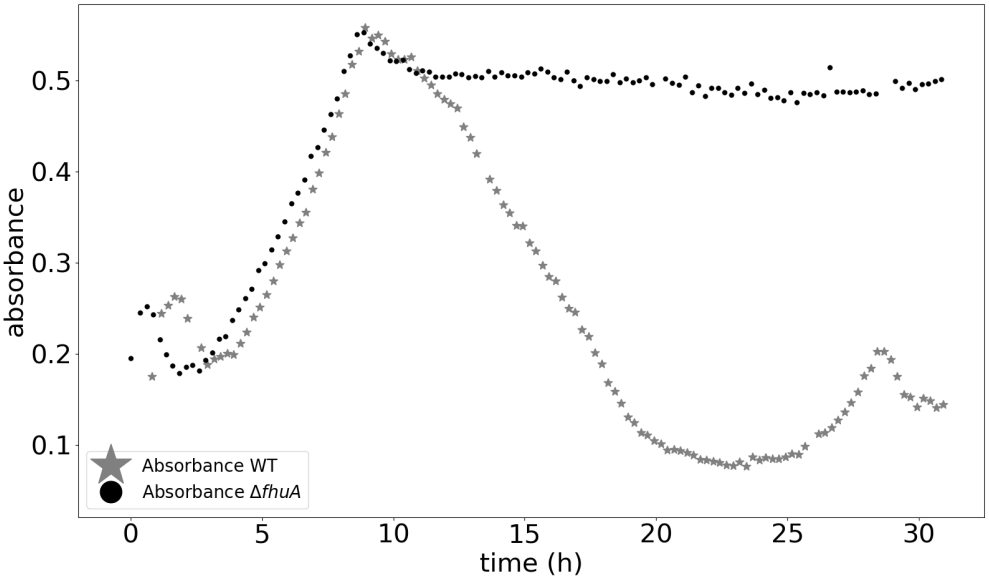

Figure 23: Absorbance dynamics for the WT and the *FhuA* knock-out in chemostat. The *FhuA* knock-out is in steady-state from 11 to 30 hours, whereas the WT culture collapses immediately after having reached steady-state.

Keeping a constant volume

As described in the introduction, the dilution rate in a chemostat is equal to the flow rate in and out of the reactor divided by the reactor volume. As a result, in order to run an experiment with a certain stable dilution rate, we need to be sure that the reactor volume is approximately stable. A change of reactor volume would change the dilution rate, which would mean that we are running our experiment at a different dilution rate than intended. To keep the volume constant, we need first of all to take care not to take too many measurements. A measurement sample V_{sample} has a volume of about 350 μL. The volume of medium coming into the reactor is equal to the dilution rate (D) times the reactor volume ($V_{reactor}$). The maximum number of samples taken per hour (S) is given by Equation (15).

$$S = \frac{DV_{reactor}}{V_{sample}} \tag{15}$$

For a dilution rate of 0.15 h^{-1}, this would mean $S = 0.15 * 15/0.35 = 6$. In practice, the amount of samples that we can take is much less, due to evaporation of the culture and overflow due to bubbling. For a dilution rate of 0.15 h^{-1}, we take a sample every 1 hour and 15 minutes.

A second factor that can lead to a reduction in culture volume is excess bubbling. Whereas bubbling is needed to stir the culture and to provide it with oxygen, too much of it can lead the bubbles to reach the output needle even if the culture volume is below the desired volume, leading to a slow but steady reduction of the culture volume. In our experiments we therefore take care that there are enough bubbles to stir the culture but not enough for culture spilling.

The last factor of importance for the stability of the culture volume is the height of the

output needle. If this height changes, the culture volume does as well. Initially, we were using 80mm long needles for the output that we would insert to be at the right height. However, they tended to move down into the reactor during the experiment, leading to a reduction in culture volume. Therefore, we started using shorter 40 mm needles that we insert all the way into the reactor, so that they are unlikely to change height, keeping the culture level stable.

2.2.5 A typical experiment

A typical bioreactor experiment follows the following protocol. More details are given in the Materials and Methods.

- Preparation:
  - Make precultures in the desired carbon source
  - Measure the absorbance and fluorescence of a fluorescence standard
  - Clean the reactor
  - Set up all the connections, the inflow bottles, and the waste bottles
  - Determine the pump speed for the desired dilution rate
  - Set-up an ODIN campaign with the desired algorithms
- Starting the experiment:
  - Dilute the precultures in the desired amount in the reactors
  - Insert needles in the reactors
  - Start influx and outflux pumps and algorithms in the campaign
- During the experiment:
  - Take manual samples to measure extracellular metabolite concentration
  - Take manual samples for flow cytometry measurements
- Stopping/cleaning up the experiment:
  - Turn off algorithms
  - Recalibrate the pumps, to see if the dilution rate has changed
  - Clean the reactor
  - Turn of pumps and disconnect all the tubing

2.3 Experimental characterization of the individual strains

In Section 2.1, we showed how we constructed an acetate and a glucose specialist. We aimed to study a consortium consisting of these two constructed strains. We asked whether the community would display any emergent properties, i.e. does it display characteristics that could not be predicted from the features of the individual strains? In order to answer this question, we first experimentally characterized our individual strains. In Section 2.3.1 we compare the growth rate of the glucose specialist and the acetate specialist during batch growth on glucose. We show that the glucose specialist grows faster than the acetate specialist and that the glucose specialist excretes acetate in these conditions. Then, we compare the growth rate of the glucose specialist and the acetate specialist in batch on acetate and show that the acetate specialist grows faster. In Section 2.3.2 we look at the growth of the glucose specialist in a chemostat and show that it excretes acetate in this set-up as well.

2.3.1 Batch growth

As described in the Introduction, batch experiments are an appropriate means to characterize the growth of microbes: one starts with a certain amount of carbon source and a small amount of cells. Then, the (exponential) growth of the cells on the carbon source is monitored. In our lab, we did these experiments using a plate reader with a 96-well plate. This way, we could test different conditions in parallel in the same plate, as well as multiple technical replicas.

Batch growth on glucose

In order to understand the properties of our strains when they are cultured on glucose, and to verify that they are good candidates to be grown together in a cross-feeding consortium, we grew them individually in a plate reader starting with 1 g/L of glucose. We tried different glucose concentrations and found that at glucose concentrations higher than 1 g/L, the biomass yield was suboptimal, indicating that growth was no longer glucose-limited, but likely oxygen-limited due to impaired stirring at high cell densities (see supplementary Figure S1). Therefore, we decided to execute all experiments with a starting concentration of 1 g/L of glucose.

Figure 24 shows the growth curves of both strains grown individually in 1 g/L of glucose. We observe that the glucose specialist (WT) grows faster than the *ptsG* knock-out on glucose. The growth rates of the strains were respectively 0.60h^{-1} and 0.25h^{-1} as calculated by a line fit through the exponential part of the curve. The full acetate specialist ($\Delta ptsG$ and added Pta-AckA plasmid) had the same decreased growth rate as the *ptsG* knock-out. During the experiment, we took manual samples to determine the metabolite concentration in the medium: the lower panel in Figure 24 shows the excretion and uptake of acetate by the glucose specialist (WT). As expected from the literature on overflow metabolism [51–53], the glucose specialist excretes acetate during exponential growth on glucose. After having finished taking up glucose, it is able to continue growth on acetate. This makes it a good candidate for our cross-feeding consortium, since acetate will be available for the acetate specialist to grow on. The acetate specialist indeed grows slower on glucose than the glucose specialist after the knock-out of *ptsG* which makes it a suitable acetate specialist: it will not

exert a strong competition on the glucose specialist for glucose, but it will be able to grow at intermediate dilution rates.

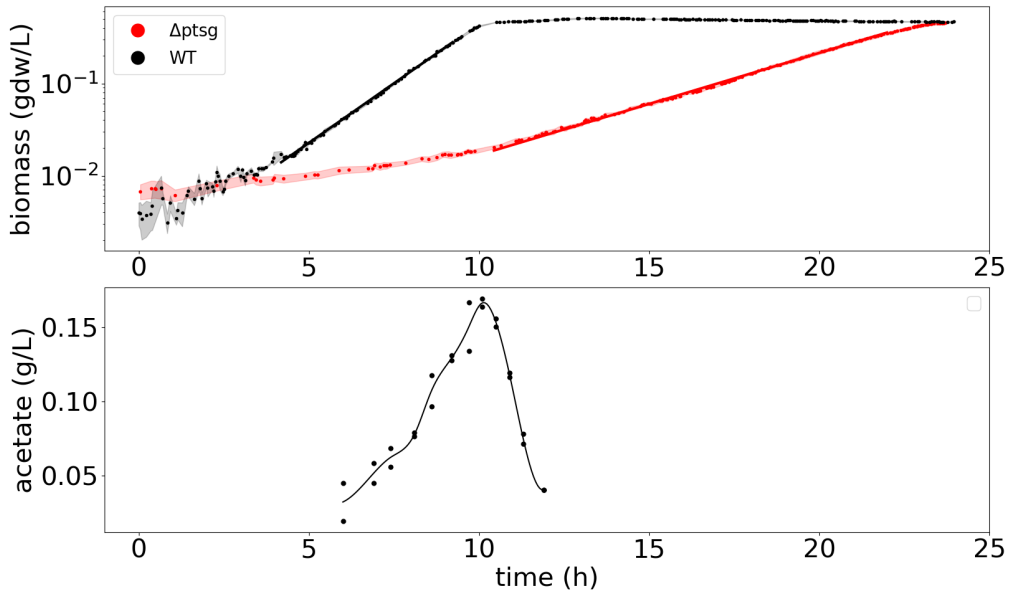

Figure 24: Upper panel: Biomass accumulation of the glucose specialist (WT) and the *ptsG* knock-out grown individually in batch on 1 g/L of glucose. The dots indicate the mean of 6 technical replicas. The shaded area marks the SEM. The lines represent a line fit through the linear part of the growth curve. Lower panel: Acetate excretion and uptake by the glucose specialist in the same experiment as the upper panel. The dots indicate individual data points of two technical replicas. The line shows the mean.

Batch growth on acetate

In order to measure the growth rate of our glucose specialist strain when cultured on acetate, and to assess the effectiveness of the plasmids constructed for the overexpression of *acs* and *pta-ackA*, we grew the glucose specialist as well as the constructed strains in a plate reader starting with 0.72 g/L acetate. Since the overexpressed genes had an IPTG inducible promoter, we grew the strains both with and without IPTG, expecting that the addition of IPTG would lead to faster growth on acetate. Figure 25 shows that the growth rate of the glucose specialist (WT) on acetate is 0.13 h^{-1}, and adding the plasmid expressing *acs* does not increase the growth rate, unless IPTG is added. The plasmid expressing *pta-ackA*, however, increases the growth rate on acetate both with and without IPTG. This could be due to a leaky promoter, so that even in the absence of IPTG, the genes are sufficiently overexpressed to increase the growth rate on acetate.

All together, these results show that the addition of the Acs or Pta-AckA plasmid increases the growth rate of our acetate specialist on acetate, allowing it to grow on the acetate excreted by glucose specialist. If we want to control the amount of (or 'turn on/off') acetate uptake, the Acs plasmid is useful since it has a bigger dynamic range: there is a bigger difference in acetate uptake rate between the off (without IPTG) and the on (with IPTG)

state. The Pta-AckA plasmid, on the other hand, cannot really be turned on and off, since the acetate uptake rate is similar with and without IPTG. If there is no need for control the Pta-AckA plasmid is a good candidate to be used. Since it is effective even without its inducer, we can use this plasmid to obtain an acetate specialist that grows faster than the glucose specialist without the expensive addition of IPTG.

To confirm that the plasmids can increase the growth rate of the *ptsG* knock-out (and not just the WT) on acetate, we also tested the *ptsG* knock-out with added Pta-AckA (without IPTG) and showed that its growth rate was the same as the WT with added Pta-Acka, see Figure 26.

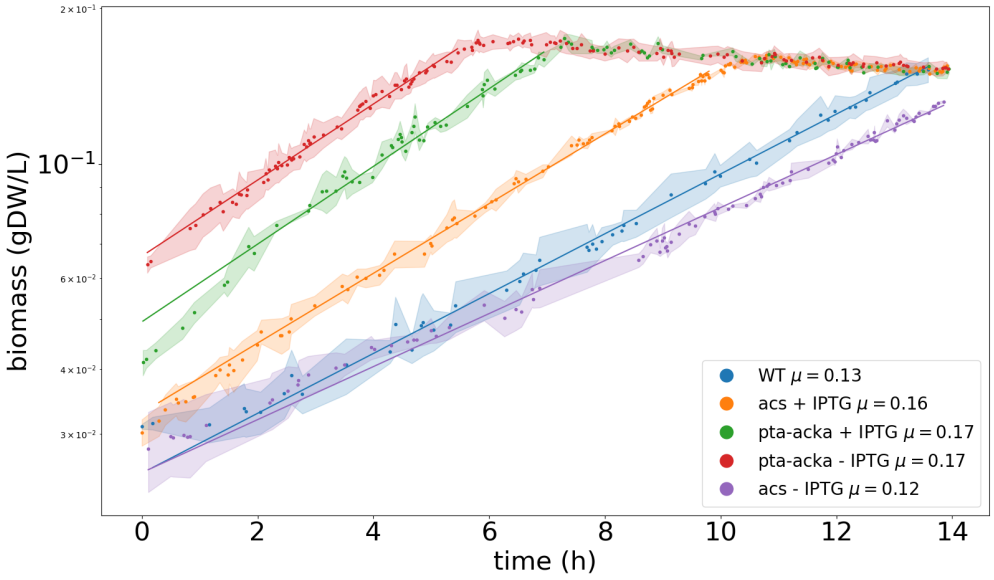

Figure 25: Biomass accumulation of three different strains with and without IPTG during batch growth on 0.72 g/L of acetate. Growth rates (in h^{-1}) are mentioned in the legend, as calculated by the slope of the straight lines. The dots indicate the mean of 6 technical replicas. The shaded area marks the SEM.

2.3.2 Chemostat growth

In the previous section we have shown that our strains seem to have the characteristics necessary to coexist during growth on glucose: the glucose specialist excretes acetate during growth on glucose and we have constructed an acetate specialist that is impaired during growth on glucose but that has an increased growth rate on acetate. In theory, therefore, there could be cross-feeding of acetate between the glucose specialist and the acetate specialist. In practice, the goal of this project is to grow the two strains in a chemostat, and have them coexist in steady-state. To assess whether this might be possible with the constructed strains, we first grew the glucose specialist individually in a chemostat, in our automated mini-bioreactor platform, and measured the extracellular concentration of glucose and acetate manually (see Section 4.8 for the technical details).

Figure 27 shows the results of a chemostat experiment where we grew the glucose specialist at an intermediate dilution rate for about 45 hours and then attempted to flush it out at a

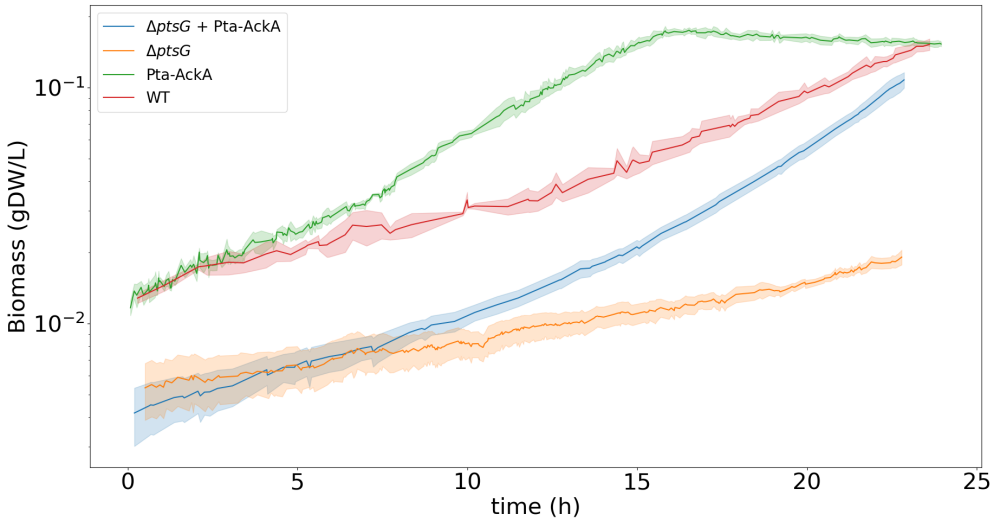

Figure 26: Biomass accumulation of four different strains without IPTG during batch growth on 0.72 g/L of acetate. By the steepness of the lines, it can be observed that the *ptsG* knock-out have the same growth rate. Likewise, the WT with added Pta-AckA has the same increased growth rate as the knock-out with added Pta-AckA. The lines indicate the mean of 6 technical replicas. The shaded area marks the SEM.

high dilution rate. It can be observed that the glucose concentration decreases rapidly at the start of the experiment (first 3 hours), and eventually reaches a low residual concentration (15 hours). Upon flush-out of the cultures, the glucose concentration initially increasing (45 hours), before decreasing. The increase is expected as the culture is flushed out, since fewer cells are present to take up the glucose entering the bioreactor. It seems that the cells are not completely flushed out, but reach a new steady-state with a new steady concentration of acetate and glucose (49 hours).

The acetate concentration initially increases (first 3 hours), which is in accordance with the results from the batch experiment (Section 2.3.1): the cells excrete acetate during exponential growth on glucose. The acetate concentration then also reaches a residual concentration (15 hours) which is low but seems slightly higher than the glucose concentration. However, when we compare the measured residual acetate concentration to a negative control with known zero acetate concentration, we cannot distinguish them, see Figure S2. Therefore, even though we can observe acetate being excreted in the initial growth phase, we cannot be sure of the presence of acetate in steady-state. In conclusion, from growing the glucose specialist in a continuous culture on glucose, we can show that acetate excretion happens, but we cannot confirm with certainty that there is enough acetate in steady-state for the acetate specialist to grow on. We can only find this out by growing the two strains together, as described in Section 2.5.

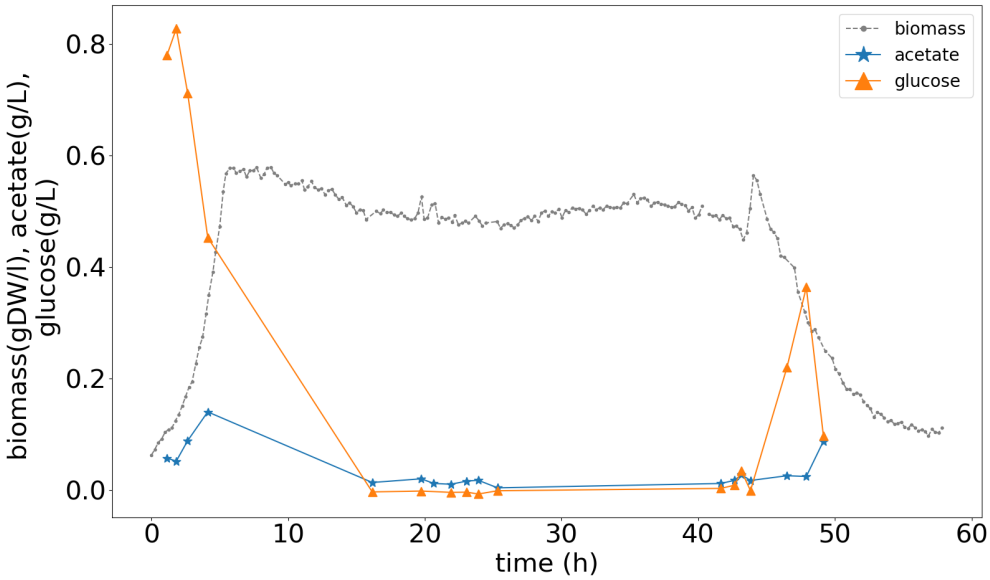

Figure 27: Dynamics of glucose, acetate and biomass in the bioreactor during growth in a chemostat on 1 g/L glucose. The glucose specialist was grown at D=0.3h^{-1}, and then flushed out at D=0.6h^{-1}

2.4 Fitting the model to the individual strains

Now that we have characterized the individual strains qualitatively and shown that they are good candidates for a cross-feeding interaction, we can investigate their properties more quantitatively. For a start, we are interested to see if we can fit the model suggested by our group [24] (see Section 1.4) to the data of the individual strains. A schematic of this model is shown in Figure 7.

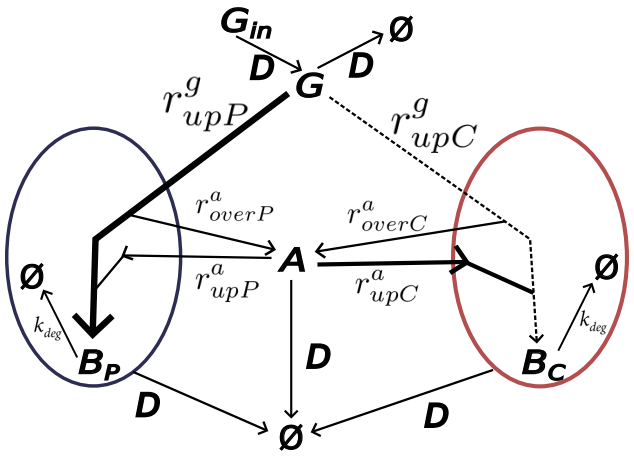

Figure 7: A schematic of the model in [24] of glucose and acetate metabolism for a glucose specialist (subscript $_P$) and an acetate specialist (subscript $_C$). During glucose-fueled growth, glucose (G) is taken up and transformed into biomass (B) through r^g_{up}. In the case of overflow metabolism, the glucose can be excreted as acetate (A) through r^a_{over}. Acetate can be taken up from the medium through r^a_{up}. In a chemostat, G is supplied from the inflow (G_{in}) with the dilution rate D. Both the cells and the medium are flushed with D. Biomass is degraded for maintenance metabolism through k_{deg}. For clarity of the figure, the negative impact of acetate inhibition and carbon catabolite repression are not indicated here. (repeated from page 23)

The parameter values in the model were originally estimated using literature data obtained from the *E.coli* wild-type strain MG1655, grown in batch in minimal medium with different concentrations of glucose and acetate [56]. For our experiments, we use the BW25113 strain (see Materials and Methods), which has different growth dynamics. Since we would like to compare our experiments to the model, we want to adapt the model to the strain we use, and change parameters accordingly. Therefore, we refitted the model to the data as described in this section. First, we fit the model to batch growth on glucose: we fit the growth of the glucose specialist in Section 2.4.1. We fit the growth of the acetate specialist in Section 2.4.2. Then, we fit the growth of the glucose and acetate specialist on acetate (Section 2.4.3)

2.4.1 Glucose specialist on glucose

In this section, we first fit the model to the biomass data to match the growth rate of our strain. Then, we fit the model to biomass data and extracellular acetate concentrations to correctly parameterize our strain's diauxic growth.

First of all, we noticed that the growth rate of BW251133 was higher than that of MG1655. To increase the growth rate on glucose of our strains in the model, we can increase either Y_g or k_g (via simulation, the sensitivity of the growth rate to K_g was found to be negligible over a range of realistic values), see Equation (6):

$$r^g_{upP} = k_g \frac{G}{G + K_g} \frac{\theta^n_a}{A^n + \theta^n_a}, \qquad \text{(6 revisited)}$$

To find new values for these parameters, we fit the growth curves of the WT to the growth curves produced by the model (in batch mode: D=0) while allowing Y_g and k_g, as well as the unknown initial biomass concentration y_0, to vary freely. Using python package lmfit [99], we minimized Equation (16):

$$\sum_i^N [y_i^{meas} - y_i^{model}(v)]^2 \qquad (16)$$

where y_i^{meas} is the biomass data as measured in the experiment, y_i^{model} is the biomass calculated by the model, using the set of variables v=(Y_g, k_g, y_0).

It was found that $Y_g = 0.52$, $k_g = 1.58$, see Table 4. The previous values were respectively 0.44 and 1.53. We therefore conclude that our model fits the data best when we increase the glucose yield as compared to the previous version, but leave the maximal glucose uptake rate approximately the same. One might ask about the identifiability of these two parameters. Could we change k_g instead of Y_g for the same result? We investigated this question and found that Y_g determines the biomass plateau of the growth curve: the parameter dictates how much biomass can be made from the initial amount of carbon source. Therefore, increasing the value of k_g instead of Y_g would lead to a similar growth rate but an incorrectly estimated biomass plateau.

Fitting the biomass and the measured acetate concentrations

As explained in the Introduction, our strain shows diauxic growth when grown in glucose in batch; it grows at two different rates before it stops growing. This is because the strain first grows on glucose and when this resource is exhausted, it continues growth on acetate. In the model this diauxie is reflected by the second part of Equation (**??**).

$$r^a_{upP} = k_a \frac{A}{A + K_a} \frac{\theta^m_g}{r^g_{upP} + \theta^m_g} \qquad \text{(10 revisited)}$$

The term $\theta_g/(r^g_{up}(G, A) + \theta_g)$ in Equation (10) models the carbon catabolite repression: the larger the glucose uptake rate (r^g_{up}) of the cells, the smaller the acetate uptake rate (r^a_{up}). The extent of the diauxie is determined by the value of θ_g: the smaller the value of θ_g with respect to r^g_{up}, the lower the concentration of glucose in the medium has to be before the

strain starts taking up acetate, the clearer the separation between the two growth phases: in a model assuming a low θ_g, the cells first have to take up all the glucose before they can start taking up the excreted acetate. This leads to a biomass curve with a sharp transition between the two growth phases. In a model assuming a high θ_g, on the other hand, the cells can start taking up the excreted acetate while they are also still growing on glucose. This leads to a smooth biomass curve. In our data, it is clear that there is a sharp separation between the first growth phase on glucose and the second growth phase on acetate (red region in Figure 28). To let our model reflect the shape of the growth curve present in our data, we therefore suspected that the value of θ_g would have to be lowered.

So far, we have only talked about the biomass data. To have a better idea of the accuracy of our model, we measured a second variable: the acetate concentration in the medium. The result is shown Figure 28 (brown dots). As expected, the glucose specialist excretes acetate during growth on glucose and takes it up in a second growth phase. This was already the case with the parameters from [24] but to reflect the exact shape of the acetate profile with the model (brown line Figure 28), we had to change the parameters l and k_{over}, two parameters in the equation for acetate overflow:

$$r^a_{overP} = k_{over}\max(0, r^g_{upP} - l), \qquad \text{(8 revisited)}$$

where l represents the threshold glucose uptake rate at which overflow takes place and k_{over} is a constant determining the rate of overflow. To better reflect the diauxie as observed in the data, we fitted the biomass and acetate concentration to those predicted by the model while allowing θ_g, l and k_{over}, as well as the unknown initial biomass concentration, to vary freely. Using python package lmfit [99], we minimized an equation analogous to Equation (16), comprising a term for biomass plus a term for acetate concentration. Figure 28 shows the result of the biomass as well the acetate fit. See Table 4 for the new parameter values.

2.4.2 Acetate specialist on glucose

To make sure that most of the glucose is available for the glucose specialist when growing the consortium, we diminished the acetate specialist's glucose uptake by knocking out the main glucose uptake system (see Section 2.1). Figure 29 shows that the growth rate is now much lower than that of the glucose specialist. This is because of a lower maximum glucose uptake rate, which we will denote $k_{\Delta PTS}$. The value of $k_{\Delta PTS}$ was determined by fitting the model to the data, leaving $k_{\Delta PTS}$ and the initial biomass concentration free, see Table 4.

2.4.3 Glucose specialist and acetate specialist on acetate

To allow the acetate specialist to coexist with the glucose specialist, we had to enhance the former's acetate uptake rate. We put two acetate uptake systems on a plasmid (see Strain constructions) and saw that the Pta-AckA pathway enhanced acetate uptake most (see Section 2.3.1). In our model, an enhancement of acetate uptake is modeled by Equation (17) (same as Equation (11) but we use $_{Pta}$ instead of $_{Acs}$ as a subscript).

$$r^a_{upC} = k_a \frac{A}{A + K_a} \frac{\theta_g}{r^g_{up} + \theta_g} + k_{Pta} \frac{A}{A + K_{Pta}} \qquad (17)$$

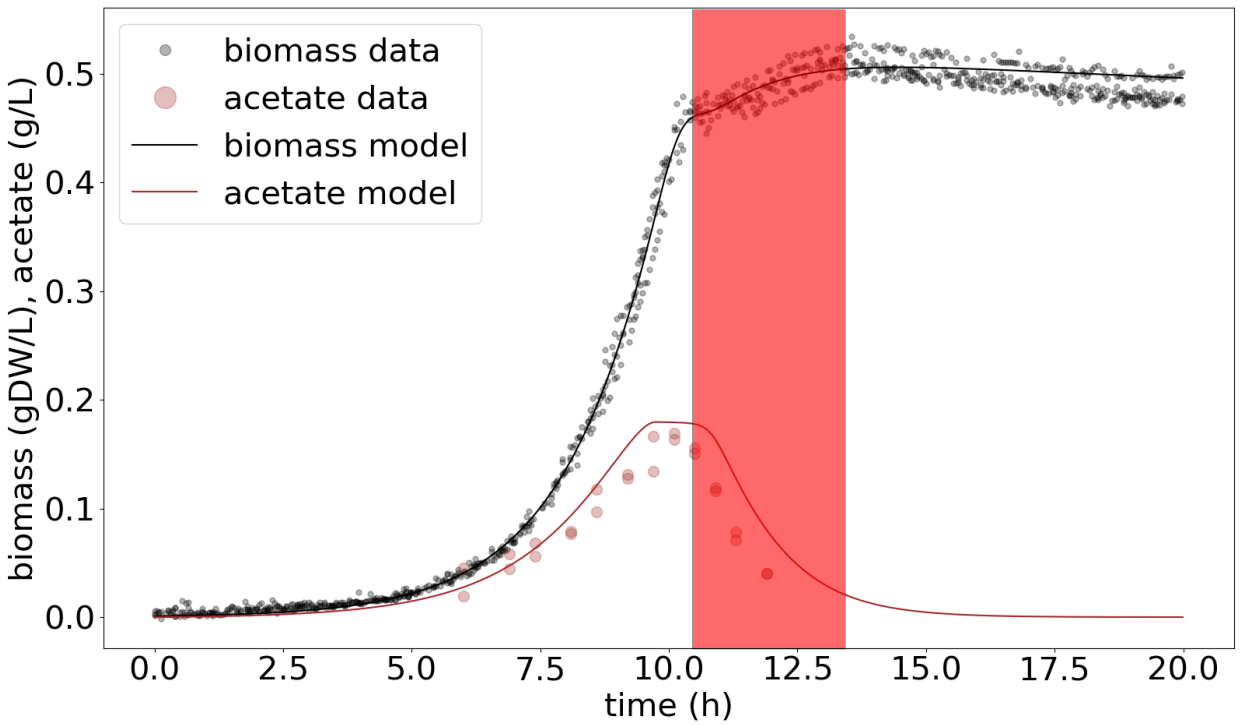

Figure 28: Acetate and absorbance data and model dynamics for the glucose specialist growing in batch on glucose. The region marked in red marks growth on acetate. The model parameters were taken from [24] except those described in the text and given in Table 4.

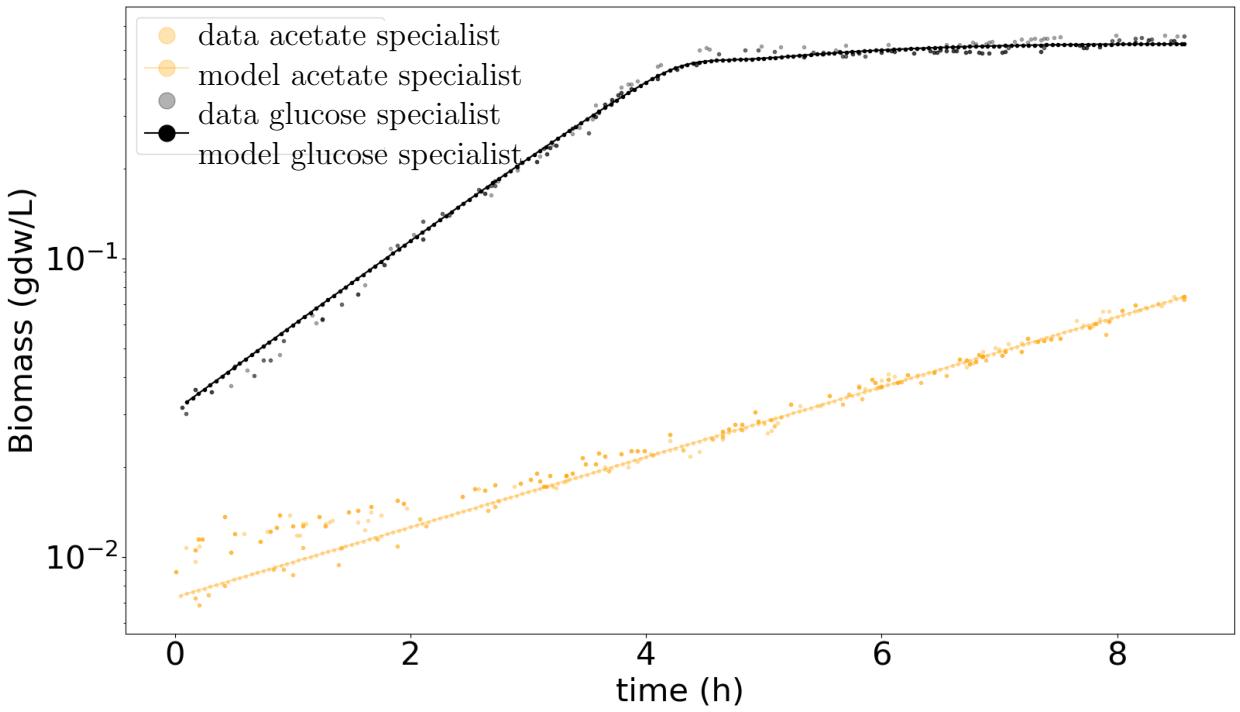

Figure 29: Absorbance data and model dynamics for the glucose specialist and the acetate specialist growing in batch culture on 1 g/L glucose

It is considered that the acetate specialist has the same acetate uptake rate as the glucose specialist (see Equation (10)), plus an additional term describing the enhanced uptake. The overexpression appears as a separate term summed with the first, because it is not considered subject to carbon catabolite repression, so it is not multiplied by the term $\theta_g/(r^g_{up} + \theta_g)$. To obtain a model for the acetate specialist growing on acetate, we left k_a, k_{Pta} and the initial biomass concentration free and minimized the residual between the model and the data (Equation (16) with $v = (k_a, k_{Pta}, y_0)$). Figure 30 shows that we can fit the individual growth of the acetate specialist and the glucose specialist on acetate with the model, using the parameters shown in Table 4.

Table 4: Values of the model parameters that are different from the parameters in [24]. *Growth on acetate only **Growth on a mix of glucose and acetate (diauxic growth)

Parameter	**Value**	**Value in [24]**	**Units**	Meaning
Y_g	0.52	0.44	$\mathrm{gDW\,g^{-1}}$	biomass yield for growth on glucose
k_g	1.58	1.53	$\mathrm{g\,gDW^{-1}\,L^{-1}}$	maximal glucose uptake rate of the glucose specialist
θ_g	8×10^{-3}	0.35	$\mathrm{g\,gDW^{-1}\,h^{-1}}$	inhibition constant of acetate uptake
l	1.0	0.7	$\mathrm{g\,gDW^{-1}\,h^{-1}}$	threshold for acetate excretion
k_{over}	1.0	0.17	NA	proportionality constant for acetate excretion
$k_{\Delta PTS}$	0.51	0.38	$\mathrm{g\,gDW^{-1}\,h^{-1}}$	maximal glucose uptake rate of the acetate specialist
k_a*	0.63*/0.97**	0.97	$\mathrm{g\,gDW^{-1}\,h^{-1}}$	maximal acetate uptake rate
k_{Pta}	0.42	1.46	$\mathrm{g\,gDW^{-1}\,h^{-1}}$	maximal acetate uptake rate of Pta-AckA
θ_a	3.5	0.52	$\mathrm{g\,L^{-1}}$	inhibition constant of acetate on the glucose uptake rate

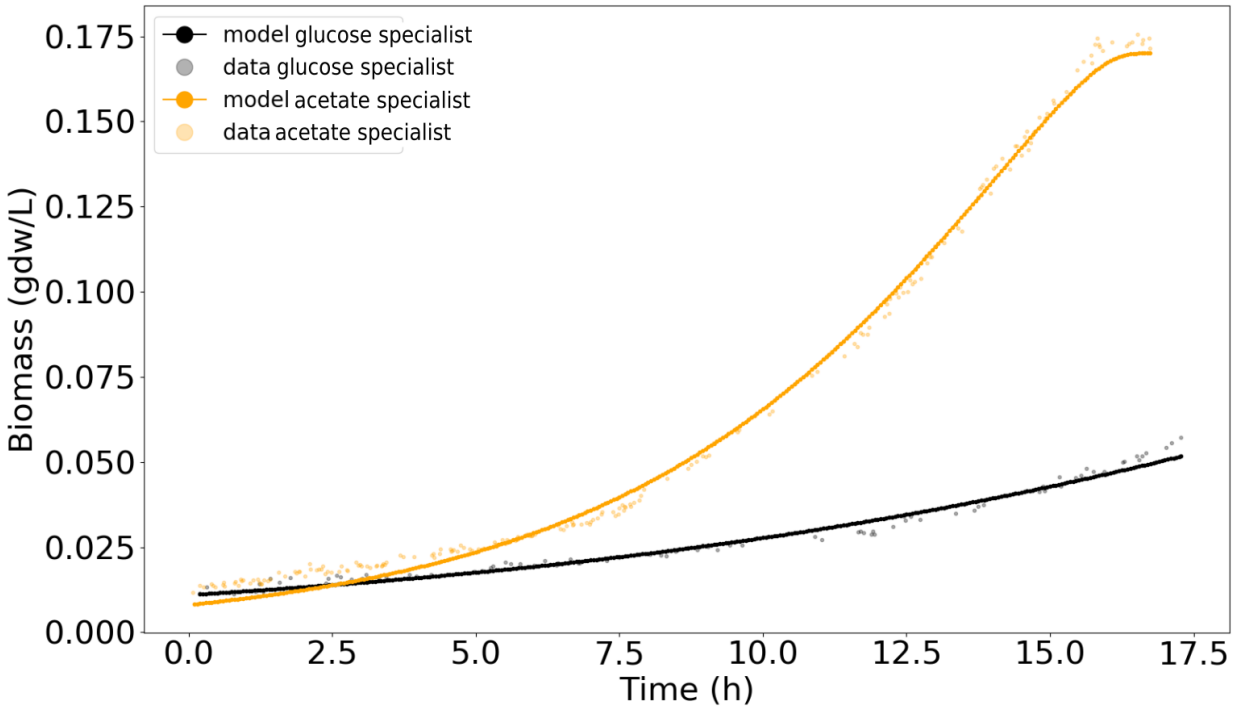

Figure 30: Absorbance data and model dynamics for the glucose specialist and the acetate specialist growing on 0.56 g/L acetate

2.5 Looking for coexistence

After we characterized our individual strains experimentally (Section 2.3) and adapted the parameters in our mathematical model to match the growth dynamics of our individual strains (Section 2.4), we can now start looking at the potential for coexistence of the two glucose specialist and the acetate specialist. First, we will show that cross-feeding likely happens in a batch co-culture (Section 2.5.1). Secondly, we look at our model as parameterized in Section 2.4 and show that coexistence in the chemostat is unlikely to happen considering our current model assumptions (Section 2.5.2). Then, we will experimentally investigate the community in a chemostat (Section 2.5.3).

2.5.1 Experimental characterization of the community in batch

In Section 2.3 we showed that the individual strains constructed for this PhD have the potential to cross-feed; the glucose specialist excretes acetate during growth on glucose and the acetate specialist is impaired during growth on glucose but grows faster on acetate. Eventually, we will grow both strains as a consortium in a continuous culture. First, however, we tested the consortium in batch culture, to see if we could demonstrate cross-feeding in this set-up. We added small amounts of both strains to an initial amount of medium with glucose. We expected the glucose specialist to grow much better in these conditions than the acetate specialist. In addition, it should excrete acetate that could be taken up by the acetate specialist.

Unlike in continuous culture (that runs as long as one keeps supplying medium) a batch experiment ends when the carbon source initially present in the reactor runs out. Therefore, the initial conditions are crucial in this kind of experiment; the way the two species grow is dependent on their initial concentration. Keeping this dependence in mind, we tested the consortium with two different initial conditions. In one experiment, we started with a relatively high amount of acetate specialist and a much lower amount of glucose specialist. The reasoning behind this was that we wanted to give the acetate specialist the time to grow (and profit from glucose at its reduced uptake rate, then from the acetate excreted by the glucose specialist), before the glucose specialist took over the whole population.

The result of this experiment is shown in Figure 31. It can be observed that most of the culture is acetate specialist throughout the experiment. Only in the last 5 hours before stationary phase is reached, some glucose specialists also appear. As shown in Figure 24, the glucose specialist should excrete acetate when it starts producing biomass. We cannot directly measure the acetate flux from the glucose specialist to the acetate specialist, but we measured the acetate concentration in the medium and did not find any. This is an indication that the acetate excreted by the glucose specialist is immediately taken up by the acetate specialist.

Since we started with a low concentration of glucose specialist, its effect on the consortium was only minor. Therefore, with the aim to get a clearer interaction between the two strains, we did a second batch experiment in which we grew the species starting each at approximately the same biomass concentration. The results of this experiment are shown in Figure 32. We can observe that there is a lag phase (blue circle) for both the glucose and the acetate specialist. Moreover, we can observe that the growth rate of the glucose specialist in the

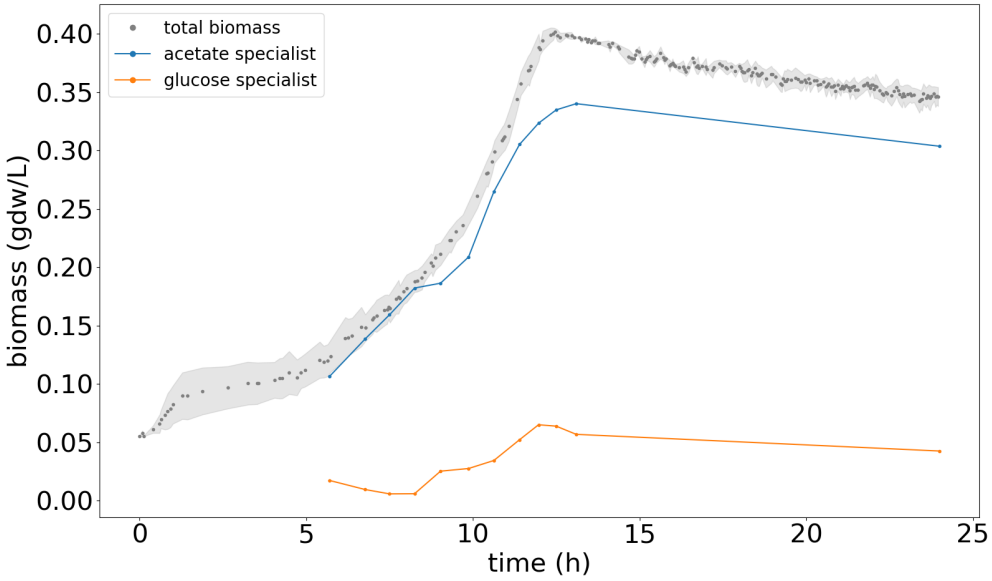

Figure 31: Dynamics of the consortium in a batch culture with 1 g/L glucose. The experiment was started with 0.037 gDW/L acetate specialist and 0.00093 gDW/L glucose specialist. The total biomass was determined from the absorbance in a plate reader, whereas the amount of acetate specialist and glucose specialist was derived from the fraction of each as determined by flow cytometry, which was multiplied with the total biomass to get the biomass concentration of each strain.

consortium (orange) is the same as the growth rate of the glucose in monoculture (black), indicated by the similar slopes of the growth curves in log scale; the acetate specialist does not seem to affect the growth rate of the glucose specialist. In this experiment, we did not manage to measure the acetate concentration in the medium, but we can see the effect of acetate in the growth curve in the last, slower growth phase (red circles). In the monoculture of glucose specialist (black) this phase is longer than in the consortium (grey). This suggests that after the glucose growth phase, there was more acetate in the medium to be taken up in the monoculture than in the coculture. It seems that the acetate excreted by the glucose specialist in the coculture is directly taken up by the acetate specialist.

All in all, while it is impossible to measure a flux of acetate going from the glucose to the acetate specialist during batch growth on glucose, our mono-culture and co-culture results combined strongly suggest that cross-feeding of acetate is taking place. Therefore, we decided to continue our experiments with these strains.

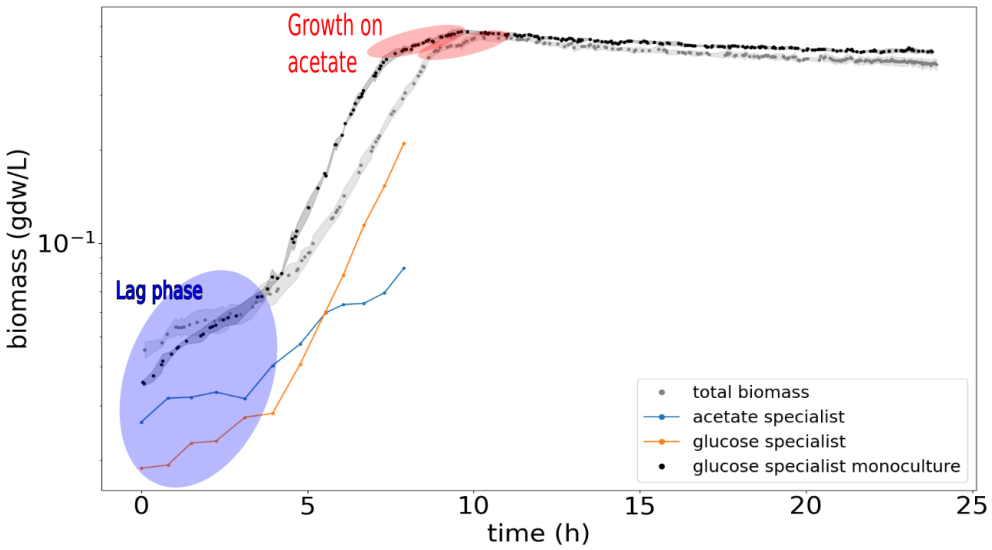

Figure 32: Dynamics of the consortium in a batch culture with 1 g/L glucose. The experiment was started with 0.037 gDW/L acetate specialist and 0.037 gDW/L glucose specialist. The total biomass was determined from the absorbance in a plate reader, whereas the amount of acetate specialist and glucose specialist was derived from the fraction of each as determined by flow cytometry, which was multiplied with the total biomass to get the biomass concentration of each strain. In black, the biomass dynamics of a culture of only glucose specialist are shown. The blue circle indicates the lag phase. The regions circled in red show where we suspect the cultures are growing on previously excreted acetate.

2.5.2 Predicting coexistence with the model

In this section, we explain how we used the calibrated model to predict if, in theory, we could expect coexistence of the consortium in a chemostat. First we looked at the conditions for coexistence by analyzing the steady-state mathematically. Then, we simulated the model over a range of dilution rates and looked for coexistence at steady-state.

Approximate mathematical prediction of coexistence

Since we knocked out the acetate specialist's main glucose uptake system, its glucose uptake rate is lower than that of the glucose specialist. In order to know by how much, we looked at the model in steady-state. Then, we looked at the acetate uptake rate needed to compensate for the lower glucose uptake. Finally, we evaluated whether, with the current model and the current parameters, there could be a state of coexistence, i.e. whether there are steady-state conditions where i) the glucose specialist produces acetate and ii) the growth rate of the acetate specialist is high enough to not be flushed out.

In steady-state, we know that the change in biomass concentration is zero:

$$\frac{dB_p}{dt} = (Y_g r^g_{upP} + Y_a(r^a_{upP} - r^a_{overP}))B_p - k_{deg}B_p - DB_P = 0, \tag{18}$$

$$\frac{dB_c}{dt} = (Y_g r^g_{upC} + Y_a(r^a_{upC} - r^a_{overC}))B_C - k_{deg}B_C - DB_C = 0. \tag{19}$$

It follows that:

$$Y_g r^g_{upP} + Y_a(r^a_{upP} - r^a_{overP}) = k_{deg} + D. \tag{20}$$

Given carbon catabolite repression, $r^a_{upP} \approx 0$, so

$$Y_g r^g_{upP} = k_{deg} + D + Y_a r^a_{overP}. \tag{21}$$

Since we know that the expression for the glucose uptake rate is the same for the glucose and the acetate specialist, namely:

$$r^g_{up} = k_g \frac{G}{G + K_g} \frac{\theta_a^n}{\theta_a^n + A}, \tag{22}$$

and $\frac{k_{gP}}{k_gC} = \frac{1.58}{0.51} \approx 3$ (see Table 4), it follows that

$$Y_g r^g_{upC} = \frac{1}{3} Y_g r^g_{upP} = \frac{1}{3}(k_{deg} + D + Y_a r^a_{overP}). \tag{23}$$

We could call the expression $Y_g r^g_{upC}$ the growth rate of the acetate specialist on glucose only, while $Y_g r^g_{upP}$ is the growth rate of the glucose specialist on glucose only. Equation (23) tells us how fast the acetate specialist can maximally grow on glucose when growing together with the glucose specialist in steady-state: The acetate specialist can only grow at 1/3 the rate of glucose specialist, since its maximum glucose uptake rate is 3 times smaller and both strains have the same amount of glucose available: For the same glucose concentration, the acetate specialist grows 3 times slower. The rest of the growth of the acetate specialist has

to come from growth on acetate. So in order for the acetate specialist to be in steady-state (Equation (19)) the following equation has to hold:

$$Y_g r^g_{upC} + Y_a(r^a_{upC} - r^a_{overC}) = k_{deg} + D. \tag{24}$$

Given our current knowledge about overflow metabolism, $r^a_{overC} \approx 0$, so:

$$Y_a r^a_{upC} = k_{deg} + D - Y_g r^g_{upC}, \tag{25}$$

$$Y_a r^a_{upC} = k_{deg} + D - \frac{1}{3}(k_{deg} + D + Y_a r^a_{overP}), \tag{26}$$

$$Y_a r^a_{upC} = 2/3(k_{deg} + D) - \frac{1}{3} Y_a r^a_{overP}. \tag{27}$$

$Y_a r^a_{upC}$ is the growth rate of the acetate specialist on the available acetate. Equation (27) tells us the minimum growth rate of the acetate specialist on acetate to keep up with dilution rate and coexist with the glucose specialist at steady-state (condition ii). To evaluate whether there can be a state of coexistence, we now need to see over which dilution rate condition (i) holds according to our model. To do this, we look at the equation for acetate overflow:

$$r^a_{over} = k_{over} max(0, r^g_{up} - l). \tag{28}$$

From Equation (28), it follows that for acetate production to occur, $r^g_{up} > l$. From Equation (21), it follows that:

$$(k_{deg} + D + Y_a r^a_{overP})/Y_g > l. \tag{29}$$

Since we are looking at the point of transition (we are considering the minimum dilution rate for acetate excretion, where overflow is still zero, but will start as soon as the dilution rate increases), we can consider $r^a_{overP} = 0$.

$$D > lY_g - k_{deg}. \tag{30}$$

We had determined that $l = 1, Y_g = 0.5, k_{deg} = 0.004$, so $D > 1 \cdot 0.5 - 0.004 = 0.50$

So the minimum dilution rate for the presence of acetate is 0.50h^{-1}. Is it possible for the acetate specialist to stabilize at non-zero biomass at this dilution rate? We insert the minimum dilution rate in Equation (27). We set $r^a_{overP} = 0$, since we are still at the critical condition where there is exactly no acetate overflow:

$$\begin{aligned} Y_a r^a_{upC} &= 2/3 \cdot 0.50 = 0.33, \\ r^a_{upC} &= 0.33/0.3 = 1.1. \end{aligned} \tag{31}$$

Is this a feasible value for r^a_{upC}? The rate is defined as:

$$r^a_{upC} = k_a \frac{A}{A + K_a} \frac{\theta_g}{r^g_{upC} + \theta_g} + k_{Pta} \frac{A}{A + k_{Pta}}. \tag{32}$$

At $D = 0.50$, $r^g_{upC} = \frac{1}{3}(k_{deg} + D)/Y_g = 0.33 \cdot 0.50/0.5 = 0.33$. Therefore, $\frac{\theta_g}{r^g_{upC}+\theta_g} = 8 \times 10^{-3}/(0.33 + 8 \times 10^{-3}) = 0.024$. We can therefore write Equation (32) as:

$$r^a_{upC} = 0.024 \cdot k_a \frac{A}{A + K_a} + k_{Pta} \frac{A}{A + k_{Pta}}. \tag{33}$$

So far, we measured $k_a = 0.63$ and $k_{Pta} = 0.42$. So the maximal acetate uptake rate for the acetate specialist at this dilution rate is $r^a_{upC} = 0.024 \cdot 0.63 + 0.42 = 0.43$. This is smaller than the necessary uptake rate of 1.1 (Equation (31)). In addition, this is the maximum rate, which only occurs if $A >> K_a = 0.5$. In reality, the acetate concentration A is not likely to be that high. In conclusion, it is unlikely, that both condition (i) and (ii) will hold at the same time: the acetate specialist will likely not be able to grow fast enough at the dilution rate above which acetate starts to be excreted in the reactor by the glucose specialist.

Numerical prediction of coexistence

To confirm the analytical results in the previous section, and to evaluate the model further, we simulated the model numerically at different dilution rates and looked at the steady-state concentration of glucose and acetate specialists in the reactor. We used $G_{in} = 1$ g/L and started with 0.1 gDW/L of each strain. We simulated 100 hours of chemostat to make a sure a steady-state was reached. Figure 33 shows the model prediction: at none of the dilution rates, the acetate specialist is predicted to be present at steady-state. As anticipated by the mathematical analysis, this can be explained by the high dilution rate above which the glucose specialist starts excreting acetate according to our model (see green line). Apparently, even though the acetate specialist has an enhanced acetate uptake rate, and should be profiting from the acetate excreted by the glucose specialist, the dilution rate above which acetate excretion starts is too high for the acetate specialist to stay in the reactor: Its combined growth rate on glucose and acetate is lower than the dilution rate.

From the analytical and numerical analysis of the model, it can be understood that there are various reasons for the lack of coexistence. First of all, the model predicts that the glucose specialist does not excrete acetate for the majority of dilution rates. This high threshold is determined by the value of the parameter l. Secondly, the acetate uptake rate of the acetate specialist is too low to compensate for its lack of glucose uptake. This is determined by two parameters. k_{Pta} indicates the additional acetate uptake of the acetate specialist, whereas θ_g determines to what extent the acetate specialist is able to take up acetate during partial growth on glucose: since the value of this parameter is currently low, there is almost no basal acetate uptake rate by the acetate specialist in the model. Thirdly, the acetate concentration in the medium resulting from acetate overflow might be too low, or the affinity for acetate of the acetate specialist might be too low. In the model, k_{over} impacts the rate of overflow and thereby the acetate concentration in the medium. K_a and K_{Pta} affect the affinity of the cells for acetate.

As explained in Section 2.4, the parameter values were initially determined by fitting the model to batch growth on glucose. In these conditions, the parameters are not entirely identifiable: the effect of one parameter might be compensated by another without significant effects on the data fit. Therefore, the values of the parameters critical for coexistence might have slightly different values than those determined by the initial model fit. This gives

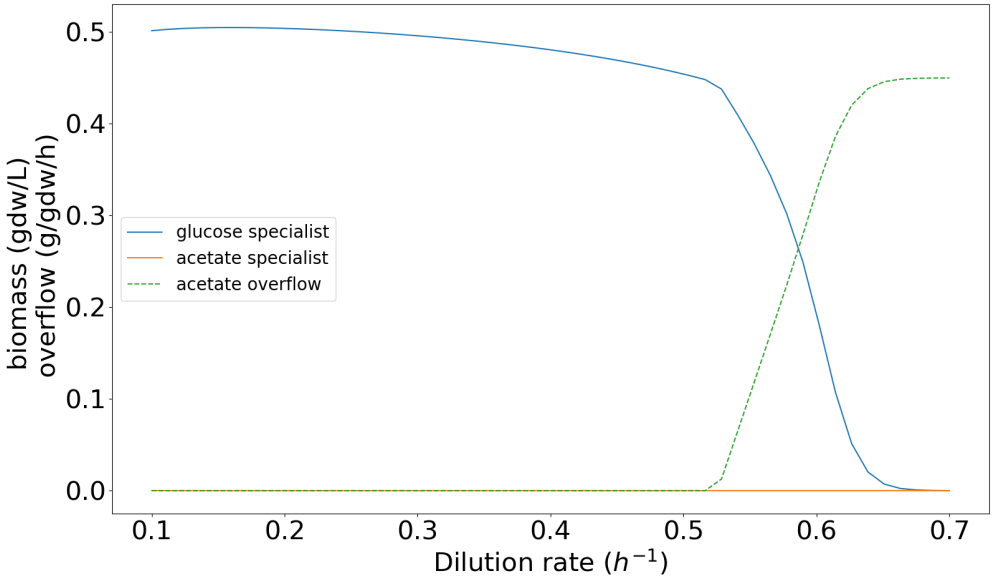

Figure 33: Predicted steady-state concentration of the two strains in a co-culture, as a function of dilution rate. The acetate overflow rate by the glucose is also depicted with a green dotted line.

a potential for coexistence, despite our initial assessment showing that it is not possible. Indeed, in our model, if we increase k_{Pta}, or decrease l, coexistence is predicted to happen, see Figure 34. With an increase in k_{Pta}, coexistence occurs at high dilution rates (Figure 34(a)). For a decrease in l, the strains can coexist at low dilution rates (Figure 34(b)). When k_{Pta} is increased and l is decreased at the same, coexistence can occur at intermediate dilution rates (Figure 34(c)).

In this case, the parameters were not refitted to the data, but manually explored, so the fit to the data as shown in Section 2.4 is likely worse. However, this manual exploration illustrates that it is not the model structure that prohibits coexistence, but rather the used parameter values. In the Discussion (Sections 3.2.4 and 3.3.3) we give some more perspectives on the importance of model parameterization for this study.

In conclusion, our model analysis shows that coexistence is not possible with the current parameters, but that coexistence might be obtainable if some parameters were to be different than found in the fits with the data of individual growth curves. We speculated that measurements co-culturing the strains could still lead to modifications of the parameters or the model structure. For example, the presence of the acetate specialist (and consumption of acetate by the acetate specialist) might cause the glucose specialist to excrete more acetate, or the acetate specialist might improve its ability to grow on acetate. Therefore, we still continued to investigate the constructed community in the chemostat. If we were to find coexistence, it would point to an inaccuracy in our parameter values, or even in the model structure.

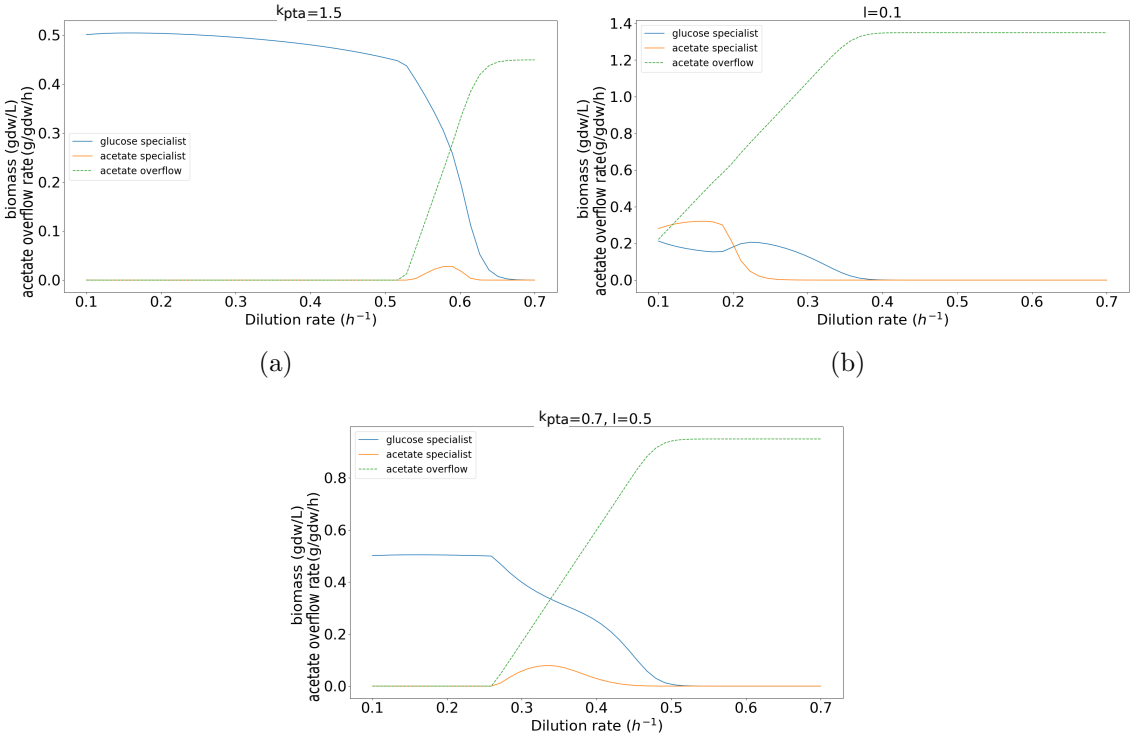

Figure 34: Possible parameter changes to achieve coexistence with the current model. (a) Increasing k_{Pta} improves the performance of the acetate specialist at high dilution rates. (b) Decreasing l increases the overflow of the glucose specialist at low dilution rates. (c) Decreasing l slightly and increasing k_{Pta} slightly leads to coexistence at intermediate dilution rates.

2.5.3 Experimental characterization of the community in chemostat at different dilution rates

To answer the question whether the glucose and the acetate specialist can coexist in a chemostat, we inoculated our bioreactors with small starting concentrations of glucose and acetate specialists and let the chemostat run for 10 residence times. One residence time is the time needed to replace the entire bioreactor volume. At a given dilution rate D, the number of residence times corresponding to an experiment lasting a time T is equal to $T \cdot D$. So, for a dilution rate of 0.1h^{-1}, 10 residence times amount to 100 hours, whereas for a dilution rate of 0.6h^{-1}, 10 residence times represent only about 17 hours. We rescale the time unit to residence times in order to be able to compare the flush-out of the acetate specialist across different dilution rates: if the acetate specialist does not keep up with the dilution rate, its concentration in the bioreactor will decrease faster at a high than at a low dilution rate, because the cells are replaced by medium more quickly. Using residence times as time unit allows us to factor out this bias, and to compare the speed of flush-out between different dilution rates. As a proxy for the amount of acetate specialist, we use red fluorescence, since the acetate specialist expresses the mScarlet-I protein constitutively (see Section 2.1.1). Since the loss of cells due to the dilution is exponential with rate $-D$, we look at the red fluorescence on a log scale. On this scale, if the acetate specialist was purely flushed out by the dilution rate, without taking up glucose or acetate, its disappearance at rate D (relative to time units) would look like a decreasing straight line with negative slope independent of D in residence time units.

The collective result of five chemostat experiments with the consortium at five different dilution rates is shown in Figure 35. The expected loss of cells due to the dilution rate only is shown as well.

When looking at the total biomass (Figure 35 upper panel), we notice that it reaches a steady-state for all dilution rates except $D = 0.6\text{h}^{-1}$. At this high dilution rate, cells are flushed out by medium faster so, for cells that are multiplying equally fast, it takes longer to reach steady-state. On top of that, the plotted result for this dilution rate corresponds to the shortest time period across all dilution rates, since profiles are reported relative to residence times.

Another thing we notice when looking at Figure 35 is that the steady-state does not amount to the same biomass concentration for all dilution rates. We observe a correlation between dilution rate and steady-state biomass concentration: the higher the dilution rate, the higher the steady-state biomass concentration. This correlation was not something we expected from chemostat theory or from our model, although variations of biomass concentration with dilution rate have been observed before in the literature [100, 101]. We hypothesized that, for unknown reasons, the biomass yield of our strains increases with the dilution rate.

Coming back to the main purpose of the figure, when looking at the red fluorescence (Figure 35 lower panel), we observe that the acetate specialists are flushed out quickly at high (0.6) and intermediate (0.4) dilution rates. At low (0.1, 0.15, 0.2) dilution rates, the acetate specialist stays in the bioreactor for a higher amount of residence times and the flush-out rate is lower, judging by the less steep slope of the red fluorescence curve. Note that time is normalized by the dilution rate, so that slopes should be comparable if the cells

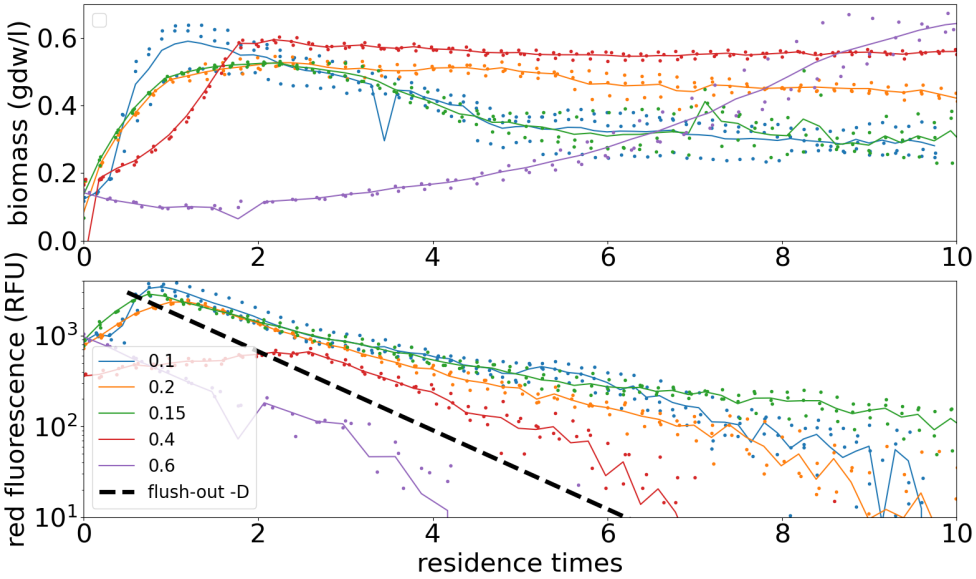

Figure 35: Dynamics of total biomass (upper panel) and red fluorescence (lower panel) at increasing dilution rates. To compare experiments properly, time is rescaled in residence time units. The lines represent the mean of three technical replicates, whose values are indicated by the dots. The black dashed line indicates the expected flush-out if the cells were simply flushed out by the dilution rate. The slope of this flush-out is independent of the dilution rate because time is rescaled in residence time units.

were growing at the same speed.

At all dilution rates except 0.6, the acetate specialist is not immediately flushed out: before steady-state is reached there is enough glucose and possibly acetate in the medium for it to grow faster than the dilution rate and to accumulate some biomass. With decreasing glucose concentration, the acetate specialist's growth rate decreases until it is no longer able to keep with the dilution rate and it is slowly flushed out. That is, at 0.1 and 0.2h^{-1} the acetate specialist is flushed out.

At 0.15h^{-1}, however, the red fluorescence seems to reach a steady-state: the acetate specialist is not flushed out. This is confirmed by a flow cytometry measurement that still shows 1 to 3 % acetate specialist after 10 residence times (see Figure S3). It seems that, at 0.15h^{-1}, we reach the balance explained in Section 2.5.2: there is both acetate in the medium, and the growth rate of the acetate specialist is high enough not be flushed out. As we stated in Section 2.5.2, our model currently does not predict such a balance to be possible. The fact that the acetate specialist does seem to be coexisting with the glucose specialist in the chemostat suggests an inaccuracy in our model's parameter values, or even in the model structure. In the next section, we explain why we suspect our model structure might be incomplete and we propose a more complete model for *E.coli* glucose metabolism that could explain our chemostat results.

2.6 A model of acetate cycling that allows for coexistence at low dilution rates

In Section 2.5.3 we found that the acetate specialist seems to coexist with the glucose specialist at the low dilution rate of 0.15h^{-1}. This suggests that, at this dilution rate, acetate is excreted by the glucose specialist that can be taken up by the acetate specialist fast enough to compensate for its impaired glucose uptake. With the model of *E.coli* metabolism that we initially proposed, this is not possible, because the model supposes the presence of a threshold for acetate excretion: below a specific dilution rate, no acetate is excreted at all. Above the threshold, acetate is excreted proportionally to the glucose uptake rate. The threshold is represented by the parameter l, see Equation 8. One way to allow the model to predict acetate excretion at lower dilution rates would therefore be to decrease the threshold for acetate overflow or even remove it completely, so that acetate is always excreted proportionally to the glucose uptake rate. However, as discussed in Section 1.3, earlier studies on the metabolism of acetate strongly imply that a threshold for acetate secretion exists and that it is located at intermediate dilution rates [51–53].

Therefore, rather than decreasing or even eliminating it, we thought of a way to preserve an acetate overflow threshold in our model, while at the time implementing acetate secretion at all dilution rates. We hypothesized that this might be done by modeling the mechanism of acetate cycling as proposed by Enjalbert et al. [56]; Enjalbert et al. showed that acetate overflow is the result of two gross fluxes: acetate excretion and acetate uptake. The balance between uptake and excretion is determined by the internal metabolite concentration and the extracellular acetate concentration. A high extracellular acetate concentration results in more uptake than excretion, resulting in a net uptake. Low extracellular acetate concentrations cause more excretion than uptake, resulting in a net overflow. Even in the case of a net zero overflow, however, there is a still a gross uptake and excretion flux of acetate in and out of the cell; acetate is cycled through the medium continuously. This mechanism of acetate cycling could result in an apparent threshold of acetate overflow: At low dilution rates, excretion equals consumption, leading to a net zero overflow. Above the observed acetate overflow threshold, excretion of acetate exceeds its consumption, leading to a net positive overflow.

We hypothesized that a cycling model of acetate could explain what is happening in our consortium at low dilution rates: even though the glucose specialist does not seem to excrete acetate at low dilution rates when observed in a monoculture, it is nonetheless continuously cycling acetate in out of its cells. When we grow the glucose and the acetate specialists together, the acetate specialist might be profiting from this cycled acetate.

In this section, we therefore propose a model for glucose and acetate metabolism that allows for acetate cycling (gross acetate secretion and uptake) at all dilution rates while still maintaining a threshold for net acetate excretion. We calibrate this model with data from the literature and show that it can reproduce the data generated in our lab. Then, we show the possibilities of coexistence according to this new model.

2.6.1 Model structure

A schematic of the new model (which we refer to as the 'cycling model') is shown in Figure 36. Unlike the initially proposed model ('threshold model', schematic in Figure 7), the cycling model uses a variable C to represent the internal metabolites. The amount of acetate overflow and uptake is assumed to depend on the equilibrium between these internal metabolites and the external acetate (A) concentration. This relects the way the Pta-AckA pathway works. During glucose-fueled growth, glucose (G) is taken up and transformed into central metabolites (C). The central metabolites can be either converted into biomass (B) or excreted as acetate by a reversible pathway, whose direction is determined by the concentration of central metabolites and acetate. Acetate can also be taken up by another, irreversible, pathway; this models the function of the Acs enzyme in *E.coli*, which is known to take up acetate irreversibly.

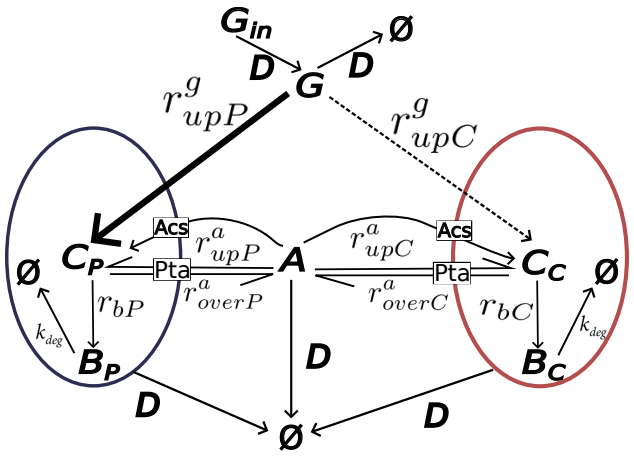

Figure 36: A schematic of our model of glucose and acetate metabolism for a glucose specialist (subscript $_P$) and an acetate specialist (subscript $_C$). During glucose-fueled growth, glucose (G) is taken up and transformed into central metabolites (C) through r^g_{up}. The central metabolites can be either converted into biomass (B) through r_b or excreted as acetate (A) through r^a_{over} by Pta. Acetate can be taken up from the medium through r^a_{up} by both Acs and Pta. In a chemostat, glucose is supplied from the inflow (G_{in}) with the dilution rate D. Both the cells and the medium are flushed with D. Biomass is degraded for maintenance metabolism through k_{deg}.

2.6.2 Definition of the cycling model

The differential equations of the cycling model are similar to those of the threshold model. Its variables are given in Table 5. Because of the addition of central metabolites C we add two differential equations modeling their respective concentration in the acetate specialist and the glucose specialist. We use the subscript P to denote the glucose specialist and the subscript C to denote the acetate specialist. Whereas in the threshold model, the accumulation of biomass is determined by the acetate uptake rate and the glucose uptake rate directly (see Equation (1)), in the cycling model the change in biomass is determined by the biomass synthesis rate r_b. The glucose uptake rate and the acetate uptake rate jointly determine the

change in central metabolites whose concentration in turn determines the rate of biomass production. Note that the central metabolites are measured with respect to cell volume, not bioreactor volume, and are therefore diluted by the growth rate, see Section S5.2 for a mathematical explanation.

Table 5: Meaning of the variables in the cycling model

Parameter	Meaning	Units
B	concentration of cells in the reactor	$\mathrm{gDW^{-1}\,L^{-1}}$
G	glucose concentration in the reactor	$\mathrm{g\,L^{-1}}$
A	acetate concentration in the reactor	$\mathrm{g\,L^{-1}}$
G_{in}	glucose concentration in the inflow	$\mathrm{g\,L^{-1}}$
C_P	concentration of central metabolites in the glucose specialist	$\mathrm{g\,gDW^{-1}}$
C_C	concentration of central metabolites in the acetate specialist	$\mathrm{g\,gDW^{-1}}$
μ_P	growth rate of the glucose specialist	$\mathrm{h^{-1}}$
μ_C	growth rate of the acetate specialist	$\mathrm{h^{-1}}$

$$\frac{dB_P}{dt} = (Y_g r_{bP} - k_{deg})B_P - DB_P \tag{34}$$

$$\frac{dB_C}{dt} = (Y_g r_{bC} - k_{deg})B_C - DB_C \tag{35}$$

$$\frac{dG}{dt} = -r^g_{upP}B_P - r^g_{upC}B_C + D(G_{in} - G) \tag{36}$$

$$\frac{dA}{dt} = (r^a_{overP} - r^a_{upP})B_P + (r^a_{overC} - r^a_{upC})B_C - DA \tag{37}$$

$$\mu_P = Y_g r_{bP} - k_{deg} \tag{38}$$

$$\frac{dC_P}{dt} = r^g_{upP} + r^a_{upP} - r^a_{overP} - r_{bP} - \mu_P C_P \tag{39}$$

$$\mu_C = Y_g r_{bC} - k_{deg} \tag{40}$$

$$\frac{dC_C}{dt} = r^g_{upC} + r^a_{upC} - r^a_{overC} - r_{bC} - \mu_C C_C \tag{41}$$

2.6.3 Rates

Rate equations are expressed in g/gDW/h for both glucose specialist (P) and acetate specialist (C). The biomass production rate and the glucose uptake rate are irreversible Michaelis-Menten equations. Acetate toxicity is modeled by adding the expression $\theta_a/(\theta_a + A)$ to the glucose uptake rate. The acetate uptake and excretion by Pta-AckA are modeled as a reversible Michaelis-Menten equation, with separate terms for the two directions. The uptake

by Acs again follows Michaelis-Menten kinetics, and is subject to carbon catabolite repression as modeled by the expression $\theta_g^m/(r_{upP}^{gm} + \theta_g^m)$. To represent the possibility of overexpression of Pta-AckA or Acs by the acetate specialist we added the enzyme concentration of these two enzymes explicitly. We assume that $pta_P = 1$, whereas pta_C is increased in the case of overexpression. Similarly, $acs = 1$ in both strains, whereas the acetate specialist might have $acs_C > 0$ in the case of overexpression. Notice that acs_C is not subject to carbon catabolite repression, since this repression is mostly transcriptional and therefore bypassed in the case of overexpression.

r_b: rate of conversion of central metabolites to biomass

$$r_{bP} = k_b \frac{C_P}{C_P + K_b} \tag{42}$$

$$r_{bC} = k_b \frac{C_C}{C_C + K_b} \tag{43}$$

r_g: glucose uptake rate

$$r_{upP}^g = k_{gP} \frac{G}{G + K_g} \frac{\theta_a}{\theta_a + A} \tag{44}$$

$$r_{upC}^g = k_{gC} \frac{G}{G + K_g} \frac{\theta_a}{\theta_a + A} \tag{45}$$

r_{up}^a: acetate uptake rate

$$r_{upP}^a = k_{up}^{pta} pta_P \frac{A/K_a}{1 + A/K_a + C_P/K_{cm}} + k_{acs} acs \frac{A}{A + K_{acs}} \frac{\theta_g^m}{r_{upP}^{gm} + \theta_g^m} \tag{46}$$

$$r_{upC}^a = k_{up}^{pta} pta_C \frac{A/K_a}{1 + A/K_a + C_C/K_{cm}} + k_{acs} \frac{A}{A + K_{acs}} (acs \frac{\theta_g^m}{r_{upC}^{gm} + \theta_g^m} + acs_C) \tag{47}$$

r_{over}^a: acetate overflow rate

$$r_{overP}^a = k_{over}^{pta} pta_P \frac{C_P/K_{cm}}{1 + A/K_a + C_P/K_{cm}} \tag{48}$$

$$r_{overC}^a = k_{over}^{pta} pta_C \frac{C_C/K_{cm}}{1 + A/K_a + C_C/K_{cm}} \tag{49}$$

2.6.4 Parameters

The parameters in the cycling were partly taken from the threshold model, but some had to be added. Table 6 explains the meaning of each parameter. It also gives the values as determined by calibration, as explained below.

Table 6: Values and meaning of the parameters in the cycling model.

Parameter	Value	Units	Meaning
k_{gP}	1.60	$\mathrm{g\,gDW^{-1}\,L^{-1}}$	maximum glucose uptake rate of the glucose specialist
k_{gC}	0.5	$\mathrm{g\,gDW^{-1}\,L^{-1}}$	maximum glucose uptake rate of the acetate specialist
K_g	0.009	$\mathrm{g\,L^{-1}}$	half maximal rate constant
θ_a	5.8	$\mathrm{g\,L^{-1}}$	inhibition constant of acetate on the glucose uptake rate
k_b	1.7	$\mathrm{g\,gDW^{-1}\,h^{-1}}$	maximum rate of central metabolites to biomass
K_b	0.0022	$\mathrm{g\,gDW^{-1}}$	half maximal rate constant
k_{up}^{pta}	0.12	$\mathrm{g\,gDW^{-1}\,M^{-1}\,h^{-1}}$	catalytic constant of pta in the uptake direction
k_{over}^{pta}	2.2	$\mathrm{g\,gDW^{-1}\,M^{-1}\,h^{-1}}$	catalytic constant of pta in the overflow direction
pta_P	1.0	M	concentration of Pta-AckA in the glucose specialist
pta_C	5.0	M	concentration of Pta-AckA in the acetate specialist
K_a	0.019	$\mathrm{g\,L^{-1}}$	Michaelis constant of Pta-AckA in the uptake direction
K_{cm}	0.0077	$\mathrm{g\,gDW^{-1}}$	Michaelis constant of Pta-AckA in the overflow direction
k_{acs}	0.2	$\mathrm{g\,gDW^{-1}\,M^{-1}\,h^{-1}}$	catalytic constant of Acs
acs	1.0	M	base concentration of Acs
acs_C	0.8	M	concentration of overexpressed Acs in the acetate specialist
K_{acs}	0.00012	$\mathrm{g\,L^{-1}}$	half maximal rate constant of Acs
θ_g	0.8	$\mathrm{g\,gDW^{-1}\,h^{-1}}$	inhibition constant of Acs expression
m	5	NA	exponent shaping the non-linear effect of carbon catabolite expression
Y_g	0.50	$\mathrm{gDW\,g^{-1}}$	biomass yield during growth on glucose or a mixture of glucose and acetate
Y_a	0.30	$\mathrm{gDW\,g^{-1}}$	biomass yield during growth on acetate only
k_{deg}	0.0044	$\mathrm{h^{-1}}$	degradation rate constant
D	Depends on experiment	$\mathrm{h^{-1}}$	dilution rate

2.6.5 Calibration of the cycling model

In this section, we describe how we calibrated the cycling model of the glucose specialist with data in order to obtain the parameter values as given in Section 2.6.4, Table 6. In the next section, we will show how the model was calibrated to represent the acetate specialist.

Valgepea et al. 2010 [52] measured the relative concentration of the Acs protein at different dilution rates, see Figure 37. The figure shows the value of $\theta_g^m/(r_{upP}^{gm} + \theta_g^m)$ as a function of the relative dilution rate. With higher dilution rate, r_{upP}^g increases, so the Acs expression decreases. We varied parameters θ_g and m (Equation (46)) to fit the decrease of Acs as a function of relative dilution rate. Figure 37 shows the different fits for $\theta_g = 0.8$ and varied m. The best fit is obtained for $\theta_g = 0.8$ and $m = 5$.

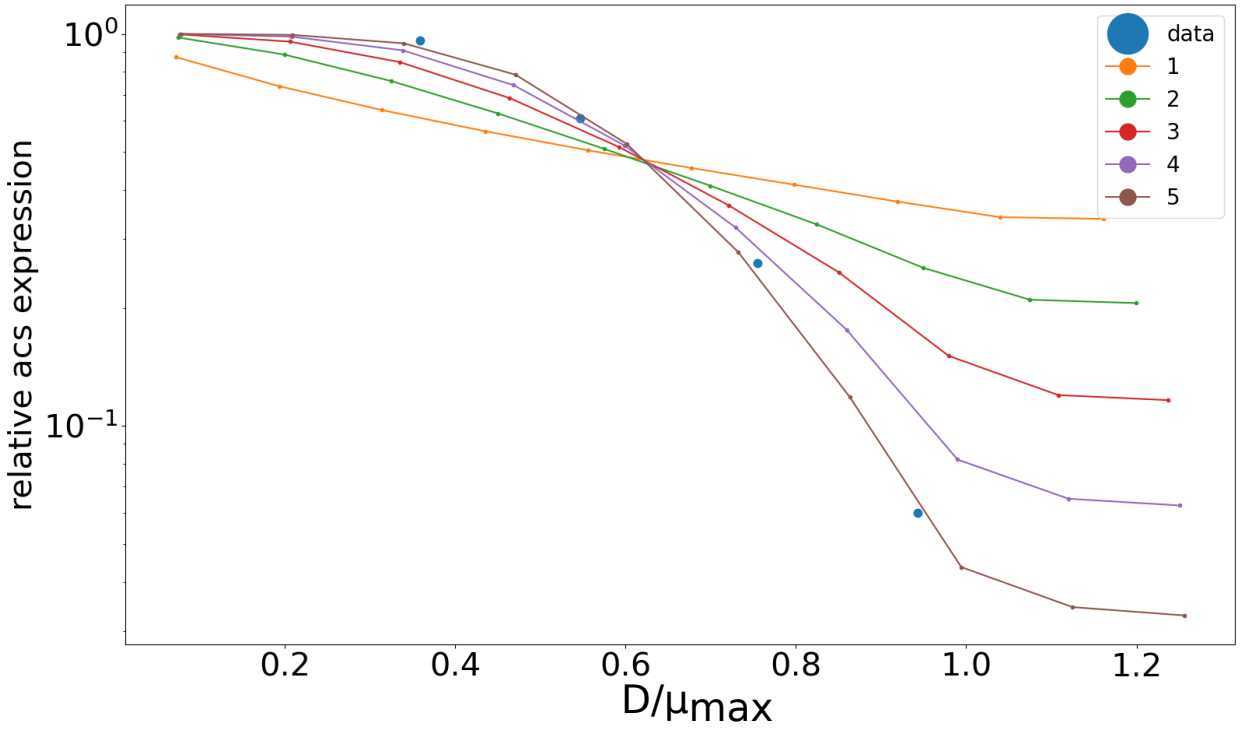

Figure 37: Acs expression as a function of relative dilution rate measured by Valgepea et al. [52] by proteomics. We simulated the model and left θ_g and m free. Here, fits are shown for $\theta_g = 0.8$ and varied m. The best fit is obtained for $m = 5$.

We determined the values of the parameters K_b, k_{up}^{pta}, k_{over}^{pta} K_a, K_{cm}, θ_a and k_{acs} by fitting several data-sets simultaneously.

Enjalbert et al. [56] measured acetate going in and out of the cell by growing cells in a batch experiment on 15 mM ^{13}C-glucose and increasing concentrations of unlabeled acetate. They measured the concentration of labeled and unlabeled acetate in the medium over time for each batch experiment. This allowed the researchers to determine net acetate uptake and secretion in the exponential phase as a function of the initial acetate concentration in the medium. To determine the parameters of our model, we fitted it to the data of net acetate overflow as a function of acetate concentration in the medium. The final model fit

to these data is shown in Figure 38. The figure also shows the gross uptake and secretion rates predicted by the model, illustrating that the cells are predicted to take up and excrete acetate simultaneously. The acetate concentration determines the net result of these two fluxes. At low acetate concentrations, net acetate is expected to be excreted by the cells. As the acetate concentration increases, the cells start taking up more acetate than they secrete.

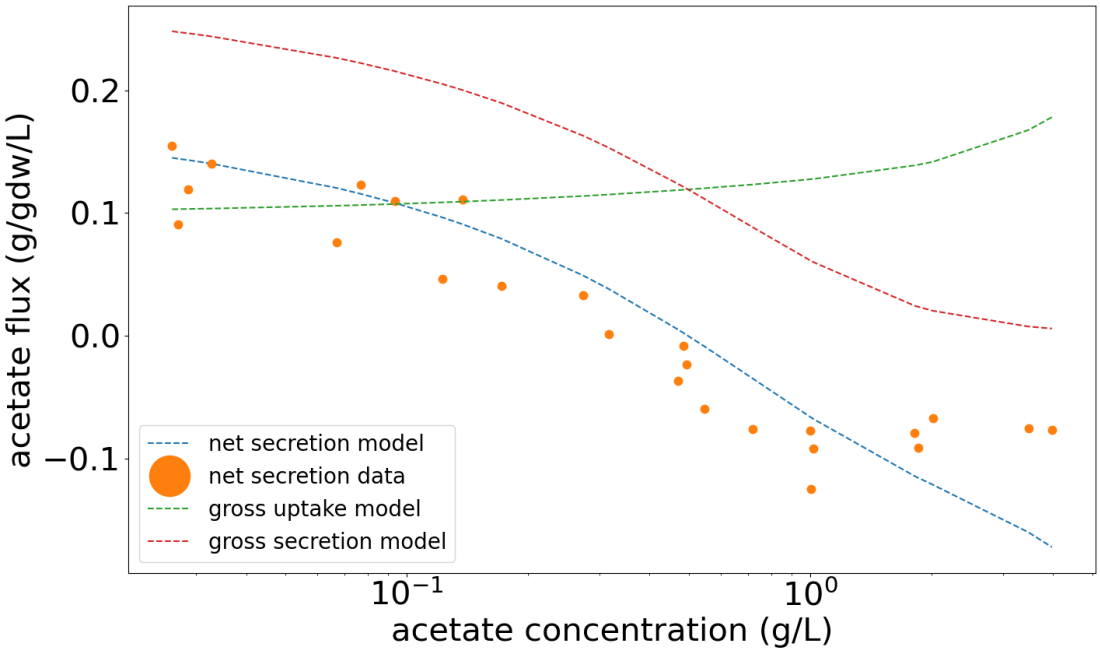

Figure 38: Best fit of the model to net acetate secretion rate data from Enjalbert et al. [56] as a function of acetate concentration in the medium. The absolute gross uptake and secretion predicted by the model are also shown (green and red lines). At low acetate concentration in the medium, secretion exceeds uptake, leading to a net positive secretion whereas at high acetate concentration, uptake exceeds secretion, leading to a net negative secretion, i.e. net acetate uptake.

Figure 39 shows that the fitted model is also in accordance with the acetate toxicity as measured by Enjalbert et al [56]; increasing acetate concentration results in a lower glucose uptake rate, as tuned in our model by θ_a.

Figure 40 shows that we can fit the new model quite well to batch data as obtained by plate-reader experiments of the glucose specialist growing on glucose in our own lab.

Figure 41 shows that our model results in an apparent threshold for overflow. This was not fitted, but is a result of the parameters found by fitting to the data in Figures 38, 39 and 40. In the resulting model predictions, the acetate uptake is almost equal to the acetate secretion at low dilution rates, resulting in a net zero overflow. This shows that it is theoretically possible to find a net zero overflow even if the glucose specialist is excreting acetate. Without imposing a threshold on acetate overflow, we can model an apparent threshold of overflow: at low dilution rates, gross acetate excretion equals gross

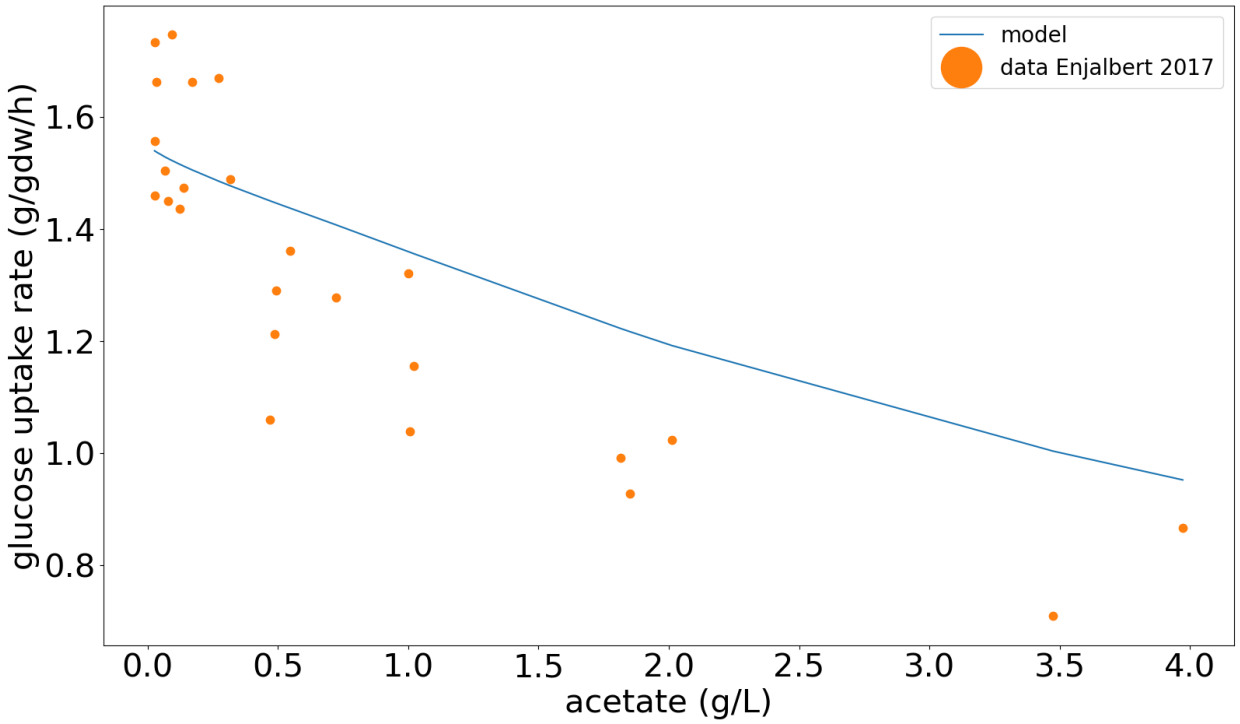

Figure 39: Fit of the model to glucose uptake data from Enjalbert et al. [56] as a function of the acetate concentration in the medium.

acetate consumption, resulting in a net zero acetate overflow. Above a certain threshold, the gross secretion is bigger than the uptake, so we observe a net acetate overflow. This model might explain the observations in our consortium at low dilution rates: even though the glucose specialist does not excrete net acetate at low dilution rates, it might nonetheless be continuously cycling acetate in and out of its cells. When we grow the glucose and the acetate specialists together, the acetate specialist might be profiting from this cycled acetate. In Section 2.6.7, we will explore whether the cycling model can indeed predict coexistence of the consortium at low dilution rates.

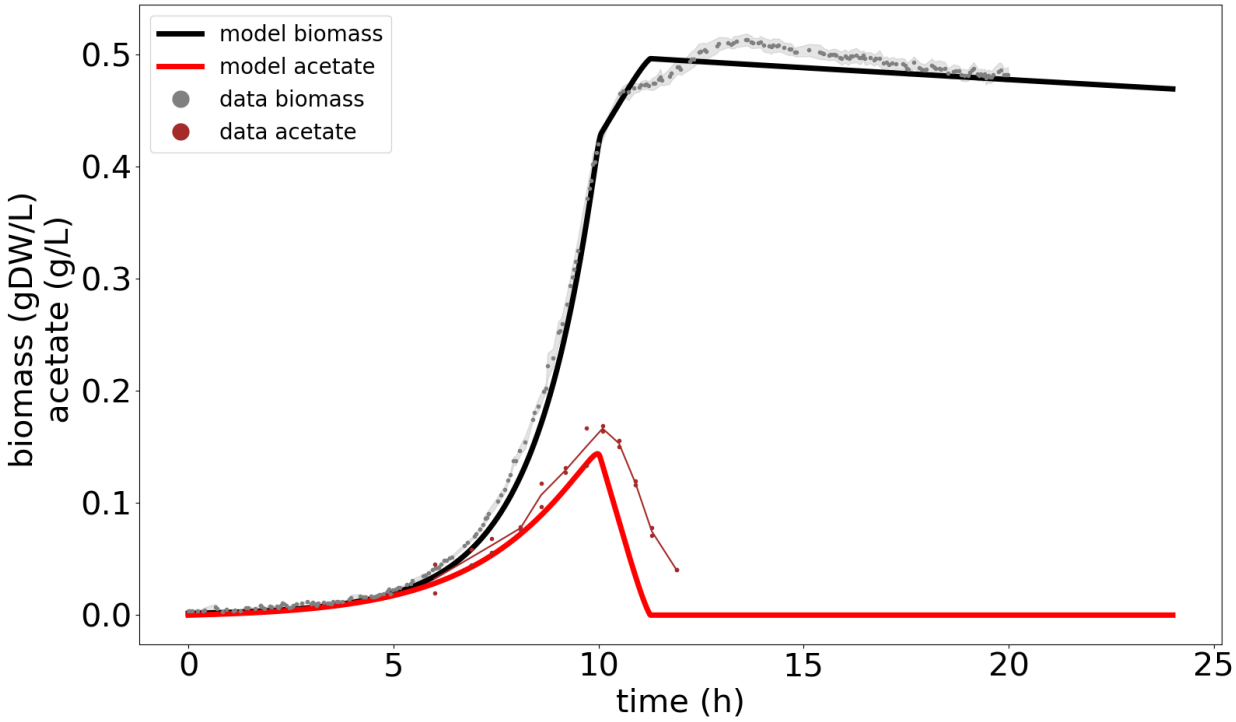

Figure 40: Black: fit of the cycling model to biomass accumulation of the glucose specialist grown individually in batch on 1 g/L of glucose. The dots indicate the mean of 6 technical replicas. The shaded area marks the SEM. Red: fit of the cycling to the acetate excretion and uptake by the glucose specialist in the same experiment. The dots indicate individual data points. The thin line shows the mean.

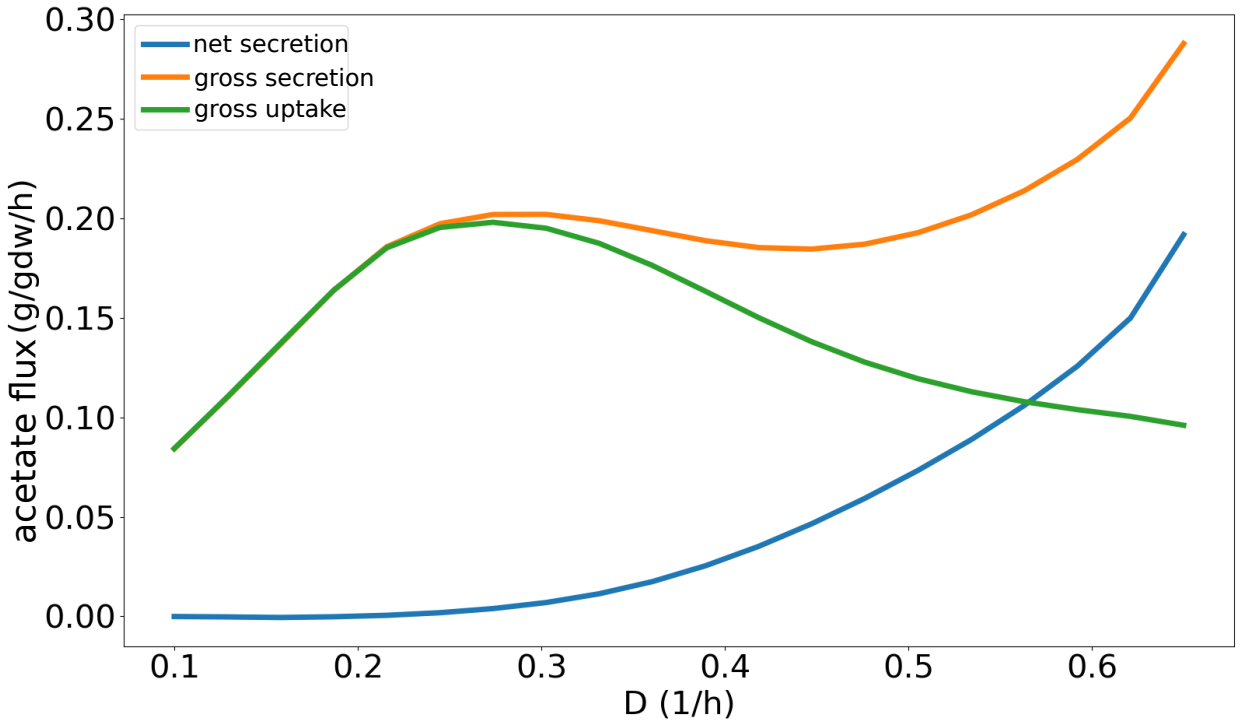

Figure 41: Acetate fluxes as a function of dilution rate as predicted by our cycling model presented in this section. We used the parameters for the glucose specialist given in Table 6, and used $G_{in} = 1$. At each dilution rate, we ran the model until steady-state and recorded the acetate fluxes. At low dilution rates, gross secretion equals uptake, leading to a zero net secretion. Above a threshold, around $D = 0.25\text{h}^{-1}$, and clearly visible above $D = 0.35\text{h}^{-1}$, gross secretion exceeds uptake, leading to a net acetate secretion (overflow). This shows that we can create an apparent threshold for acetate overflow with the cycling model. Below the threshold, the net but not the gross acetate secretion equals zero.

2.6.6 Fit of the cycling model with acetate specialist data

To see if we can also reconcile the cycling model with the growth of the acetate specialist, we used the data from batch experiments on acetate (Figure 25) and glucose (Figure 24) and fitted them to the cycling model. We set the parameters established above for the glucose specialist (Table 6) and fitted only the parameters specific for the acetate specialist. To fit the data of the acetate specialist with a plasmid carrying the Pta-AckA pathway, we fitted the model to the orange data points in Figure 42, leaving the initial biomass concentration and the parameters pta_C and Y_g free. Y_g was left free because we suspected that the biomass yield of acetate would be lower when the cells are growing on acetate only as compared to the biomass yield on glucose, or a mixture of glucose and acetate. Farmer and Jones [102], showed that, during growth on glucose, *E.coli* can make 13.9 gDW from 1 mol ATP but this value drops to 7.1 gDW/mol ATP during growth on acetate only. Renilla et al. [53] suggest that this is because energy is lost in gluconeogenesis during growth on acetate only. Indeed, we found that the model fits best for $pta_C = 5.0$ and $Y_g = 0.3$, see Figure 42 (orange) for the final fit. We rename the biomass yield on acetate only Y_a, see Table 6.

To fit the data of the acetate specialist with a plasmid carrying *acs* (blue dots in Figure 42), we set $Y_a = 0.3$ and left acs_C and the initial biomass free. We found that the data fitted best for $acs_C = 0.8$. The data and the model of the glucose specialist are shown in black in Figure 42 for comparison. The black line is not a model fit but a simulation of the model with a starting biomass concentration of 0.012 gDW/L and the biomass yield set to $Y_a = 0.3$.

To fit the cycling model to the data of the acetate specialist growing on glucose, we left k_{gC} and the initial biomass concentration free, and found $k_{gC} = 0.5$. The fit result is shown in Figure 43 in red. The glucose specialist data and model fit are shown for comparison. For this fit, only the initial biomass concentration was re-estimated.

In conclusion, we can fit the cycling model to the data of the glucose and acetate specialists growing on individually on acetate by setting $Y_a = 0.3$ and adapting pta_C and acs_C depending on the acetate uptake system that is overexpressed by the acetate specialist. We can fit the cycling model to the data of the acetate specialist growing individually on glucose by decreasing the maximal glucose uptake rate k_g as compared to the glucose specialist.

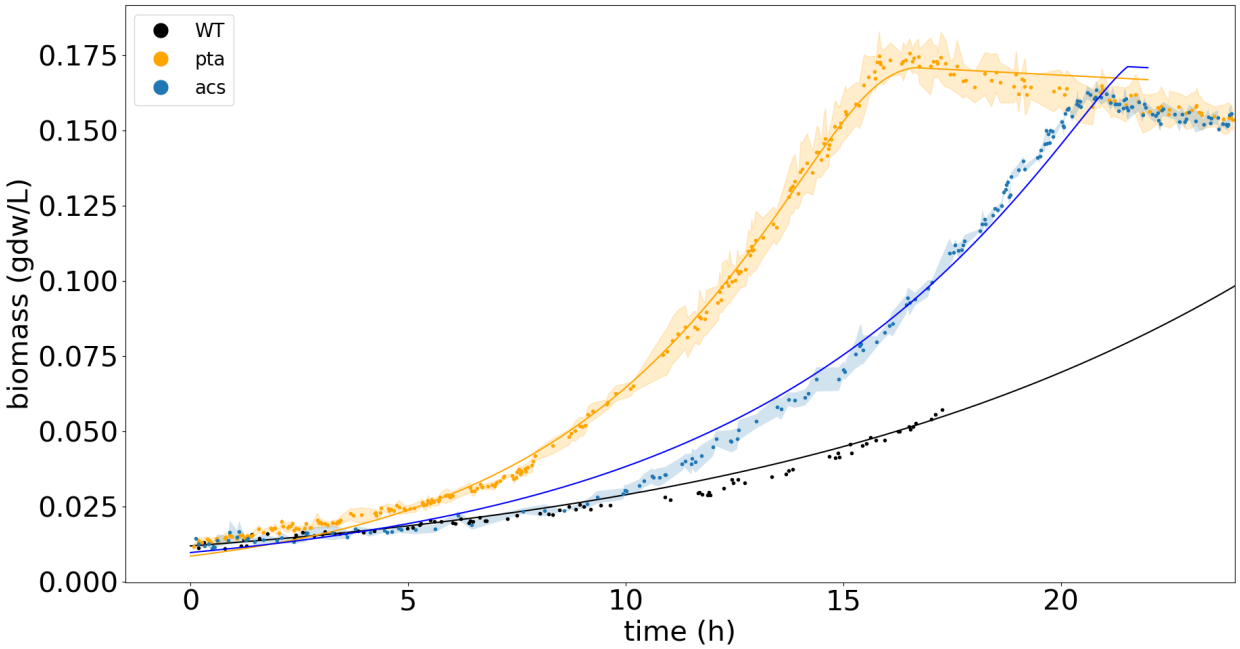

Figure 42: Fit of the cycling model with the data of the acetate specialists carrying Pta-AckA (yellow) or Acs (blue) on a plasmid, as well as the glucose specialist (black), grown in batch on 0.56 g/L of acetate. The strain carrying the Acs plasmid was grown with the addition of IPTG to induce gene expression (see Section 2.3.1 for details). The dots indicate the mean data, the shaded region shows the SEM. The orange and blue lines refer to the model fits, while the black line is a model prediction from these fits.

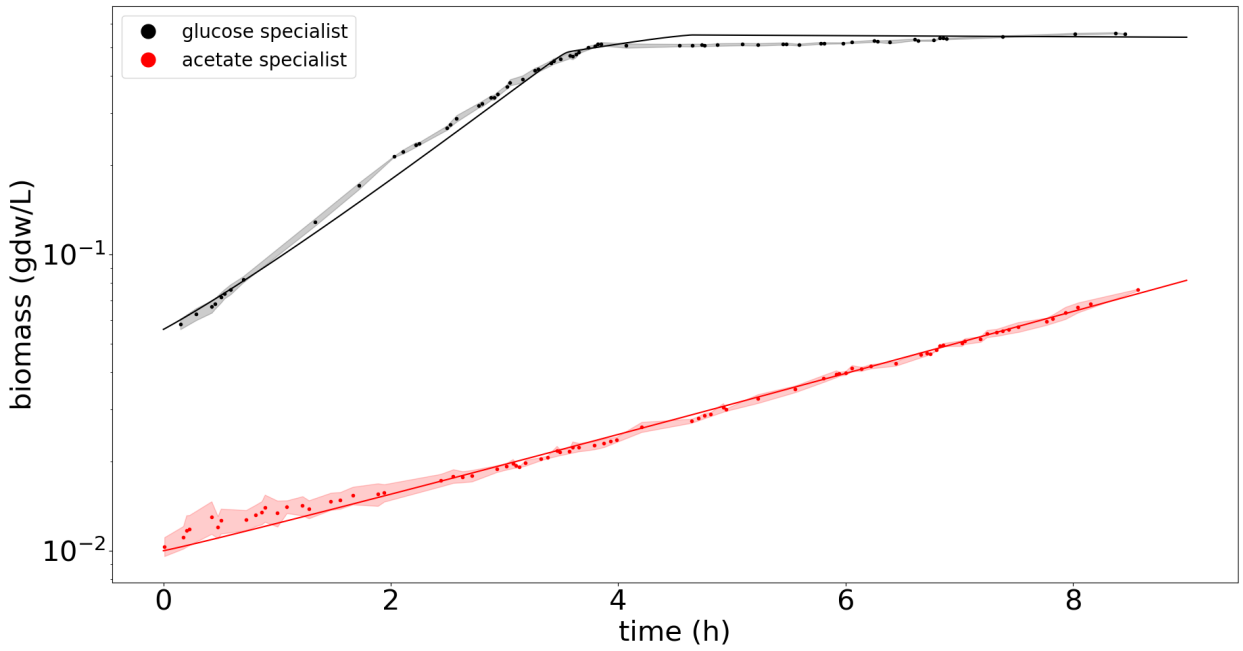

Figure 43: Fit of the cycling model with the data of the glucose and the acetate specialist during individual batch growth on 1 g/L glucose. The dots indicate the mean data, the shaded region shows the SEM. The lines refer to the model fits.

2.6.7 Predicting coexistence with the cycling model

We now have a cycling model that can explain our and others' experimental data. To evaluate whether the cycling model could predict coexistence at low dilution rates, as suggested by the results in Figure 35, we carried out the same numerical analysis as for the threshold model (Section 2.5.2): we ran the cycling model numerically at different dilution rates and looked at the steady-state concentration of glucose and acetate specialists in the reactor. We used $G_{in} = 1\,\mathrm{g/L}$ and started with 0.1 gDW/L of each strain. We simulated 100 hours of chemostat. For this analysis, we looked at three different consortia, namely the glucose specialist together with three different acetate specialists: The acetate specialist overexpressing the Pta-AckA pathway ('Pta'), the acetate specialist overexpressing Acs ('Acs'), and the acetate specialist without any overexpression of acetate uptake ('Basic'). The parameters for these three types of acetate specialist are shown in Table 7.

Table 7: Parameters used for the acetate specialist to evaluate coexistence with the glucose specialist. The rest of the parameter values are given in Section 2.6.4

Acetate specialist	pta_C	acs_C
Acs	1.0	0.8
Pta	5.0	0
Basic	1.0	0

Our cycling model predicts that the Acs acetate specialist can coexist with the glucose specialist at low dilution rates, see Figure 44. The consortia with the other two acetate

specialists no longer contained any acetate specialist in the chemostat after 100 hours of coculture with the glucose specialist (figures not shown). Figure 44 shows that the model predicts coexistence of the Acs consortium between the low dilution rates of 0.10 and 0.20h^{-1}. Interestingly, this coexistence is possible despite a net zero acetate overflow by the glucose specialist (green dotted line): The acetate specialist has access to extracellular acetate since the glucose specialist's acetate secretion rate is equal to its acetate uptake rate but is not zero. Evidently, the additional acetate uptake by Acs enables the acetate specialist to take advantage of the available acetate and increase its growth rate. As a result, its growth rate is closer to the dilution rate, so it is not flushed out as it would be when growing only on glucose.

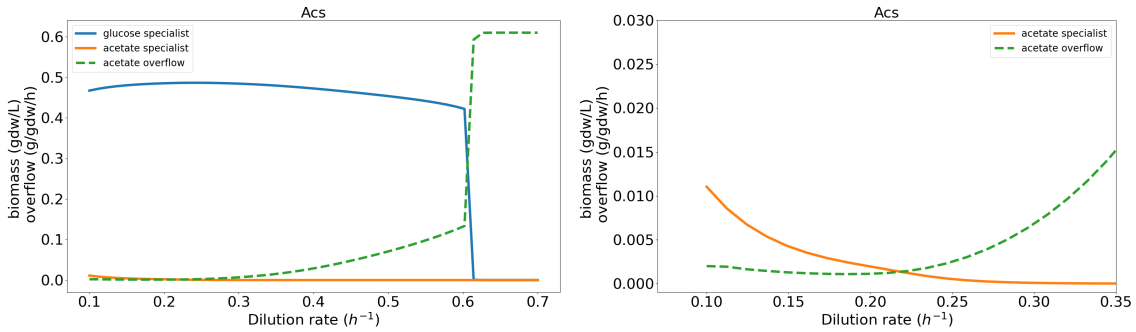

(a) (b)

Figure 44: 44(a) Predicted steady-state concentration of the Acs acetate specialist and the glucose specialist in a co-culture, as a function of dilution rate, predicted by the cycling model. For the acetate specialist, $pta_C = 1$, $acs_C = 0.8$ (see Table 7). The model predicts coexistence between D=0.1 and D=0.2. Green dotted line: net acetate secretion by the glucose specialist in the consortium. 44(b) shows an insert of the region between 0.1 and 0.35h^{-1}.

To understand better why coexistence of the consortium is predicted to be possible according to the cycling model when the acetate specialist overexpresses Acs, but not when it overexpresses Pta-AckA or when it does not overexpress an acetate uptake system, we looked at the dynamics of four different community models at D=0.15 h^{-1} on glucose. We looked at the cycling model with three different parameter settings for the acetate specialist (see Table 4) as well as the threshold model for comparison, see Figure 45. The figure shows the predicted dynamics of the concentration of acetate specialist (upper panel) in the consortium, as well as the predicted acetate uptake rate by the acetate specialist (lower panel).

First of all, we see that the simulation with the Acs acetate specialist (red) is actually not yet in steady-state. It seems that the acetate specialist will eventually be flushed out, but the flush-out is substantially slowed down, to the extent that the slow flush-out is hard to distinguish from a steady-state at a low biomass concentration.

Furthermore, we notice that even an acetate specialist without any overexpression of an acetate uptake system (green) is predicted to be taking up acetate (lower panel) and thereby slowing down its flush-out. Remarkably, the cycling model predicts that the Pta acetate specialist (orange) is actually flushed out faster than the other two acetate specialists,

because in the long run, the overexpression of Pta-AckA leads to enhanced acetate overflow instead of uptake (lower panel; the acetate uptake rate is negative). As expected, the threshold model (blue) predicts no acetate overflow by the glucose specialist at this dilution rate. As a result, the acetate specialist is not predicted to take up any acetate and is flushed out of the chemostat quickly.

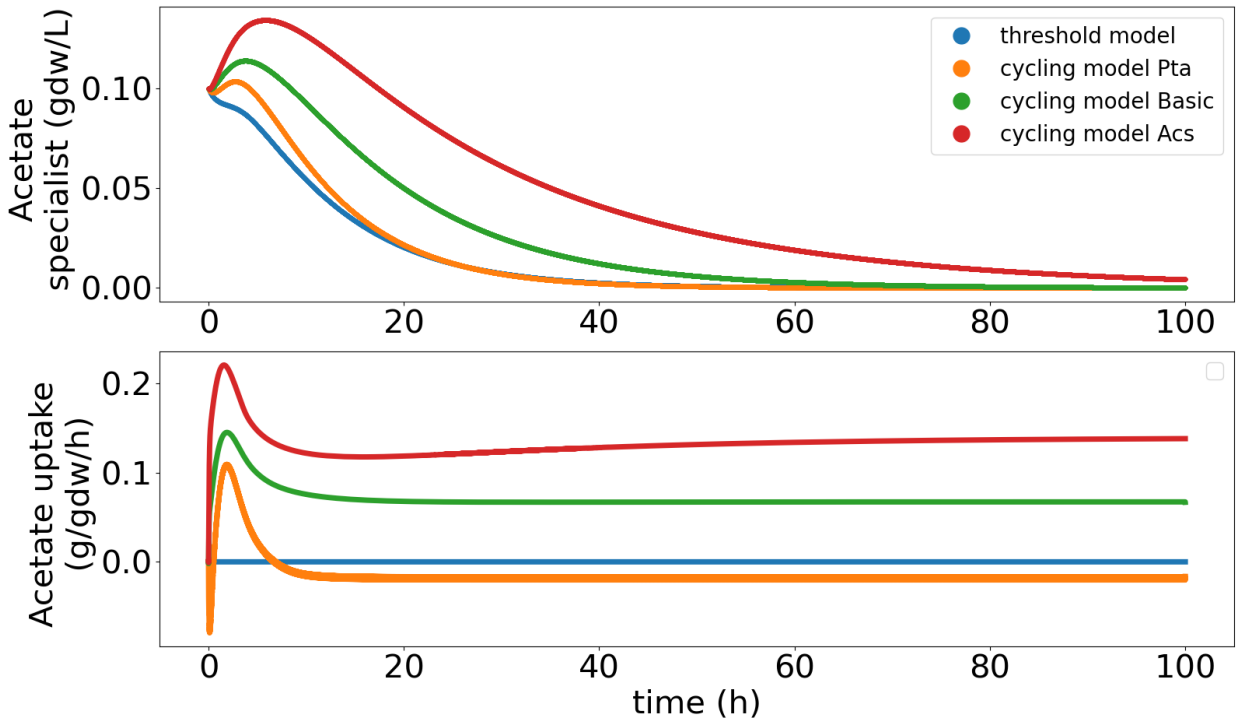

Figure 45: Upper panel: Dynamics of the acetate specialist concentration in the consortium growing in a chemostat with only glucose in the inflow, predicted by four different models. For all of the models, $D = 0.15$, $G_{in} = 1$, starting concentrations of both strains is $B = 0.1$. Lower panel: net acetate uptake by the acetate specialist (uptake minus secretion) for the same simulations. A negative net acetate uptake rate corresponds to a net overflow of acetate.

In summary, we explained in Section 2.5.2 that the initially proposed threshold model does not predict coexistence of the consortium at steady-state, regardless of the dilution rate. In Section 2.5.3 we showed that, in contrast with the model predictions, the consortium does seem to get close to coexistence when grown in a chemostat on glucose in our bioreactor system at low dilution rates. This discrepancy led us to suggest a cycling model of acetate metabolism in this section that allows for acetate excretion by the glucose specialist at low dilution rates. In this section, we outlined the model and showed that it can be parameterized to correspond with data from the literature as well as data generated in our lab (Section 2.6.5 and 2.6.6). We showed that, although the cycling model does not predict coexistence of the consortium in steady-state either, it does allow for substantially slower flush-out of the acetate specialist, to the point where it is hard to distinguish from a steady-state at low biomass concentration. Surprisingly, according to the cycling model, there will be a significant difference in the rate at which the acetate specialist is flushed out depending on

whether an enzyme is overexpressed (Acs, Pta-AckA, or none at all, see Figure 45). In the following section, we will investigate whether these predictions correspond to the data.

2.7 Investigating the community at D=0.15

In Section 2.5.3 we showed that the acetate specialist is able to coexist with the glucose specialist for 10 residence times at $D = 0.15\text{h}^{-1}$. This was in disagreement with the modelling predictions from our initial threshold model of acetate metabolism (Section 2.5.2). In an attempt to resolve this disparity, in Section 2.6 we proposed a cycling model of *E.coli* glucose and acetate metabolism that allows for acetate excretion by the glucose specialist at low dilution rates. This cycling model was successfully parameterized, and led to two main predictions: first of all, the acetate specialist could coexist with the glucose specialists at low dilution rates, but not at high ones. Secondly, the model predicts a difference in flush-out rate depending on the acetate uptake system that is over-expressed. The first prediction was already confirmed in Section 2.5.3. In this section, we assess the cycling model's second prediction: do we find a difference in the flush-out rate between different acetate specialists in our data, as the model predicts?

To answer this question, we let the consortium grow in our bioreactor system at the low dilution rate of $D = 0.15\text{h}^{-1}$. We did this experiment with three different acetate specialist strains: one without any plasmid (Basic), one carrying the Acs uptake system on a plasmid (Acs) and one carrying the Pta-AckA pathway on a plasmid (Pta). Figure 46 shows the result of this experiment. The figure shows both the data (solid line and points) and the model predictions (dashed line).

To find the model predictions, we fitted the models' initial conditions as well as a constant f relating the acetate specialist biomass to its red fluorescence. The initial conditions affect the shape and height of the initial 'bump' in red fluorescence, but not the decay rate. This is because the initial concentration of acetate and glucose in the reactor, as well as the initial concentration of internal metabolites, enable the acetate specialist to grow at a faster rate than it can under conditions of residual extracellular metabolite concentrations. Once the excess acetate and glucose are consumed, the red fluorescence starts decaying at a rate independent of the initial conditions.

As can be observed in Figure 46, the difference between the three acetate specialists is not as big in the data as in the model prediction. Rather, it seems that the dynamics of all acetate specialists are close to the model prediction for an acetate specialist without plasmid (Basic). Especially when comparing the flush-out rates in log scale (Figure 46(a)), we see clearly that the decay of the acetate specialist predicted by the Pta model is too fast, whereas the decay of the Acs model is too slow. It seems that, in the chemostat, the plasmids overexpressing the acetate uptake enzymes do not affect the acetate specialist in the way that was predicted by the batch results (Section 2.6.6) and the model (Section 2.6.7). One possible explanation could be that the acetate specialist loses the plasmid with the overexpression system during the experiment. This was falsified; we isolated the acetate specialist after a bioreactor experiment of 70 hours and showed that it still had an improved growth rate on acetate as compared to the WT, see Figure S6. We will discuss other possible reasons for this discrepancy between the cycling model predictions and the data in the Discussion (Section 3).

In conclusion, the data do not show a big difference between the three acetate specialists, in terms of how quickly they are flushed out of the chemostat at $D = 0.15\text{h}^{-1}$. In these conditions the three strains seem to be represented best by the Basic model that supposes

no overexpression of an acetate uptake system.

In the next section, we will discuss further long-term stabilization of our chemostat experiments.

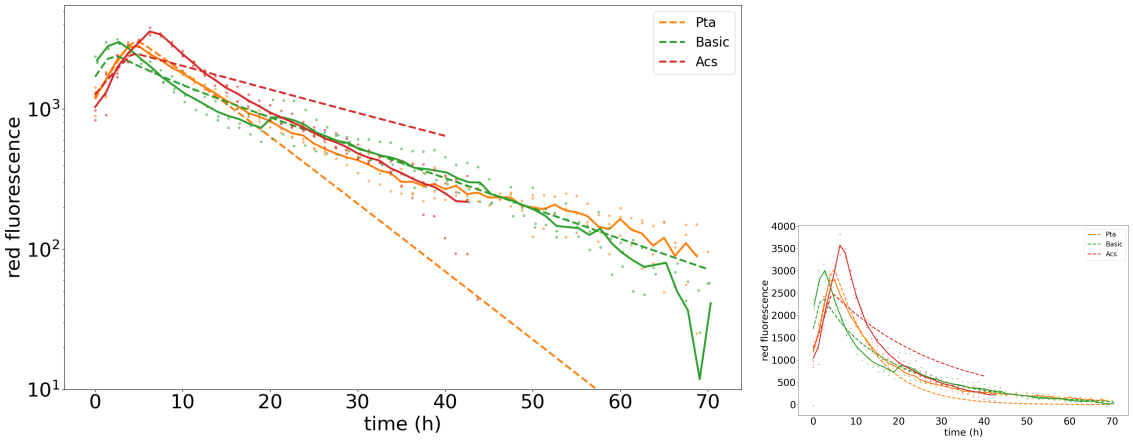

(a) (b)

Figure 46: Decay of the red fluorescence in the consortium grown at $D = 0.15\text{h}^{-1}$ in a chemostat in minimal medium with 1 g/L glucose, compared to the model prediction, in log-scale (a) and linear scale (b). Lines: mean red fluorescence of 3 bioreactors monitored during the experiment. Dots: red fluorescence in individual bioreactors. Dashed lines: prediction by the three different cycling models. For the model predictions, we fitted the models to their respective data-sets: parameters were left unchanged, but initial conditions and the constant f relating acetate specialist biomass and red fluorescence were left free.

2.8 Further improvements of long-term stability

In the previous sections we showed that the acetate specialist can coexist with the glucose specialist for 10 residence times in our bioreactor platform at $D = 0.15\text{h}^{-1}$. We showed that this is best explained by a cycling model of acetate metabolism, as opposed to the previously proposed threshold model. One observation from our research that piqued our interest and that we wanted to investigate further, was the variation in the biomass concentration at steady-state, see Figure 35 and Section 2.5.3. Because this variation seemed to correlate with the dilution rate, we hypothesized that the biomass yield of our strains was increasing as the dilution rate increased. However, we did not have a satisfying explanation as to why this would be case. Following the observation that the cultures tended to become less homogeneous and more clumpy towards the end of the culture period, we speculated that the cultures suffered from a contamination after a long experiment at a low dilution rate.

To test this hypothesis, we decided to do a negative control: we added antibiotics to the culture medium to prevent contamination and observed the biomass concentration at steady-state for a low dilution rate of $D = 0.15\text{h}^{-1}$. If contamination is indeed the cause of the lower biomass plateau, the latter should increase after contamination is eliminated by the addition of antibiotics.

In this section, we first show that the addition of antibiotics leads to a more stable culture of the acetate specialist grown individually in the chemostat (Section 2.8.1). Then, we show that the addition of antibiotics to the consortium leads to a more stable and higher total biomass plateau (Section 2.8.2). Finally, we show that the addition of antibiotics alters the flush-out dynamics of the acetate specialist, but that it still manages to coexist with the glucose specialist in these conditions and even recovers some biomass at the end of the experiment, probably thanks to a mutation in its glucose uptake system (Section 2.8.3).

2.8.1 Stabilizing the acetate specialist with antibiotics

As a first test to examine whether we can improve long-term stability of the culture by preventing contamination with antibiotics, we grew the acetate specialist in glucose individually, with the addition of kanamycin to the inflow. As explained in Section 2.1, the acetate specialist carries a kanamycin resistance gene in the place of its glucose uptake system, so it should be resistant to the antibiotic while possible contaminants will be impeded to grow. The result of this test is shown in Figure 47.

It is clear that, without antibiotics, the biomass steady-state varies between bioreactors and is not very stable. More importantly, the red fluorescence diminishes after the biomass steady-state has been reached, indicating that some contaminant lacking a red fluorescent protein on its chromosome is taking over the culture (Figure 47(a)). The presence of a contaminant was confirmed by plating (Figure S4) and flow cytometry (Figure S5). When we added antibiotics, on the other hand, the red fluorescence, as well as the biomass, stayed in steady-state for 60 hours (Figure 47(b)). This result implied strongly that contamination could, in the long run, disturb our experiments during chemostat growth at the low dilution rate, and that the addition of kanamycin could solve this issue. Therefore, we decided to grow the consortium in the presence of antibiotics as well, to see if this would impact its growth dynamics.

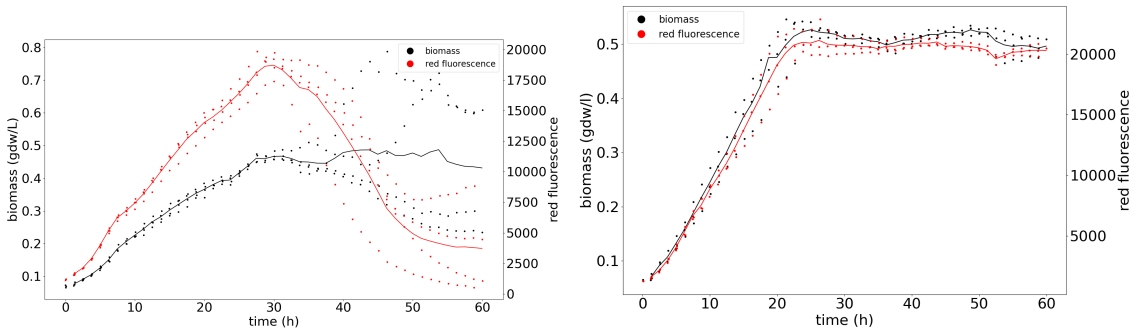

(a) (b)

Figure 47: Dynamics of biomass (black) and red fluorescence (red) in an individual acetate specialist culture grown at $D = 0.15\text{h}^{-1}$ in 1 g/L glucose, without (a) and with (b) the addition of antibiotics. The lines represent the mean of 4 technical replicates, whose values are indicated by the dots.

2.8.2 Stabilizing the consortium with antibiotics

Since we showed in the previous section that antibiotics can help to stabilize the growth of the acetate specialist, we wanted to try and add antibiotics to the consortium as well, to see if this could impact the results previously obtained. Our acetate specialist contains a gene expressing kanamycin resistance, but our glucose specialist was not resistant to any antibiotics. Therefore, instead of our glucose specialist, we used a strain previously constructed in the lab by PhD student Antrea Pavlou: a WT carrying a plasmid expressing GFP and kanamycin resistance. Except for the presence of the plasmid and the lack of mCeruleanME on the chromosome, this strain was identical to our glucose specialist. In this section, we will therefore refer to it as the glucose specialist. As an acetate specialist we used the strain overexpressing Pta-AckA. So, we grew the acetate specialist and the kanamycin resistant glucose specialist together in a chemostat in glucose at $D = 0.15\text{h}^{-1}$. Figure 48 shows the results (red) as well as a comparison with the experiment in the same conditions but without antibiotics (orange).

Three conclusions are apparent from this comparison. First of all, the concentration of biomass in steady-state has increased by the addition of antibiotics. This suggests that the decreased biomass plateau at low dilution rates as observed in Section 2.5.3 might have been caused by a contamination. Second of all, we notice that despite the suspected presence of a contamination, the decay of red fluorescence is comparable with and without the addition of antibiotics. The total red fluorescence in the antibiotics culture is somewhat lower but the slope of its decay is similar.

The third, most striking observation from Figure 48 is that in the culture with antibiotics the red fluorescence starts to increase for three out of four bioreactors after about 45 hours of culture. In the next section, we discuss an experiment we did to investigate the origin of this surprising increase of red fluorescence, corresponding to an increase of the concentration of the acetate specialist.

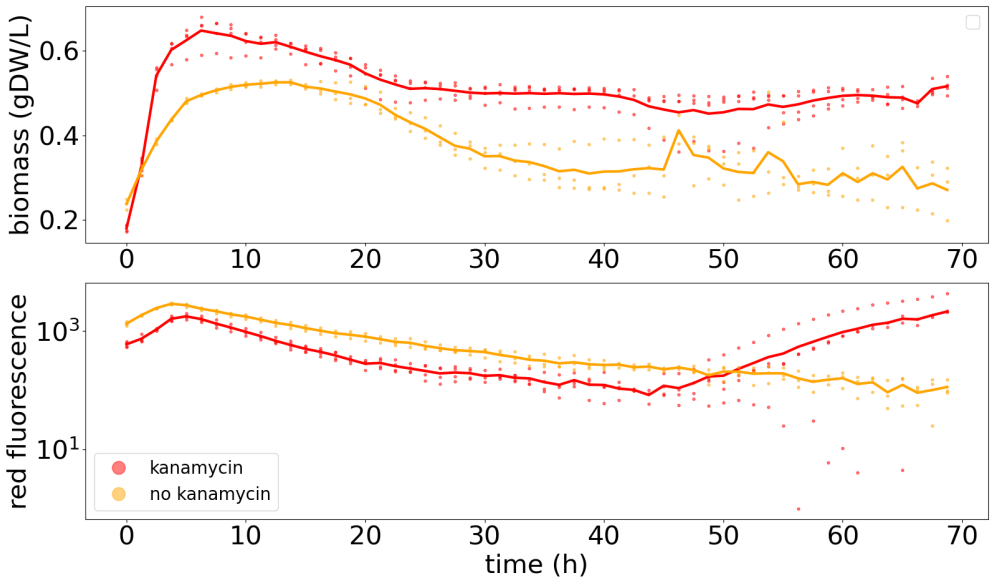

Figure 48: Dynamics of biomass (upper panel) and red fluorescence (lower panel) in the consortium grown at $D = 0.15\text{h}^{-1}$ in 1 g/L glucose, with and without the addition of antibiotics. The lines represent the mean of 3-4 technical replicates, whose values are indicated by the dots.

2.8.3 Acetate specialist adaptation in the coculture

As shown in Figure 48, the acetate specialist managed to increase its biomass after about 50 hours of decay in the chemostat. We wondered whether this was possible because the acetate specialist had improved its growth rate on either glucose or acetate. To answer that question, we examined the strains present in the bioreactor after the experiment in Figure 48.

Since we did the same experiment in 4 bioreactors, we took the culture medium from the bioreactor which seemed to contain the highest amount of acetate specialist. To separate the glucose and acetate specialists, we plated the culture on M9 agar plates with glucose. The two strains form colonies of different sizes on these plates: the acetate specialist colonies are smaller than the glucose specialist colonies (see Figure S7). We made cultures from the small colonies and compared their growth rate in acetate and glucose to the growth rate of the strains with which we had started the bioreactor experiment. If the acetate specialist had improved its growth rate on one of these carbon sources during the chemostat experiment, we should see a difference between the growth rate of the original acetate specialist and the acetate specialist isolated after the chemostat experiment.

Figure 49 shows that the isolates have indeed improved their growth on glucose as compared to the original acetate specialists: their growth rate is now about 1.5 higher. We hypothesize that this is thanks to a mutation in one of the acetate specialist's non-specific glucose uptake systems: although we knocked out its main glucose uptake system, PtsG, the acetate specialist still has ways to take up glucose that could potentially be improved by advantageous mutations.

This adaptation is an indication that the acetate specialist is adapting to chemostat

growth by improving its glucose metabolism, allowing it to compete for resources with the glucose specialist. Presumably, the improved growth on glucose in combination with acetate cross-feeding are allowing the cleaner to recover some of its biomass. In conclusion, we showed in this section that antibiotics can improve the long-term stability of the consortium. This improved stability allowed us to uncover that the acetate specialist can improve its growth on glucose during long-term chemostat growth in the community. Ways to investigate this adaptation further are suggested in the Discussion in Section 3.3.2.

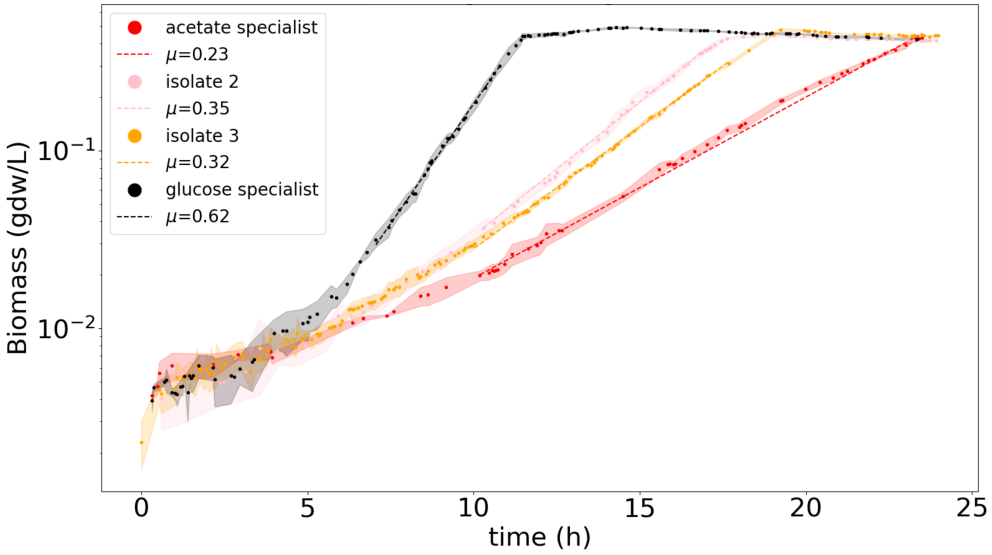

Figure 49: Isolates of the acetate specialist taken after the consortium bioreactor experiment in Section 2.8, grown on 1 g/L glucose in a plate-reader (pink and yellow). They have a higher growth rate than the acetate specialist before the experiment (red), but lower than the glucose specialist (black). Dots indicates the mean of three technical replicates. Shaded region signifies the SEM. The growth rates of the strains are given in the legend in h^{-1}

3 Discussion

> Living beings defy neat definition. They fight, they feed, they dance, they mate, they die. At the base of the creativity of all large familiar forms of life, symbiosis generates novelty. It brings together different life-forms, always for a reason.
>
> Lynn Margulis

3.1 Main results

In this PhD thesis, we aimed to investigate cross-feeding in an *E.coli* consortium. Specifically, we examined a consortium in which one strain, the glucose specialist, would grow on glucose and excrete acetate while a second strain, the acetate specialist, would grow poorly on glucose but profit from acetate excreted by the glucose specialist, as proposed by our group in previously published research [24]. We sought to grow the consortium in a chemostat and investigate the conditions of coexistence of this consortium: is there a dilution rate at which both strains can coexist stably? We were interested in studying the impact of acetate cross-feeding on the coexistence of the consortium: could acetate cross-feeding stabilize the growth of the consortium? How does the acetate specialist affect the growth of the glucose specialist and vice versa?

To answer these questions we first constructed a glucose specialist and an acetate specialist strain with the desired properties, see Section 2.1. We added fluorescence proteins to the strains in order to be able to track them in the consortium. We knocked out a key gene of the acetate specialist's main glucose uptake system (*ptsG)* and improved its growth on acetate by adding plasmids expressing either *acs* or *pta-ackA*. We made the strains resistant to phage infections by knocking out *fhuA*.

In Section 2.3 we showed that the constructed strains have the properties desired for a potential cross-feeding interaction: The glucose specialist excretes acetate during growth on glucose, and the acetate specialist has a reduced growth rate on glucose but an increased growth rate on acetate.

In parallel, in order to grow the consortium, and experimentally characterize its interaction dynamics, we developed a custom-made, automated platform of mini-bioreactors (Section 2.2). We developed hardware as well as software to run experiments (Section 2.2.1), developed an experimental protocol (Section 2.2.2), designed calibration and processing procedures for the bioreactor data (Section 2.2.3), and improved the long-term stability of chemostat experiments (Section 2.2.4). The platform can now be used to grow cultures under sterile conditions for several days and monitor their absorbance and fluorescence by spectrometry as well as by flow cytometry.

In order to quantify the growth of the individual strains we used a model previously proposed by our group. This model describes *E.coli* growth on glucose and acetate overflow

metabolism by means of a threshold for acetate excretion; acetate is supposed to be excreted during growth on glucose above a certain glucose uptake rate. We found that this model could be fitted to data of the acetate and glucose specialist growing individually in batch experiments with glucose and acetate (Section 2.4). Analysis of the parameterized threshold model showed that it predicted no coexistence of the glucose and acetate specialists in the chemostat at steady-state, regardless of the dilution rate (Section 2.5). This was explained by the model's assumptions about acetate overflow; no acetate overflow is predicted by the model at low dilution rates, whereas at high dilution rates acetate is excreted, but the dilution rate is too high for the acetate specialist to grow. In contrast to the model predictions, we found experimentally that the consortium seems to coexist for extended periods of time at low dilution rates; the acetate specialist stays in the reactor for at least 10 residence times (Section 2.5.3).

This discrepancy between the threshold model and the data made us reconsider the modelling assumptions of the threshold model. The threshold model supposes that there is no acetate exchange at low dilution rates; both strains grow only on the glucose fed into the reactor. As the acetate specialist has a lower growth rate than the glucose specialist on the low glucose concentrations in the bioreactor, it is predicted to be diluted out of the reactor in the long term. However, since the flush-out rate of the acetate specialist at low dilution rate was lower than predicted by the model (at $D = 0.15\text{h}^{-1}$ the acetate specialist concentration even seemed to reach a non-zero steady-state), we suspected that acetate was being exchanged between the glucose and the acetate specialists, allowing the acetate specialist to coexist with the glucose specialist. Since acetate exchange at low dilution rates was in disagreement with the threshold model, we proposed a different model for glucose and acetate metabolism, that we called the cycling model (Section 2.6). In contrast to the threshold model, the cycling model assumes that the acetate overflow is the net result of three gross acetate fluxes: the acetate secretion by Pta-AckA, the acetate uptake by Pta-AckA and the acetate uptake by Acs. The balance between these three fluxes is determined by the concentration of intracellular metabolites and extracellular acetate.

The cycling model was fitted to data from the literature as well as data from our lab (Section 2.6.5 and 2.6.6). The calibrated cycling model predicted that, at low dilution rates, the balance between the three gross acetate fluxes was such that the net acetate overflow was zero. At higher dilution rates, the acetate secretion by Pta-AckA exceeds the uptake by Pta-AckA and Acs, leading to a net acetate overflow. Together, this model results in an apparent acetate overflow threshold: above a certain dilution rate, there is a net acetate overflow, but even at low dilution rates, acetate is excreted and re-taken up by the cells. For the consortium grown in a chemostat, the cycling model predicts that the acetate excreted by the glucose specialist at low dilution rates can be taken up by the acetate specialist, thereby resulting in a net flow of acetate from the glucose specialist to the acetate specialist and slowing down the flush-out of the acetate specialist substantially (Section 2.6.7). As such, the cycling model is better at predicting the dynamics of the consortium than the threshold model at low dilution rates.

In conclusion, the consortium investigated during this thesis is able to coexist at low dilution rates but not at high ones. Our modeling results suggest that coexistence is possible thanks to the continuous cycling of acetate in and out of glucose specialist cells: This acetate can be taken up by the acetate specialist to increase its growth rate in the chemostat.

The results highlight the importance of studying consortia as opposed to individual strains; the study of the consortium allowed to identify possible acetate cycling at low dilution rates that is not apparent in a single strain but that we detected because the acetate cycling affected the properties of the consortium. At the same time, this thesis stresses the importance of modeling and a clear understanding of model assumptions: Since our model assumption of a threshold for acetate excretion did not predict coexistence correctly, we reconsidered this assumption and obtained an improved insight in the possible interactions between strains in an *E.coli* consortium growing on glucose in a chemostat.

Importantly, our latest results indicated that in the long-term, the acetate specialist in the consortium is adapting its metabolism to growth in the chemostat: we found that the acetate specialist improved its maximum glucose uptake rate which allowed it to regrow in the reactor starting from a low biomass concentration (Section 2.8.3). This improvement is not due to regulation, but to genetic changes (in the same microplate conditions, this acetate specialist grows faster on glucose than the acetate specialist used to start the experiment). In addition to the importance of modeling assumptions, this research therefore emphasizes that a bacterial consortium consists of living material that may evolve over time, and challenge modeling results in this sense.

3.2 Difficulties

In this section, we discuss some difficulties encountered during this thesis project and their possible solutions. In Section 3.2.1, we discuss properties of our strains that we found were not optimal or different from expectations. In Section 3.2.2 we discuss challenges in measuring the different variables in our experiments: metabolite concentrations, measurements of fluorescence, and flow cytometry measurements. In Section 3.2.3 we discuss the challenge of long-term stability in our chemostat experiments due to phage infections, contamination, and mutations. Finally, in Section 3.2.4, we touch on the parameterization of our models and to what extent we are confident about our fitted parameter values.

3.2.1 Strains

We aimed to investigate the cross-feeding of acetate in an *E.coli* consortium with properties previously proposed by Mauri et al. [24]. We managed to implement most of these properties in our strains using molecular biology techniques, see Section 2.1. However, we encountered some difficulties during the constructions and the experimental characterization of the strains that are recounted in this section.

One problem that we encountered during the constructions is that we did not manage to remove the kanamycin resistance gene from our acetate specialist (see Section 2.1.2). We replaced *ptsG* in the acetate specialist by a kanamycin cassette flanked by two FLP recognition target (FRT) sites. In theory, these sites could then be used to remove the cassette using FLP recombinase [72]. For unknown reasons (potentially a defect in the FLP recombinase plasmid) we did not manage to perform this recombination, so the kanamycin cassette is still present in our acetate specialist. We showed that the acetate specialist still had the required properties and we reasoned that the kanamycin resistance might in fact be useful for isolation of the acetate specialist from the consortium.

To allow the acetate specialist to cross-feed on acetate, we had to construct a plasmid carrying an overexpression of the acetate uptake system. We constructed two plasmids, of both the Pta-AckA and the Acs pathway under the control of an IPTG inducible promoter, by Gibson assembly (Section 2.1.3), and we showed that both plasmids could be used to increase the acetate uptake rate of the acetate specialist in batch (Section 2.3.1). However, we found that the strains carrying the Pta-AckA plasmid displayed the same increased acetate uptake both with and without addition of the inducer IPTG. For the other uptake system, Acs, addition of IPTG did lead to higher acetate uptake rates, see Figure 25. We hypothesize that, in the case of Pta-AckA, the leaky expression of the enzyme is enough to achieve the maximum growth rate on acetate. The addition of IPTG to the cells carrying the Pta-AckA plasmid leads to more expression of the Pta-AckA enzyme but the cell cannot grow faster on acetate than it already does, likely due to downstream constraints in the cell or due to limits in active transport of acetate into the cell [103]. In the case of Acs on the other hand, it seems that the leaky expression is not increasing the acetate uptake much. More overexpression is needed to maximize the acetate uptake rate. This result also indicates that, even if we managed to express more Pta-AckA or Acs enzymes, this would not increase the cells' growth rate on acetate since it seems that acetate cannot currently be used faster by the cells potentially due to downstream limits in the their acetate metabolism, or due to limits in active transport of acetate into the cell.

Although we showed that, in batch culture on acetate, the plasmids are increasing the growth rate of the individual acetate specialist on acetate, in the consortium in chemostat we did not observe a difference in growth rate between the different acetate uptake plasmids and the acetate specialist without a plasmid (Section 2.7, Figure 46). One reason for this could be that the acetate uptake systems are not effective enough in the bioreactor to have an effect on the acetate uptake rate. Ways to improve the acetate specialist's growth rate on acetate are discussed below in the Perspectives.

Another reason why addition of a plasmid for additional acetate uptake does not seem to make a difference in our consortium could be that there is no, or not enough, acetate available to the acetate specialist for changes in its acetate metabolism to have a sufficient impact on growth. Indeed, while our experiments support the presence of acetate cycling, we have no direct measurement of acetate exchange, since in both presence or absence of this cycling the residual acetate concentration in the culture would be nearly zero. To confirm the relevance of the acetate cycling model, it would be important to have a more direct proof of acetate secretion at the growth rates of interest. Additional ways to validate that acetate cycling is happening and relevant in our consortium are proposed in the Perspectives.

3.2.2 Measurements

To monitor the growth of the consortium in the bioreactor, we measured the variables of our system using different measurement techniques, see Section 2.2.3. To determine the total cell concentration of the culture, we quantified its optical density. To monitor the growth of the two individual strains, we marked them with a fluorescent protein on the chromosome (Section 2.1.1). Using the total fluorescence from one strain, we can also calculate the concentration of each of the two strains. A second way to quantify the concentration of each of the two strains is by flow cytometry. With this method, we can detect the fluorescence of

individual cells and, by counting the cells displaying a given fluorescent marker, determine the the relative species abundance in the consortium. Lastly, we can estimate the extracellular concentration of glucose and acetate using an enzyme kit, see Section 4.8 for the technical details. In this section, we recount the challenges that we encountered with some of these measurement techniques.

To measure the concentration of the two strains in the consortium, we marked the glucose specialist with the blue fluorescent protein, mCerulean-ME, whereas we marked the acetate specialist with a red fluorescent protein, mScarlet-I. We could detect the emission by both proteins in the spectrometer, but we noticed that the cells give a significant blue background emission at the same wavelength as mCerulean-ME. This background fluorescence is probably due to flavins secreted by the cells into the medium [104].

In a monoculture, the background fluorescence can be subtracted by growing a control culture without a fluorescent protein in the same conditions. In a consortium, however, it is more complicated to estimate how much fluorescence comes from the fluorescently labeled glucose specialist, and how much derives from the flavins secreted by the two strains in the consortium. We attempted to monitor the blue background fluorescence in order to find a pattern that could be modeled and subtracted from the total fluorescence, but we have not yet found a way to reliably model the dynamics of the background fluorescence (see Figure S10).

Therefore, to monitor the individual strains in the consortium, we made use mostly of the red fluorescent protein mScarlet-I. The cells do not produce any red background fluorescence. However, mScarlet-I does come with an additional challenge, which is its maturation time [93]. Since mScarlet-I has a maturation time of 20 minutes (meaning that it takes 20 minutes for half of the proteins to mature), the red fluorescent protein observed at a certain time does not correspond exactly to the amount of gene transcribed at that time. In dynamic experiments, this has to be taken into account if one wants to relate the red fluorescence to the cell concentration; the response of the red fluorescence is delayed with respect to the cell concentration.

During this thesis, we did some (unreported) work on modeling this maturation properly, using the methods from Pavlou et al. [93]; this work needs to be extended in the future if we want to use the red fluorescence as a reporter for cell concentration in dynamic conditions. However, in the current study, we were primarily interested in the achievement of steady-states, so dynamics as fast as the 20-minutes maturation time were not of concern. Therefore we can assume that the red fluorescence relates approximately linearly to the acetate specialist concentration. Moreover, we use flow cytometry as a complementary method to monitor the fraction of acetate specialists. This method also makes use of the cells' red fluorescent label, but it is not affected by the protein's maturation time since it detects the presence or absence of a fluorescence marker in single cells as opposed to the total red fluorescence of the population.

Although we showed that flow cytometry can be used to estimate the fraction of acetate specialist in the consortium (Section 2.2.3), we encountered another problem with flow cytometry measurements; we found that dust particles present in the buffer used to dilute the culture were the same size as the cells and the two could not be distinguished from each other in the flow cytometer based on size only. This was a problem, since one of the two strains in the consortium was marked with a fluorescent protein whose wavelength could not

be detected by the cytometer.

We solved this issue in two ways. First of all, we made sure to filter the buffer through a 0.22 μm filter which led to considerably less dust particles, but did not eliminate them completely. Therefore, secondly, we ran a sample with only buffer in parallel to our measurements to quantify the concentration of dust in the buffer so that we could subtract this concentration from our samples. These solutions worked well for manual measurements, but for the automated set-up with the bioreactor we found that dust accumulated over time, which obscured our estimations of acetate specialist fraction. As a result, we decided to stick with manual flow cytometry measurements. In the future, it would be important to improve the automatic flow cytometry set-up to exclude dust particles. This could help us give more detailed information about the dynamics of the acetate specialist fraction in the consortium.

An additional variable that we could manually extract from the bioreactor experiments was the extracellular metabolite concentrations. A limitation of the enzyme assays we used to determine these concentrations, was that they were not precise enough to measure the low residual concentration of glucose and acetate in the reactor (see Section 2.3.2). Potentially, we could optimize the assay for very low concentrations by taking bigger sample volumes and making a more fine-grained calibration curve for low concentrations of acetate and glucose. Alternatively, we could use more sensitive detection methods, such as mass spectrometry [105], NMR [106], or HPLC [107]. A limitation of the metabolite measurements remains that it will be hard to automate them, since the procedure contains too many precise dilution steps and movement of a plate in and out of a plate reader. Therefore, the estimates of extracellular acetate and glucose will most likely only be used to analyze our system offline, not to monitor the culture in real-time.

3.2.3 Long-term stability

As described in Section 2.2.4, we encountered some issues with the long-term stability of the culture in the chemostat. We solved some of them but others are still work in progress. As explained in Section 2.8, contamination of the culture remains a problem at low dilution rates.

Besides the fact that these experiments are long and therefore susceptible to contaminants, we hypothesize that at low dilution rates, external contaminants can compete with the consortium more easily than at high dilution rates. We found that the dynamics of the consortium as well as the individual acetate specialist's growth were more robust after the addition of antibiotics. This made us suspect that the experiments done without antibiotics were affected by a contamination at prolonged incubation times. The results obtained in Section 2.5.3 and Section 2.7 should therefore be repeated with the addition of antibiotics. In Section 2.8.2, we compare the consortium dynamics with and without antibiotics, and show that the decay of the acetate specialist is similar in both conditions. This is a promising result in the sense that the suspected contamination does not seem to affect our findings on the dynamics of the acetate specialist in the consortium.

Besides contamination, the long-term stability of the consortium also seems to be affected by adaptation of the individual strains to the conditions. In a long-term chemostat experiment with the consortium with added antibiotics we found that the acetate specialist

increased its growth rate on glucose (Section 2.8.2 and 2.8.3). This increased growth rate seems to allow the acetate specialist to recover some biomass in the consortium, thereby increasing its biomass concentration with respect to the steady-state. It would be interesting to run the experiment shown in Figure 48 for a longer period of time to see if the consortium will eventually reach a steady-state, or whether the biomass concentrations will keep oscillating due to adaptations of the two substrains [108].

3.2.4 Model parameterization

As explained in Section 2.6.5 we determined the values of the parameters in the cycling model by fitting a number of datasets in parallel. Some datasets were taken from the literature and were generated using different *E.coli* strains than the one used for this study. Very these datasets are qualitatively similar to those that would be obtained with the strain from our lab. Quantitatively, however, there might be differences that we have not taken into account during the model fitting procedure. These differences could affect our subsequent modeling results.

Specifically, the data on carbon catabolite repression were taken from Valgepea et al. [52], who used *E.coli* K12 MG1655 as opposed to *E.coli* BW25113 as we did. The data indicate to what extent Acs expression (and thereby acetate uptake) is repressed with higher glucose uptake rates. The data and model fit of the relative Acs expression as a function of the relative dilution rate for a strain growing on glucose are shown in Figure 37. We observe that, the higher the dilution rate, the higher the glucose uptake rate, the lower the Acs expression; see Figure 50 for a schematic depiction of this trend. As observed in this figure (solid line), at low glucose uptake rates, Acs expression is predicted not to decrease; the glucose specialist growing on glucose is predicted to have the same Acs expression at $D = 0.3\text{h}^{-1}$ as at $D = 0.1\text{h}^{-1}$, despite a higher glucose uptake rate at the higher dilution rate. This also means that a strain growing on glucose alone at $D = 0.3\text{h}^{-1}$ has the same Acs expression as a strain growing on partly glucose and partly acetate at that dilution rate (compare blue and red vertical line). At higher dilution rates, in contrast, the acetate uptake rate of a strain growing on only glucose will be repressed more than the acetate uptake rate of a strain growing on a mixed substrate.

For the consortium, this balance is important; the acetate specialist could profit more from acetate cycled by the glucose specialist if the Acs expression of the acetate specialist were higher than that of the glucose specialist (see intersection of the blue and red line with the dotted line). With the current parameters, the Acs expression and, as a result, the acetate uptake rate of the glucose specialist and the acetate specialist are predicted to be equal at low dilution rates, despite the glucose specialist having a higher glucose uptake rate. It would interesting to know the true extent of carbon catabolite repression in our lab strain, so that we can parameterize it correctly in our model, and understand the effect of Acs expression and acetate uptake by both strains at low dilution rates. We hypothesize that, for our strain, the Acs expression might follow something like the dotted line in Figure 50, rather than the solid line. If this were indeed the case, the slow flush-out of the acetate specialist at low dilution rates could in part be explained by increased Acs expression of the acetate specialist as compared to the glucose specialist.

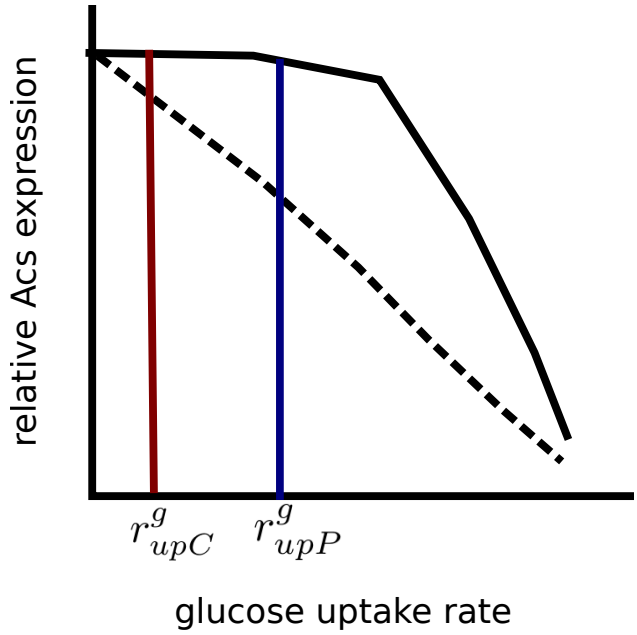

Figure 50: Schematic Acs expression as a function of glucose uptake rate. The solid black line shows an abstraction of the data by Valgepea et al. [52] (Figure 37). The dotted line shows a scenario in which Acs expression drops faster. In this scenario, the Acs expression would differ between the glucose specialist (blue vertical line) and the acetate specialist (red line).

3.3 Perspectives

In this section, we discuss further research directions that we identified during this thesis. First, in Section 3.3.1, we propose ways to improve acetate growth in the acetate specialist, in order to improve the coexistence of glucose and acetate specialists. In Section 3.3.2, we suggest ways to further investigate the adaptation of the acetate specialist as observed in the consortium. Section 3.3.3 outlines ways to continue our efforts to model the consortium of glucose and acetate specialists. In Section 3.3.4, we discuss the observed cross-feeding interaction: how to improve it, how to confirm that cross-feeding is indeed taking place and possible ecological implications. Finally, Section 3.3.5 sheds light on the opportunities and directions for feedback control of the consortium composition.

3.3.1 Improving growth on acetate

In Section 2.3.1 we showed that the acetate specialist grows faster on acetate than the glucose specialist. However, we did not find an effect of this improved growth rate in the consortium in chemostat (Section 2.7) and speculated that the improvement is insufficient (Section 3.2.1). Potentially, if we manage to improve acetate specialist's growth capabilities on acetate, this could lead to a more stable coexistence with the glucose specialist at low dilution rates. Additionally, an improved growth rate on acetate could widen the range of dilution rates at which the acetate specialist is capable of achieving steady-state growth.

There are several ways to improve the acetate specialist's uptake rate. One way would

be to put the acetate uptake systems Acs or Pta-AckA on a higher copy plasmid. This would result in more copies of the enzyme. However, as explained above, this is not likely to have an affect on the cells' growth rate, since the cells seem to be limited by a downstream bottleneck, or by a lack of acetate transporter, rather than by the acetate uptake rate itself.

An additional approach to improve the acetate uptake by the Acs enzyme, was described by Novak et al. [60]. The researchers found that Acs is not only subject to transcriptional carbon catabolite repression but also is affected by translational repression during growth on glucose, in the sense that the enzyme is acetylated during growth on glucose, making it less effective. By changing one amino acid in the enzyme, Novak et al. managed to make Acs insensitive to acetylation, thereby improving *E.coli's* acetate uptake rate during growth on glucose. This could improve the effect of the Acs plasmid in the chemostat given that the acetate specialist cells are growing on a mix of glucose and acetate in the consortium.

A third method to improve the acetate specialist's growth on acetate would be by directed evolution. By selecting the strains with the fastest growth rate on acetate we could likely not only improve the acetate uptake rate of the acetate specialist but also the downstream metabolic reactions or potentially the expression of acetate transporter. One question that we would have to consider is whether we aim to increase the affinity or the maximal growth rate of the acetate specialist. By growing the cells for a large number of generations in a chemostat with acetate we would probably increase the affinity of the cells for acetate, since this would expose them to low residual concentrations of acetate [83, 109]. For improving the maximal growth rate, however, we would need to grow the cells in a turbidostat with a feed of acetate [110]. In a turbidostat, cells have to grow at their maximal growth rate; this is done by keeping the density (turbidity) of the culture constant. If the density increases, the dilution rate is increased. If the density decreases, the dilution rate is decreased. For both long-term bioreactor experiments, we would need to take care of contaminations, potentially by adding antibiotics to the culture medium. Another risk in long-term directed evolution experiments, is that one selects not for the mutants best growing on the given substrate, but for the mutants best sticking to the walls of the reactor [107]. A way to prevent this would be to empty and rinse the reactors periodically.

3.3.2 Investigating the adaptation of the acetate specialist

In Section 2.8.3 we showed that, after about 50 hours in the chemostat at $D = 0.15\text{h}^{-1}$, the acetate specialist seems to adapt to growth in the consortium by increasing its maximum glucose uptake rate. There are a number of aspects about this phenomenon that we would like to investigate further. First of all, it would be interesting to investigate the consortium for a longer period of time. Currently, we only observed the consortium for 70 hours; we noted an increase in acetate specialist red fluorescence but we do not know whether this increase will continue or whether the acetate specialist will reach a new steady-state. Potentially, the strains will continue to evolve and adapt resulting in continuous oscillation of the strains' concentration in the consortium. Alternatively, some sort of local optimum might be achieved, leading to a more stable steady-state.

Based on previous research, we predict that the consortium will be eventually overtaken by a generalist species that has optimized growth on a mix of glucose and acetate [108]. This is because, in a chemostat, there are no spatial nor temporal niches; all cells are

always exposed to the same metabolites in the same concentrations. Although cross-feeding can temporarily create and stabilize an ecosystem with a glucose and an acetate specialist, according to the competitive exclusion principle, a generalist will probably take over the population in the long term. To prevent the evolution of a generalist, one might consider varying the environment over time, in order to create temporal niches for two different strains. This could be an interesting application of feedback control of the culture, see Section 3.3.5.

Another way to investigate this apparent adaptation of the acetate specialist would be to start a new bioreactor experiment with the newly evolved acetate specialist. We kept cultures of the bioreactor mixtures as glycerol stocks in the freezer and, as described in Section 2.8.3, we found that we can separate the glucose and the acetate specialists on M9 agar with glucose. This gives us the opportunity to regrow the consortium with the acetate specialist presumably already adapted. It would be interesting to see if it would still be flushed out of the consortium or if it would reach a steady-state biomass concentration right away.

To examine the mechanism behind the acetate specialist adaptation, we should sequence the adapted acetate specialist to see if we can pinpoint any mutations that could explain the adaptation. We hypothesize that the acetate specialist might have improved its alternative glucose uptake system. We would therefore have a look specifically at the genes coding for the mannose phosphotransferase and the galactose and maltose transporters [45].

During batch growth, we could only show that the acetate specialist had increased its maximal glucose uptake rate, since we are growing the strains on excess glucose, but we could not make any statements about the affinity of the cells for glucose. In the chemostat, however, the cells are exposed to low residual concentrations of glucose that are close to the half-maximal rate constant. In these conditions, it is therefore likely that the cells do not only increase their maximal glucose uptake rate, but also their affinity for glucose. In fact, in order to compete with the glucose specialist for glucose, this is probably necessary.

Figure 51 shows a scenario where the acetate specialist has a lower maximal glucose uptake rate, but a higher affinity (lower K_m) for acetate. In this case, for a residual glucose concentration that is around the K_m of the glucose specialist, the acetate specialist will outcompete the glucose specialist. This could allow it to compete for glucose in the consortium.

Previous research has shown that a monoculture of *E.coli* improves both maximal glucose uptake rate and affinity during chemostat growth on glucose [111, 112]. In fact, the maximal glucose uptake was shown to only increase at the start of the growth and then plateau, whereas the glucose affinity was continuously improved. Similar adaptation is likely to happen in a consortium, so it would be interesting to test if the acetate specialist also evolved an increased affinity for glucose, and if it improved to a greater or lesser extent than the glucose specialist.

To measure the strains' affinity for glucose, we would need to measure the residual glucose concentration in the chemostat. The higher the strains' affinity, the lower the resulting residual glucose concentration. As explained in Section 3.2.2, our procedure for the detection of metabolites is currently not sensitive enough to measure residual concentrations, so this should be improved before we can make any statements about the affinity of the acetate specialist for glucose.

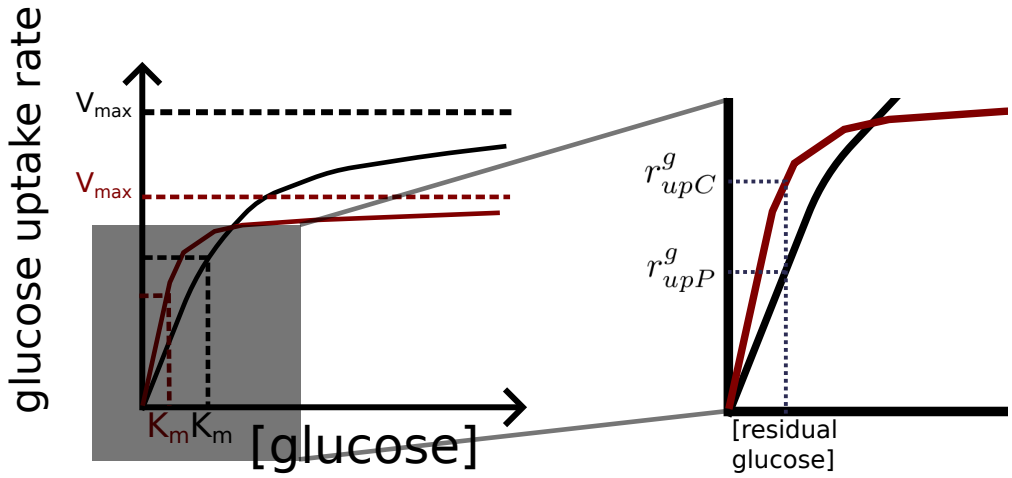

Figure 51: Left: Hypothetical reaction rate as a function of glucose concentration for the acetate specialist (red) and the glucose specialist (black), as predicted by the Michaelis-Menten equation: $r^g_{up} = v_{max}\frac{G}{G+K_m}$. The maximal glucose uptake rate (v_{max}) and the K_m are indicated with dotted lines. In this hypothetical situation, the glucose specialist has a higher maximal glucose uptake rate, but the acetate specialist has a higher affinity for glucose (lower K_m). Cut-out on the right: In this hypothetical situation, the acetate specialist has a higher glucose uptake rate (r^g_{upC}) than the glucose specialist (r^g_{upP}).

3.3.3 Modeling perspectives

In Section 2.4 and Section 2.6.5, we fitted the threshold model and the cycling model to data of the individual strains growing in batch. Our examination of both models revealed that both could fit the data of individual strains quite well. We then showed that the cycling model explained the consortium data better, since it allows for a net threshold of acetate excretion but still acetate cycling at low dilution rates. However, in Section 3.2.4, we explain that some of the data used to parameterize the threshold were taken from the literature and might therefore quantitatively deviate from our lab strain's dynamics. In order to understand the impact of this deviation on the model properties, we would have to do a more extensive sensitivity analysis of the model parameters.

Although we explored the model enough to intuitively understand the impact of most parameters on the model, a more formal sensitivity analysis could help us better understand the impact of each parameter on the model output [113]. This, in turn, might enable us to comprehend the kinds of outputs that our model is capable of producing under different parameter settings. It would also be useful to understand how much each parameter can be allowed to vary before the model output starts to be biologically implausible.

Although we observed that the proposed cycling model predicted the growth of the consortium in the chemostat quite adequately, we found that the consortium shows dynamics that are currently not predicted by the model: in Section 2.7 we observed that the acetate specialist seems to be able to mutate and improve its glucose metabolism, resulting in an oscillation in its biomass concentration. We could attempt to integrate this observation in the model, which might be possible in several ways.

First of all, we could try to implement mutations in the model by giving the modeled cells

some sort of mutable genome that is linked to their metabolic properties. An example of such a model is Evo²Sim [108]. Since we are focused on mutations in the glucose system, however, we could simplify the problem by only allowing k_g and K_g to evolve. This was previously done for a single strain by Wick et al. [112]; they could fit the successive take-over of five mutant phenotypes with progressively lower K_g and higher k_g to data of residual glucose concentration and maximum glucose uptake rate in the chemostat. It would be informative to implement such an approach for a consortium where both strains evolve to see if this evolution can explain our data.

A third approach could be to use the model as currenlty implemented, except we start the simulation with a small proportion of acetate specialists that already have an improved affinity and glucose uptake rate. In the long term, this small proportion could take over the population potentially leading to the biomass recovery as observed in Section 2.7.

3.3.4 Investigating cross-feeding

The threshold model proposed in this thesis suggests that cross-feeding happens in a consortium of glucose and acetate specialists at low dilution rates; this cross-feeding seems to help the acetate specialist to coexist with the glucose specialist. We have some ideas to study this cross-feeding interaction in more detail that we outline in this section.

First of all, it would be informative to see if we can expand the range of dilution rates in which cross-feeding can take place. One way to do this would be by improving the growth rate of the acetate specialist on acetate; ways to do this were already outlined in Section 3.3.1. If we improved the growth rate of the acetate specialist on acetate, it might be able to sustain coexistence at higher dilution rates because it might be able to grow faster on the same concentration of acetate.

A second approach could be to increase the acetate overflow by the glucose specialist, which would increase the amount of acetate available for the acetate specialist. Experiments [51] showed that a way to increase acetate overflow by the glucose specialist at a given growth rate would be to increase its metabolic load. Model analysis previously done by our group on the threshold model [24] showed that this model could reproduce this observation. It was shown that an increased metabolic load would lead to a decrease of the threshold for acetate excretion, because for a higher metabolic load (more heterologous protein production) more substrate is needed to produce a given amount of biomass. As a consequence, the glucose uptake rate must be higher to attain the growth rate set by the dilution rate. This leads to more acetate excretion at the same dilution rate. Such a strategy would be in line with a biotechnological application of the consortium where the metabolic load on the glucose specialist would be increased by the production of a desired metabolite.

We are interested to investigate if the same reasoning holds for the new cycling model, and if increasing the metabolic load could indeed extend the range of dilution rates enabling coexistence of the consortium in the bioreactor. The metabolic load of the glucose specialist could be increased by adding a high-copy number plasmid constitutively expressing a heterologous protein.

Besides expanding the range of dilution rates at which cross-feeding is happening, we think it is important to look into the acetate cycling at low dilution rates and confirm that it is taking place and that it is impacting the consortium.

Potentially, knock-outs of the current strains could be constructed to investigate if the model predicts the consortium dynamics correctly. Knocking out *pta-ackA* in the glucose specialist should inhibit acetate overflow according to the model and, as a consequence, the acetate specialist should be flushed out quicker. Knock-outs of *acs* and *pta-ackA* in the acetate specialist should prevent acetate uptake by the acetate specialist; this should increase flush-out of the acetate specialist.

Lastly, the study of this cross-feeding consortium has some implications for our understanding of the ecological interactions in these kinds of systems that could be studied in more depth. Interestingly, our model seems to suggest that, at low dilution rates, the acetate specialist is taking up acetate that, in a monoculture, would cycle back to the glucose specialist. In that sense, it looks like the acetate specialist is a kind of cheater in this community; it is benefiting from the coexistence but not giving anything back. However, as explained in the Introduction, a similar consortium as the one constructed here also evolved spontaneously in the bioreactor [22]. This might imply that there is some advantage for the community as a whole to have two specialists instead of one generalist.

On the other hand, other researchers suggested that, in the long term, the community homogenizes again to contain only one generalist [108]. Whether this would indeed happen in the long term, or whether the specialists' proportions oscillate over time, remains an open question that should be investigated, as mentioned before in Section 3.2.3.

One intriguing remaining question is whether these kinds of interactions appear in natural settings. We hypothesize that they might actually occur more frequently in the natural environment, because there is more opportunity for temporal and spatial niche creation that could keep different specialists separated and prevent the culture from homogenizing [9, 108]. It would be informative to do a specific literature review and identify systems where cross-feeding due to overflow of acetate or other products (ethanol, lactate) might be occuring at low growth rates.

3.3.5 Control

A future application of the bioreactor system that we have developed in this thesis (Section 2.2) is the control of the consortium. We already did some initial experiments with a monoculture of the glucose specialist and showed that we could essentially use the bioreactor as a turbidostat: we could keep the density of glucose specialist at a given value, using proportional–integral–derivative (PID) and model predictive control (MPC) strategies [114]. The work done in this thesis lays the basis for control of glucose and acetate specialists' proportions in the consortium in the chemostat. We could use fluorescence and flow cytometry measurements to estimate the proportion of acetate and glucose specialists in the consortium, and use a controller to drive the system closer to the desired proportions. As control inputs, we could use dilution rate, or the composition of the inflow medium with either glucose or acetate. Controlling the relative abundance of two strains in a consortium is a lively research subject [17–19]. In addition to its interest as a proof of concept, it is of practical relevance for optimized synthesis of complex compounds [115], or for setting desired trade-offs between productivity and yield [116].

In addition to ratiometric control, an objective of the control could be to prevent a generalist from taking over the population by alternatively supplying the population with

acetate and glucose, with dynamical interventions by the controller based on a suitable feedback strategy.

In the future, we aim to use optogenetics to tune the expression of suitable genes of the consortium species, and control the proportions of the strains. The optogenetics system we aim to use is based on cyanobacterial two-component system consisting of the sensor histidine kinase CcaS and its cognate response regulator, CcaR [117]. It is currently being constructed in our lab by PhD student Thibault Clavier.

In order to perform control on the consortium, we need to improve the estimation of strain proportions in the consortium, especially when the consortium is not in steady-state but the abundance of the two species varies dynamically (as mentioned in 3.2.2). To derive the biomass concentration from fluorescence, we did some work (not reported) on estimating it using Kalman filtering and smoothing. This is an algorithm that calculates the value of biomass that has the highest probability, given a time series of noisy fluorescence data and a model relating fluorescence and biomass [93, 118]. In the future, Kalman filtering can be used to estimate the biomass concentration of the consortium species from fluorescence in real time in the bioreactor, as well as the value of other state variables such as metabolite concentrations (this is what was done in our MPC-based turbidostat, for the control of the biomass concentration of a single strain). A well-developed method to estimate state variables would enable implementation of a variety of state-feedback control strategies.

4 Materials and Methods

> How do we justify, as it were, that science would give us the truth? It works. Planes fly, cars drive, computers compute. If you base medicine on science, you cure people; if you base the design of planes on science, they fly; if you base the design of rockets on science, they reach the moon. It works ... bitches.
>
> Richard Dawkins

4.1 Bacterial strains and growth media

The WT strain used in this study was E. coli K-12, strain BW25113 [72] $\Delta intAJ23108 - ho1 - pcyA$. J23108:Ho1:pcyA is an operon coding for two phycocyanobilin-biosynthesis genes [119] that will be necessary for future optogenetic control of our strain [117]. These genes are under the control of the constitutive J23108 promoter [120]. They were put in the place of the cryptic intA gene.

The standard minimal medium (M9) contained 0.1 mM $CaCl_2$, 2mM $MgSO_4$, 5 mg/L thiamine, 1 g/L NH_4Cl, 0.5 g/L NaCl, 3 g/L KH_2PO_4, 12.8 g/L $Na_2HPO_4 \cdot 7\,H_2O$, 15 mg/L $Na_2EDTA \cdot 2\,H_2O$, 4.5 mg/L $ZnSO_4 \cdot 7\,H_2O$, 0.3 mg/L $CoCl_2 \cdot 6\,H_2O$, 1 mg/L $MnCl_2 \cdot 4\,H_2O$, 1 mg/L H_3BO_3, 0.4 mg/L $Na_2MoO_4 \cdot 2\,H_2O$, 0.3 mg/L $CuSO_4 \cdot 5\,H_2O$ and 3 mg/L $FeSO_4 \cdot 7\,H_2O$. As a carbon source, glucose was used in the amount mentioned in the text.

4.2 Construction of *E. coli* mutants

Table 8: Oligonucleotides used in this study

Primer name	Sequence (5‘ to 3‘)	Purpose
glyS-cassette-cspA_fw	TTATCGCTAAATAATACAGCAACCTTTAATAATCTTC TGCTGAATAAAGATTAGAAGAACTCGTCAAGAA	Construction
glyS-cassette-cspA_rev	TTTGTTTTCAGGAAATAAATAATCGATCGCGTAATAA AATCTATTATTATTTATATTCCCCAGAACATCA	Construction
glyS-FP-cspA_fw	TTATCGCTAAATAATACAGCAACCTTTAATAA TCTTCTGCTGAATAAAGACACAGCTAACACCACGTC	Construction
glyS-mCerulean-cspA_rev	TTTGTTTTCAGGAAATAAATAATCGATCGCG TAATAAAATCTATTATTATAGCAAAACCCGTACCCTA	Construction
rev_primer_new2	TTTGTTTTCAGGAAATAAATAATCGATCGCG TAATAAAATCTATTATTATGATAGATACATCAGAGC	Construction
primer-seq-glyS-cspA_fw	CGGATATTTCGCTGTTGC	Verification
primer-seq-glyS-cspA_rev	GGTAACGTAACCAGCCTG	Verification

keio_ptsg_fw	GAGTAAAGTTCACCGCCGA	Construction
keio_ptsg_rev	CGACAAAACCTACGATACCA	Construction
pta_acka_fw	ggaagctaaaATGTCGAGTAAGTTAGTACTGG	Construction
pta_acka_rev	ttaaaaaaatTTACTGCTGCTGTGCAGAC	Construction
acs_fw	ggaagctaaaATGAGCCAAATTCACAAACAC	Construction
acs_rev	ttaaaaaaattaCGATGGCATCGCGATAG	Construction
plasmid_acs_rev	tttggctcatTTTAGCTTCCTTAGCTC	Construction
plasmid_acs_fw	gccatcgtaaATTTTTTTAAGGCAGTTATTGG	Construction
plasmid_ackapta_fw	gcagcagtaaATTTTTTTAAGGCAGTTATTGG	Construction
plasmid_ackapta_rev	tactcgacatTTTAGCTTCCTTAGCTCC	Construction
gibson_acs_test_fw	TATTTGCTTTGTGAGCGG	Verification
pta_acka_test_Rev	GGTGGAGTAGGAGAGCAT	Verification
acs_test_rev	TCCAGTAATAGCCATCTTCATC	Verification
fhua_k7_fw	ATAATCATTCTCGTTTACGTTATCATTCACTTTA CATCAGAGATATACCATTAGAAGAACTCGTCAAGAA	Construction
fhua_k7_rev	AACAGCCAACTTGTGAAATGGGCACGGAAATCC GTGCCCCAAAAGAGAAATTATATTCCCCAGAACATCA	Construction
ssDNA_fhua_ko	AACAGCCAACTTGTGAAATGGGCACGGAAA TCCGTGCCCCAAAAGAGAAATGGTATATCTCTGATG TAAAGTGAATGATAACGTAAACGAGAATGATTAT	Construction
FhuAav_Fwd	TCTATTGCTGGTTAGGGATACCAGGGTAATCAACG CCGCTGAATCTTG	Verification
Fhuam_Rev	GGAACACTTAACGGCGCCAGAGAGACTATCGACC	Verification

The glucose specialist had the mCerulean-ME gene [92] inserted into the chromosome, under the control of the constitutive ProC promoter [121]. This was done by recombineering [69], see Figure 52. Primers glyS-cassette-cspA_fw and glyS-cassette-cspA_rev (see Table 8) were used to amplify a kan:pBAD:ccdB cassette, see Figure 53.

The PCR product was transformed into a WT expressing the λ Red recombinase (plasmid pSIM5, Figure 54). Kanamycin-resistant recombinants were selected. Primers glyS-FP-cspA_fw and glyS-mCerulean-cspA_rev were used to amplify mCerulean-ME, see Figure 55. The PCR product was recombined into the chromosome in place of the cassette. Recombinants were selected on medium containing arabinose for activation of the suicide gene *ccdB*, which kills cells that have not recombined the *mCerulean-ME* gene. The final mutant was verified by PCR and DNA sequencing (see verification primers in Table 8). To construct a red strain with mScarlet-I on the chromosome, we used same procedure, but with the rev_primer_new2 as reverse primer instead of glyS-mCerulean-cspA_rev.

In all strains, *fhuA* was knocked out to prevent phage infection, using the same recombineering approach as for the insertion of fluorescence proteins. Primers fhua_k7_fw and fhua_k7_rev were used to amplify a kan:pBAD:ccdB cassette. The PCR product was transformed into strains carrying either mScarlet-I or mCerulean-ME on the chromosome, expressing the λ Red recombinase (plasmid pSIM5, Figure 54). Kanamycin-resistant recombinants were selected. The cassette was then replaced with oligonucleotide ssDNA_fhua_ko and recombinants were selected on medium containing arabinose. The final mutants were verified by PCR using primers FhuAav_Fwd and Fhuam_Rev.

For the *ptsG* knock-out, we used the Keio collection [72], a collection of single-gene

knock-outs. We took the collection's strain with *PtsG* knock-out, and amplified the region containing the knocked-out region using primers keio_ptsg_fw and keio_ptsg_rev. This region contains a Kanamycin resistance marker. We then transformed the product into a strain carrying mScarlet-I on the chromosome and selected the Kanamycin-resistant recombinants. See Section 1.5.1 for a schematic of this deletion.

For overexpression of the Pta-AckA pathway and Acs, we placed the genes on a plasmid using Gibson assembly [74]. The plasmid was a PQE80 plasmid with a pSC101 replicon carrying spectinomycin resistance (see Figure 56). The pathway was placed under the control of an IPTG inducible *lac* promoter. For the amplification of the plasmid and insertion of Pta-AckA we used the primers plasmid_ackapta_fw and plasmid_ackapta_fw. For the amplification of the Pta-AckA pathway we used the primers pta_acka_fw and pta_acka_rev. For the amplification of the plasmid and insertion of Acs we used the primers plasmid_acs_fw and plasmid_acs_rev. For the amplification of Acs we used the primers acs_fw and acs_rev. We performed the Gibson assembly using the NEBuilder HiFi DNA Assembly Cloning Kit. To test if the assembly had happened correctly we used the primers gibson_acs_test_fw and pta_acka_test_Rev for Pta-AckA and gibon_acs_test_fw and acs_test_rev for Acs. In Table 8, lowercase letters indicate overlapping ends.

We then placed the complete plasmids in the strain with mScarlet-I on the chromosome and *PtsG* knock-out and selected the spectinomycin resistant transformants.

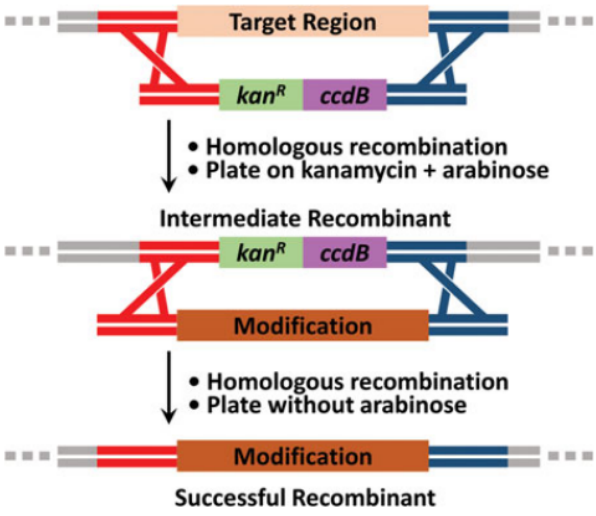

Figure 52: Image taken from [122]. Schematic of recombineering. First, we insert a cassette into the WT and select kanamycin resistant recombinants. Then, we add the desired modifaction (fluorescent proteins, *fhuA* deletion) in the place of the cassette and select recombinants growing on arabinose.

.

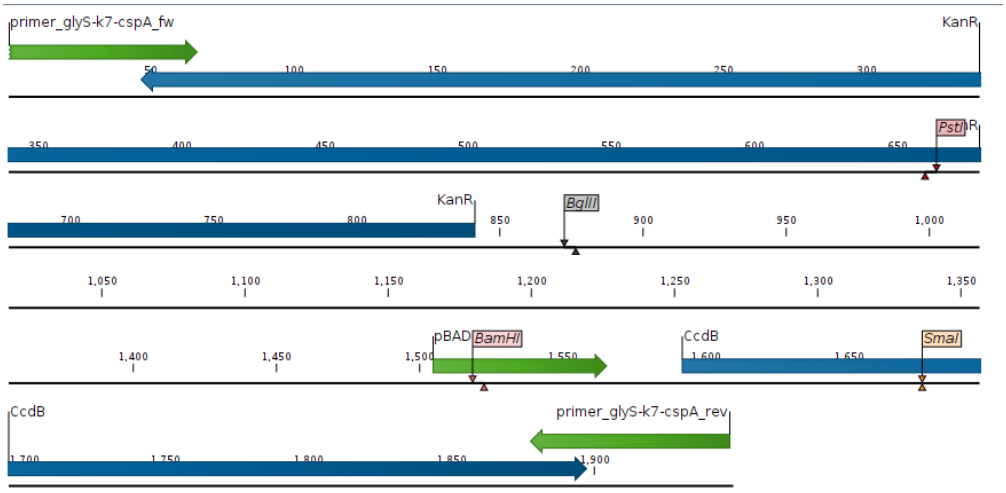

Figure 53: Amplification of the kan:pBAD:ccdB cassette using glyS-cassette-cspA_fw and glyS-cassette-cspA_rev

.

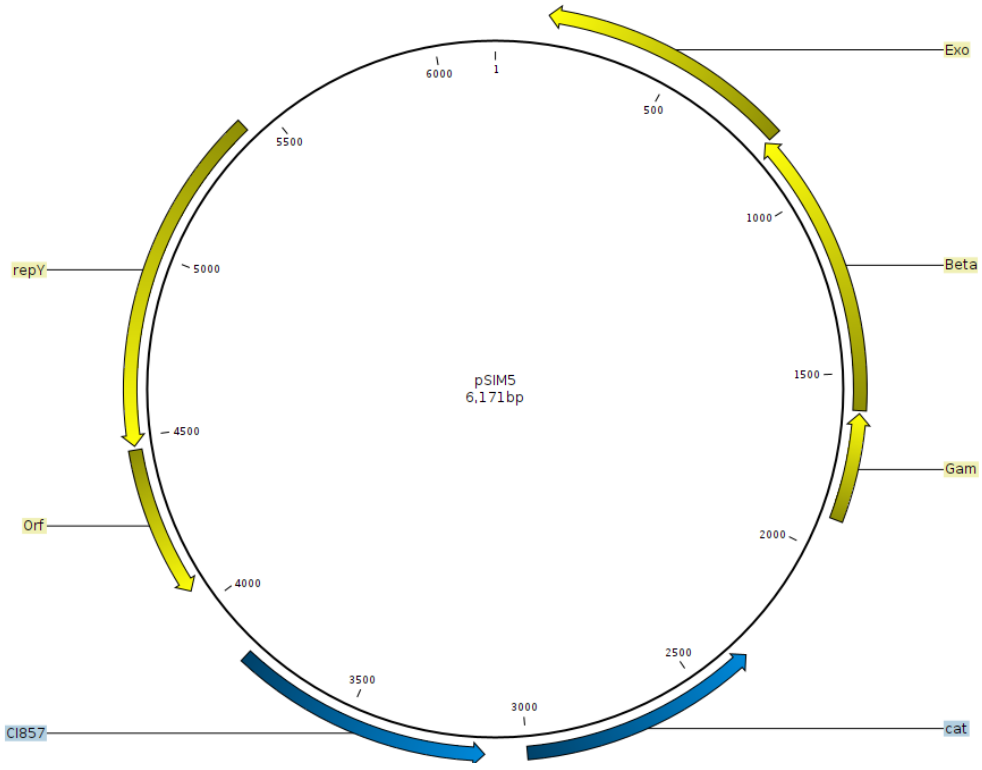

Figure 54: pSIM5 plasmid expressing the λ Red recombinase system

.

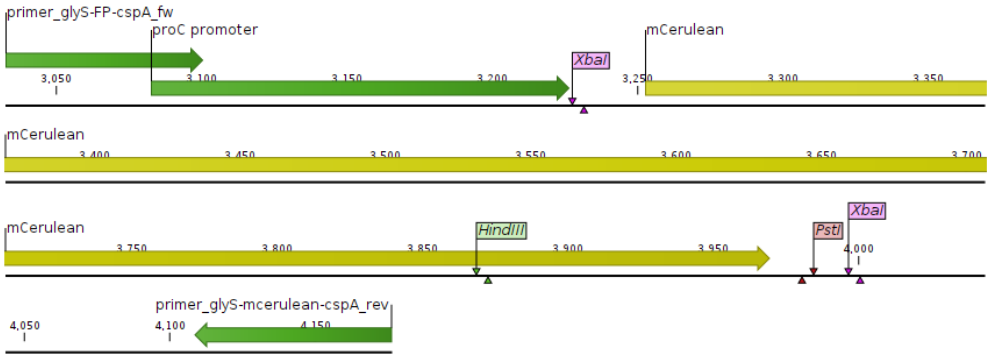

Figure 55: Amplification of *mCerulean-ME* using glyS-FP-cspA_fw and glyS-mCerulean-cspA_rev

.

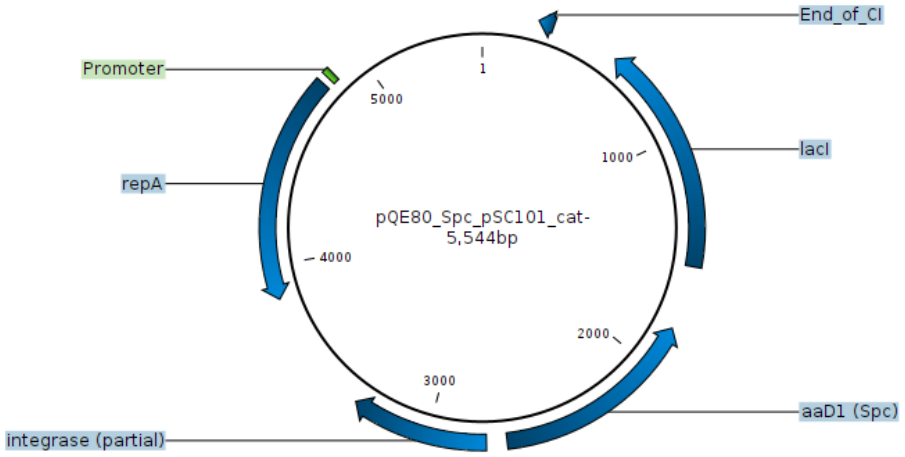

Figure 56: PQE80 plasmid with a pSC101 replicon carrying spectinomycin resistance and an IPTG inducible *lac* promoter.

.

4.3 Batch experiments for parameter identification

The batch experiments to identify growth and fluorescence parameters were performed at 37°C in an automated microplate reader (Tecan infinite F200 Pro). Precultures from glycerol stocks were grown overnight in M9 with 2 g/L glucose. They were diluted 1000 times the next day in 150 μL M9 with appropriate glucose concentration and added to a white μclear 96-well plate from Greiner Bio-one that was inserted in the microplate reader. Glass beads of 2 mm diameter were inserted into each well to improve mixing and aeration. Linear as well as orbital shaking was performed in between measurements. For OD measurements, the absorbance wavelength was 600 nm and the measurement bandwidth was 10 nm with 10 flashes and 0 ms settle time. For the blue fluorescence measurements, the excitation wavelength was 430 nm, the excitation bandwidth was 20 nm, the emission wavelength was 485 nm, the emission bandwidth was 20 nm, with 0 μs lag time, 20 μs integration time, 10 flashes, and 0 ms settle time. The gain was set to 52. For the red fluorescence measurements, the excitation wavelength was 560 nm, the excitation bandwidth was 20 nm, the emission wavelength was 635 nm, the emission bandwidth was 35 nm, with 0 μs lag time, 20 μs integration time, 10 flashes, and 0 ms settle time. The gain was set to 60. To remove outliers and substract background absorbance and fluorescence, we used the WellInverter web application [82]. The model fitting was done using the Python package lmfit, using the Levenberg-Marquardt algorithm [99].

4.4 Bioreactor experiments

Below, we give a detailed protocol for a typical experiment.

Day 0

- Make plates with single colonies of the desired strains.

Day 1

- make pre-preculture in 1 mL LB plus desired antibiotics, first thing in the morning, from single colonies made on Day 0.
  - for the acetate specialist we add kanamycin to select for $\Delta ptsG$ and spectinomycin to select for the Pta-AckA or Acs plasmid
  - leave it at 37 degrees
- measure the absorbance and fluorescence of a standard of known red fluorescence, in our case rhodamine dissolved in ethanol. We keep a box with 2 mL Eppendorf tubes of samples of the same concentration in a freezer at -20 degrees.
  - this is the first measurement of the experiment, so make sure everything is set up properly, i.e.:

  - water measurement connected and water tubing filled so the cuvette will be filled properly
  - absorbance and fluorescence leds turned on
  - absorbance LED: switch to ON, second switch to TLC
  - create a new campaign to add measurements to
  - add an observer for the red fluorescence
  - add a chart for red fluorescence on the dashboard
- prepare waste bottle: 1 L bottle with a tablet of bleach
- flush ethanol through measurement path, in order to sterilize and to remove traces of rhodamine
- flush water through measurement, in order to remove traces of ethanol. Make sure there is water in the cuvette at the end of the flushing
- determine the volume per round per minute that is pumped around by the pumps, in order to determine the necessary pump speed for the desired dilution rate.
  - $$pumpspeed = DV_{reactor}/V_{measured}$$
  - Where *pumpspeed* is the necessary pump speed of the experiment in rounds per minute (rpm), D is the desired dilution rate in h^{-1}, $V_{reactor}$ is the volume of the bioreactor in mL, and $V_{measured}$ is the volume measured during the calibration step in $mL\,rpm^{-1}h^{-1}$
  - Run for 30 minutes at 1 rpm
  - make sure that the tubing is filled with water before starting the calibration, by running it shortly at a high speed (e.g. 60 rpm)
- flush ethanol through glucose input tubing
- clean air in and output tubes with ethanol
- prepare bottle with 1M KOH to hang in the air output tubes
- connect tubes for liquid output
- make M9 medium (first without carbon, add it later when making the precultures)
- make overnight precultures in 20 mL M9
  - in the preferred carbon source:
    * the glucose specialist in M9 + glucose
    * the acetate specialist in M9 + acetate
  - make sure they are in exponential phase the next morning

Day 2

- flush M9 through glucose input tubes
- dilute cultures in the desired amount in the reactors
- write algorithms in the campaign
- insert needles in the reactors
- start measurements

Day 3

- take metabolite samples: take 1 ml from reactor, spin down, keep supernatant at -20°C
- take flow cytometry samples
  - take some sample, dilute 10.000 times in salts 1x buffer
  - run in cytometry, alongside a buffer only sample

Day 4

- See Day 3

Day 5

- calibrate pumps, see Day 1
- clean reactor, see Day 1
- turn off air
- flush ethanol through output tubing
- disconnect all tubing
- turn off algorithms
- download and backup data

4.5 Conversion of absorbance measurements to gdW/L

Since the experimental measure for cell concentration is absorbance or OD600, whereas the model uses gdW/L, we need to be able to convert from one to the other. For the conversion from OD600 to gDW/L, it is known that for *E.coli* 1 OD600 $\approx$ 0.37 gdW/L [123]. OD600 is defined for a 1 cm path length, but both the samples in the platereader and the bioreactor are not 1 cm. The bioreactor measurements cuvettes have a path length of 3mm. Therefore, to go from absorbance in the bioreactor to gDW/L, we first multiply by 3.6 to go to OD600, and then by 0.37, to go to gDW/L.

Based on the diameter of the microplates (6.96 mm) and the volume of our sample (150 μL), we calculated that our sample in the platereader is 0.39 cm high, and that we would therefore have to multiply the absorbance values with $1/0.39 = 2.5$ to convert to OD600 readings. However, when we used this conversion factor, the results of our fits were very far from our expectations, so we decided to experimentally validate the conversion factor from Tecan absorbance to OD600. For this validation, we grew our WT in M9 with glucose and took both absorbance measurements and OD600 measurements in the spectrometer every half an hour. We than calculated the conversion for 98 of these time points. We found that the conversion factor is 4.79 $\pm$ 0.06 (see Figure 57). Therefore, to compare measurements from the plate reader with the model, we first multiply by 4.79 to go from absorbance to OD600, and then with 0.37 to convert to gDW/L.

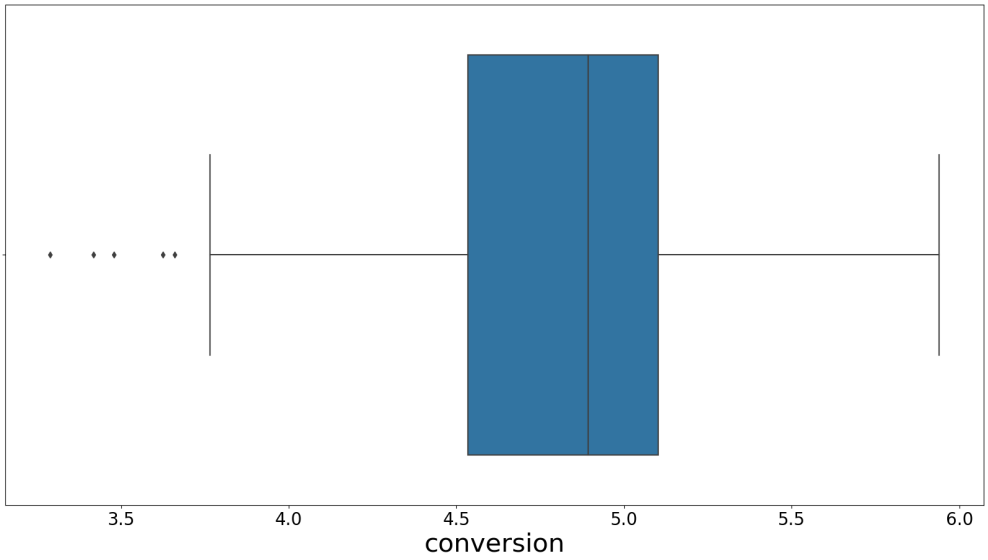

Figure 57: Boxplot of the conversion factor from absorbance in the Tecan to OD600. The outliers on the left were removed to calculate the mean conversion factor

.

4.6 Calibration of absorbance values at high cell concentrations

We know that absorbance does not scale linearly with cell concentration at high cell concentration, due to multiple scattering of cells that scatter light back into the detector [75]. This

effect can cause an underestimation of the absorbance values at high cell concentrations. Therefore, we calibrated the measured absorbance values in the plate reader to reflect the actual increase in cell concentration. To do this, we diluted a preculture of the WT various times and measured the absorbance of the dilutions in a microplate. We then plotted the resulting dilution-over-absorbance curve, and determined by a Ljung-Box test that absorbance curve in the plate reader is linear until 0.4, i.e. an OD600 of 1.9 (see Figure 58).

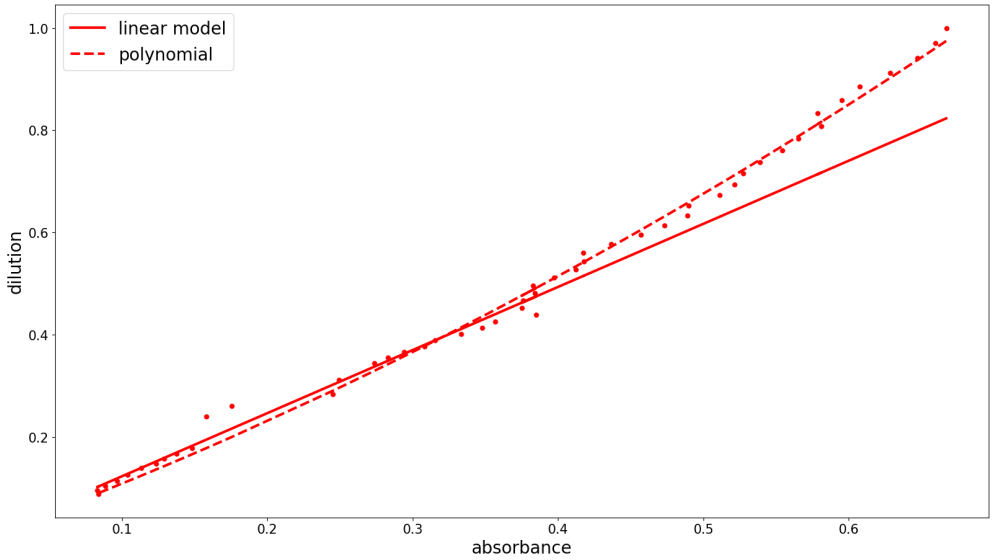

Figure 58: Dilution over absorbance, with a linear and a polynomial fit. After absorbance=0.4, the dilution goes up faster than the absorbance, meaning that the we are underestimating the absorbance values in this region. Fitting a line through data points up to absorbance=0.4 results in a Ljung-Box test statistic for the residuals of p = 0.29. It is therefore highly likely that these residuals are autocorrelated by chance. We accept the H0 that the residuals are independently distributed as would be expected for a linear fit through a data-set that actually follows a line. The Ljung-box test was also performed with a line fit through points until absorbance=0.6 and absorbance=0.5. In these cases, $p << 0.05$, which makes us reject the H0 that the residuals are correlated by chance, thus suggesting that the data-set not does follow a line until absorbances of 0.6 or 0.5.

To find the actual absorbance value of absorbances above 0.4, we set up a correction function. This function first calculates the dilution from the absorbance based on the fitted polynomial (dotted line in Figure 58). Then, the absorbance is calculated from the dilution using the slope of the linear part of the curve (solid line in Figure 58).

4.7 Flow cytometry

Samples were diluted 1000 times in water with M9 salts (1 g/L NH_4Cl, 0.5 g/L NaCl, 3 g/L KH_2PO_4, 12.8 g/L $Na_2HPO_4 \cdot 7\,H_2O$) and analyzed with a Guava easyCyte HT System flow cytometer for two minutes. A 532-nm laser was used for excitation of the red fluorescent protein. Orange Fluorescence was detected through a 620/52 nm band pass filter with a gain of 47.3. In addition, forward scatter (FSC) and side scatter (SSC) were measured and the

discriminator was set to FSC with a value of 15. Signals were amplified with the logarithmic mode for SSC, FSC, and fluorescence. To statistically analyze the data, we used the Python package cytoflow [124].

4.8 Metabolite concentrations

Acetate concentrations were assayed by a K-ACETRM (Megazyme) enzyme kit according to the manufacturer's recommendations. Quantifications were done in 96-well microplates (clear, flat bottomed, plastic). The enzymatic reactions of the kit led to the consumption of NADH. The concentration change of NADH was quantified by measuring the difference in absorbance at 340 nm with a microplate reader (Tecan infinite M200 Pro). The The concentration of the sample, $C_{metabolite}$ (diluted in order to remain within the linearity region of the assay) is then calculated as

$$C_{metabolite} = \frac{\Delta A_{metabolite}}{\Delta A_{standard}} C_{standard} \tag{50}$$

where $\Delta A_{standard}$ and $C_{standard}$ are the measured absorbance difference and the concentration of the metabolite standard. The metabolite standard solution was provided with the kit. $\Delta A_{metabolite}$ is the measured absorbance difference of the metabolite sample. In order to compute $\Delta A_{metabolite}$ and $\Delta A_{standard}$, we measured the absorbance for a minute before starting the reactions (A_1) and then for 30 minutes after starting the reactions (A_2). We fitted a straight line through the repeated measurements of A_1 and an exponential through the repeated measurements of A_2. The difference ΔA is the difference between the straight line and the minimum of the exponential.

Glucose concentrations were assayed by a K-GLUHK-220A (Megazyme) kit according to the manufacturer's recommendations using a similar procedure as described above for acetate.

5 Appendix

S5.1 Supplementary Figures

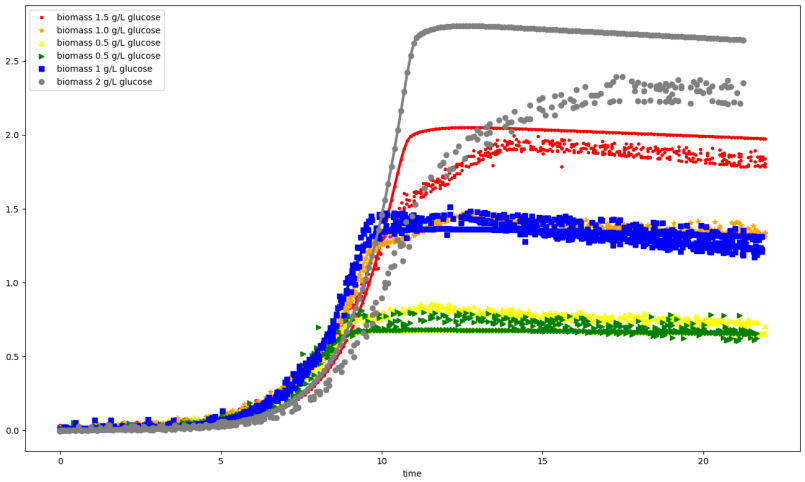

Supplementary Figure S1: Biomass for plate reader experiments at 4 different glucose concentrations. The dots indicate the data points. The lines indicate the plateau if all biomass yields were the same. As can be observed, the biomass yield at 1.5 g/L and 2.0 g/L glucose is lower than that at 0.5 g/L and 1.0 g/L glucose.

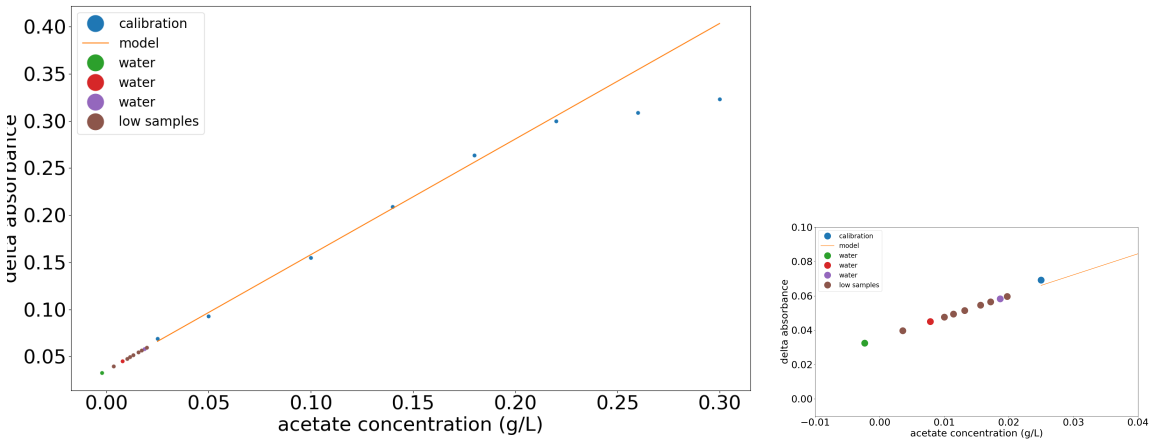

(a) (b)

Supplementary Figure S2: Change in absorbance at 340 nm as a function of acetate concentration. The blue data indicate the points used for calibration. The green, red and purple dots are negative controls: they don't contain any acetate. The brown dots indicate the measured samples with a low acetate concentration: they cannot be distinguished from the negative control. 2(b) shows a close-up of 2(a).

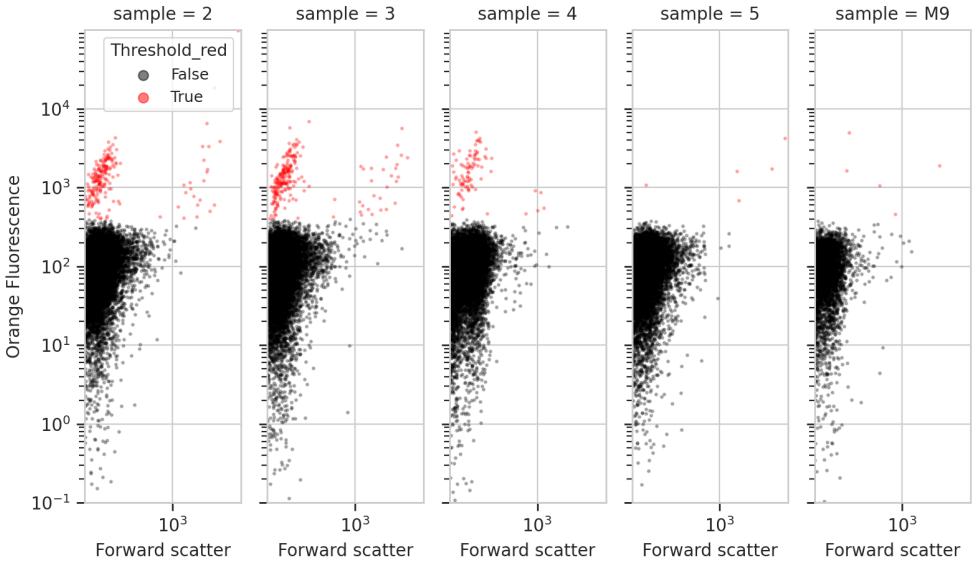

Supplementary Figure S3: Orange fluorescence over forward scatter for 4 bioreactors and a buffer (M9) sample. The red dots indicate acetate specialists, whereas the black dots are either glucose specialists or dust particles.

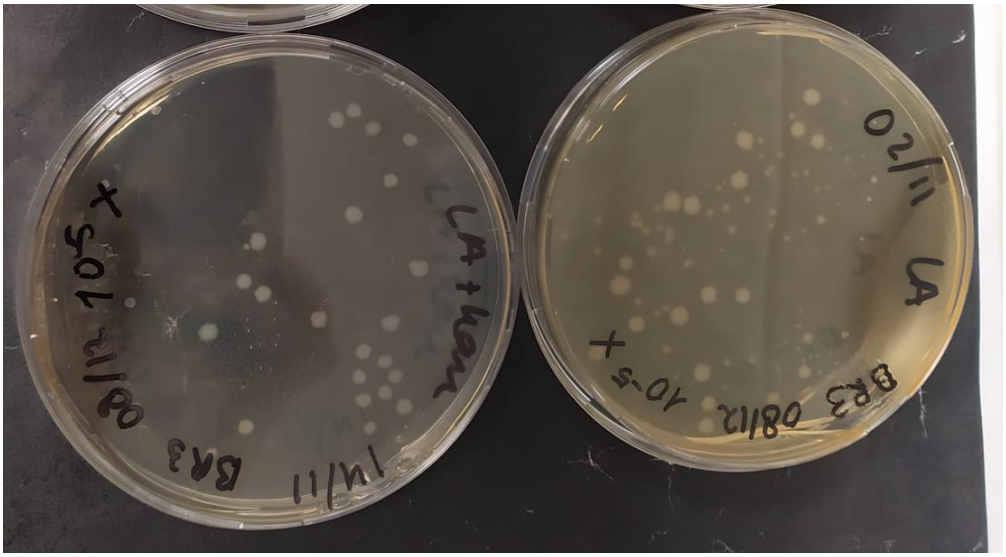

Supplementary Figure S4: Plates with cultures diluted 10^5 times after the experiment in Figure 47. We notice that on the plate with kanamycin (left), all colonies look similar, whereas on the plate without antibiotics (right), there are two different types of colonies: the smaller ones are mostly likely a contaminant that invaded the culture during the experiment.

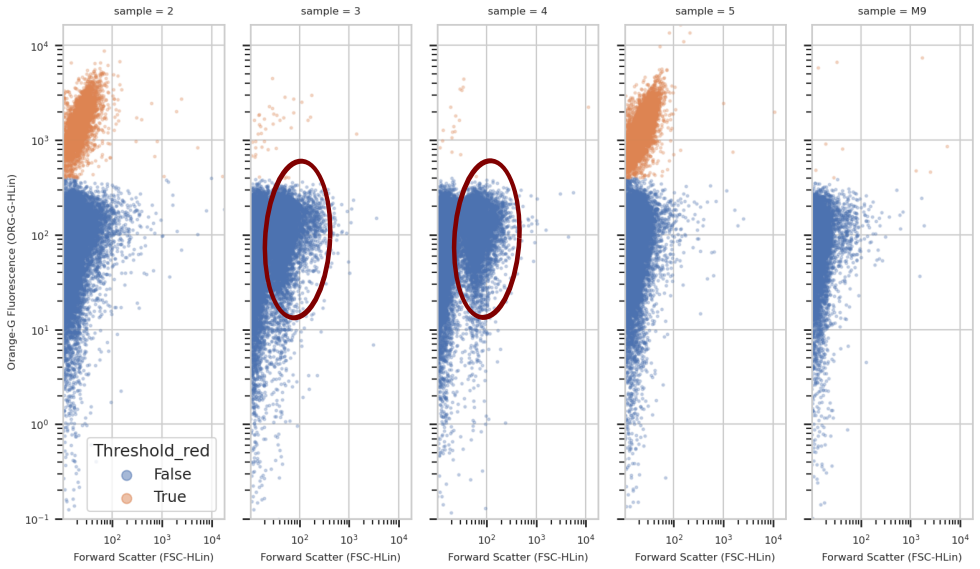

Supplementary Figure S5: Flow cytometry samples taken after the experiment in Figure 47. Here, we plot orange fluorescence over forward scattering. The samples correspond to 4 bioreactors run in parallel. Especially in bioreactor 3 and 4 we observe a cloud of cells that have a higher forward scattering value than expected (circled red). Bioreactor 3 and 4 are almost devoid of acetate specialists (orange dots). Bioreactor 2 and 5 contain respectively 36% and 44% acetate specialists. The expected amount was 100 % for all bioreactors, since it concerns an experiment with only acetate specialists. We suspect that the dots with high forward scattering indicate an unknown contaminant.

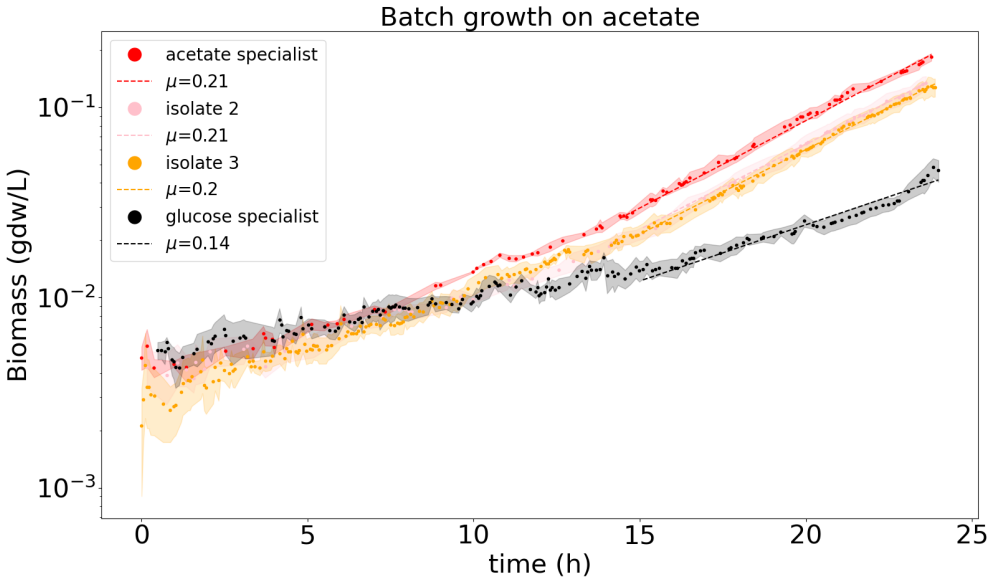

Supplementary Figure S6: Isolates of the acetate specialist taken after the consortium bioreactor experiment in Section 2.8, grown on 0.72 g/L acetate in a plate-reader (pink and yellow). They have a growth rate very similar to the acetate specialist before the experiment (red), and higher than the glucose specialist (black). Dots indicates the mean of three technical replicates. Shaded region signifies the SEM.

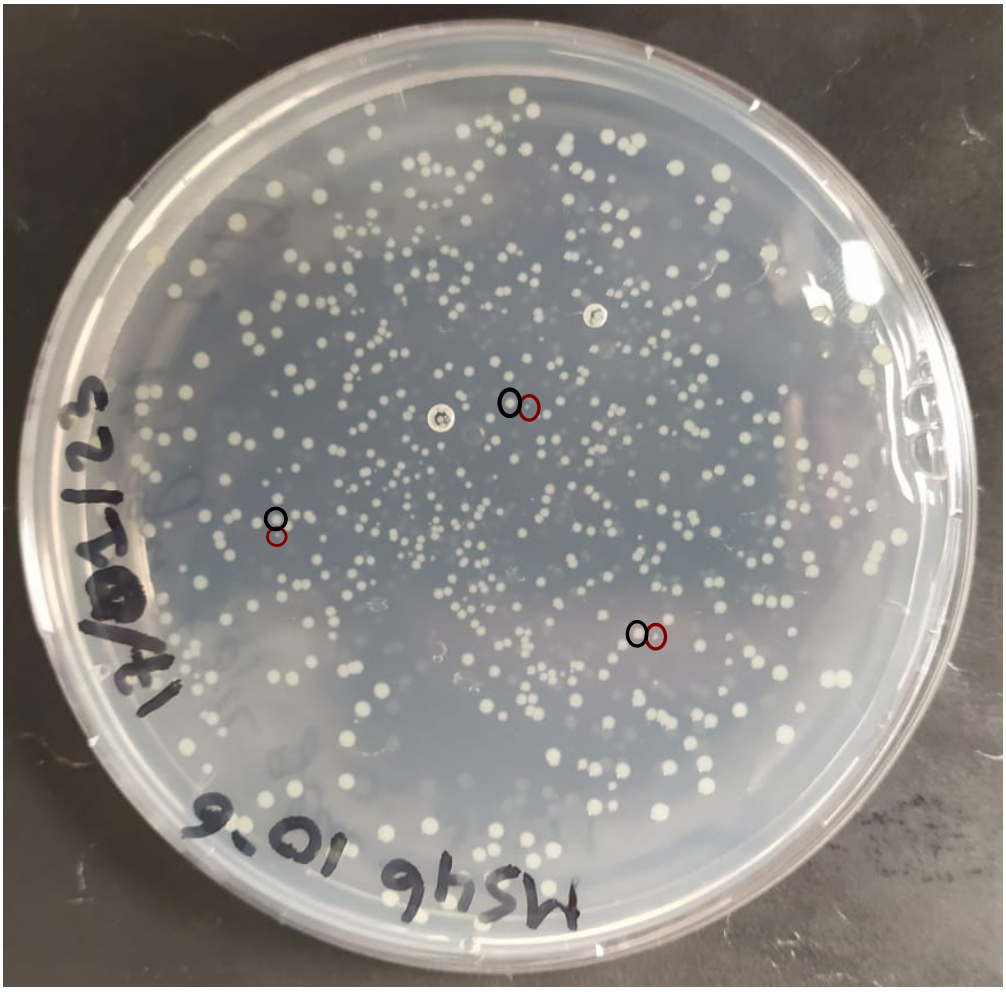

Supplementary Figure S7: A sample of one of the bioreactors taken after the experiment in Figure 47 diluted 10^6 times and plated on M9 agar with 1 g/L glucose. The acetate specialist (examples circled red) gives smaller colonies than the glucose specialist (examples circled black).

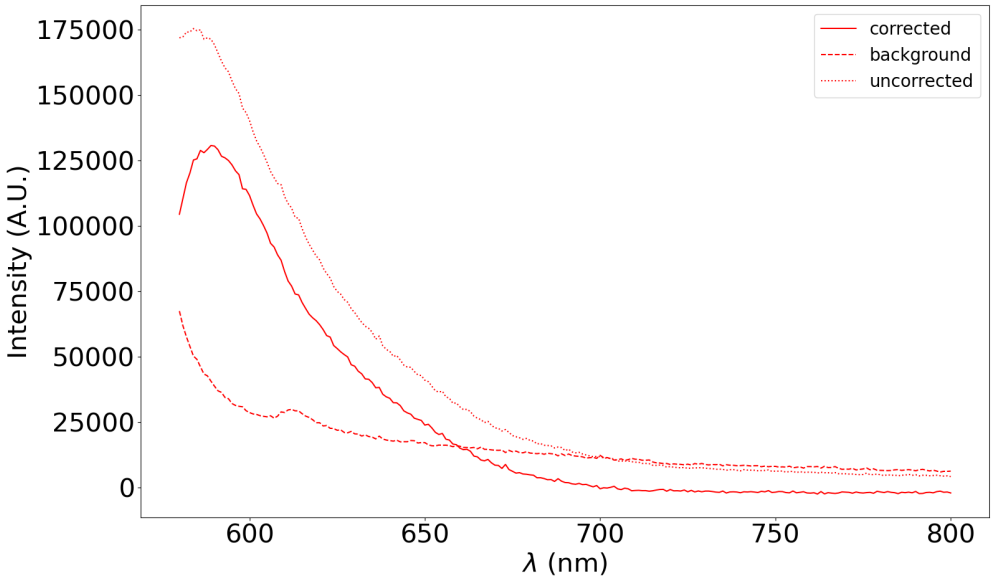

Supplementary Figure S8: Spectrum of mScarlet-I in the spectrofluorometer. We made precultures in LB of a strain carrying mScarlet-I on its chromosome under the control of the constitutive *proC* promoter. We then spun down the culture and resuspended it in M9 before recording the spectrum. The background spectrum shows the spectrum of a WT not expressing mScarlet-I.

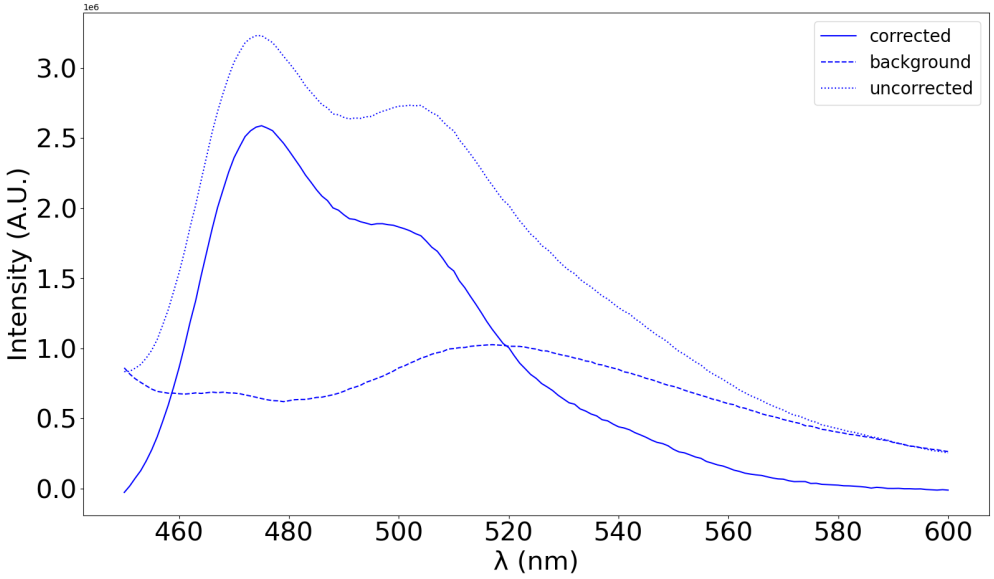

Supplementary Figure S9: Spectrum of mCerulean-ME in the spectrofluorometer. We made precultures in LB of a strain carrying mCerulean-ME on its chromosome under the control of the constitutive *proC* promoter. We then spun down the culture and resuspended it in M9 before recording the spectrum. The background spectrum shows the spectrum of a WT not expressing mCerulean-ME.

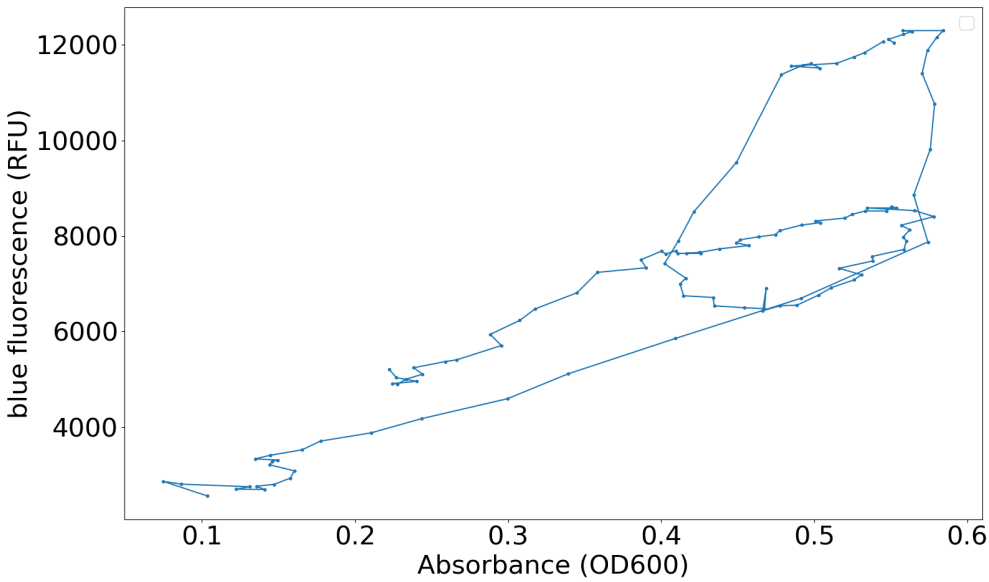

Supplementary Figure S10: Blue background fluorescence of a WT strain (not carrying any fluorescent reporter) in the bioreactor as a function of absorbance. It is not obvious how to relate the absorbance of cells to their blue background fluorescence.

S5.2 Concentration of internal metabolites

The concentration of C with respect to the bioreactor volume would be:

$$\frac{dC}{dt} = r_g B + r_a B - r_b B - DC \tag{S1}$$

However, since C is an internal metabolite, we want to model it with respect to the (time-varying) volume of the cells (biomass). Let us define a new variable $\tilde{C} = C/B$. This variable varies over time as follows:

$$\frac{d\tilde{C}}{dt} = \frac{\dot{C}}{\dot{B}} = \frac{B\dot{C} - C\dot{B}}{B^2} = \frac{\dot{C}}{B} - \tilde{C}\frac{\dot{B}}{B} \tag{S2}$$

Filling in Equation (S2) and (S1), we obtain:

$$\frac{d\tilde{C}}{dt} = r_g + r_a - r_b - D\tilde{C} - \tilde{C}(\mu - D) = r_g + r_a - r_b - \mu\tilde{C} \tag{S3}$$

References

1. Schink, B., Montag, D., Keller, A. & Müller, N. Hydrogen or formate: Alternative key players in methanogenic degradation. Environmental Microbiology Reports 9, 189–202. doi:10.1111/1758-2229.12524 (2017).
2. Bryant, M., Wolin, E. A., Wohn, M. J. & Wolfe, R. Methanobacillus omelianskii, a Symbiotic Association of Two Species of Bacteria. Archiv fur Mikrobiologie 31, 20–31 (1967).
3. Rajilić-Stojanović, M. & de Vos, W. M. The first 1000 cultured species of the human gastrointestinal microbiota. FEMS Microbiology Reviews 38, 996–1047. doi:10.1111/1574-6976.12075 (2014).
4. Sunagawa, S. *et al.* Individuality and temporal stability of the human gut microbiome. Central Asian Journal of Global Health 2, 2–3. doi:10.5195/cajgh.2013.120 (2014).
5. Wintermute, E. H. & Silver, P. A. Dynamics in the mixed microbial concourse. Genes and Development 24, 2603–2614. doi:10.1101/gad.1985210 (2010).
6. Hornung, B., Martins dos Santos, V. A., Smidt, H. & Schaap, P. J. Studying microbial functionality within the gut ecosystem by systems biology. 2018. doi:10.1186/s12263-018-0594-6.
7. Rao, C. *et al.* Multi-kingdom ecological drivers of microbiota assembly in preterm infants. Nature 591, 633–638. doi:10.1038/s41586-021-03241-8 (2021).
8. Stein, R. R. *et al.* Ecological Modeling from Time-Series Inference: Insight into Dynamics and Stability of Intestinal Microbiota. PLoS Computational Biology 9, 31–36. doi:10.1371/journal.pcbi.1003388 (2013).
9. Blasche, S. *et al.* Metabolic cooperation and spatiotemporal niche partitioning in a kefir microbial community. Nature Microbiology 6, 196–208. doi:10.1038/s41564-020-00816-5 (2021).
10. De Roy, K., Marzorati, M., Van den Abbeele, P., Van de Wiele, T. & Boon, N. Synthetic microbial ecosystems: an exciting tool to understand and apply microbial communities. Environmental microbiology 16, 1472–1481. doi:10.1111/1462-2920.12343 (2014).
11. Che, S. & Men, Y. Synthetic microbial consortia for biosynthesis and biodegradation: promises and challenges. Journal of Industrial Microbiology and Biotechnology. doi:10.1007/s10295-019-02211-4 (2019).
12. Dos Santos, A. R., Di Martino, R., Testa, S. E. A. & Mitri, S. Classifying Interactions in a Synthetic Bacterial Community Is Hindered by Inhibitory Growth Medium. mSystems 7. doi:10.1128/msystems.00239-22 (2022).
13. Rivett, D. W. & Bell, T. Abundance determines the functional role of bacterial phylotypes in complex communities. Nature Microbiology 3, 767–772. doi:10.1038/s41564-018-0180-0 (2018).

14. Brenner, K., You, L. & Arnold, F. H. Engineering microbial consortia: a new frontier in synthetic biology. Trends in Biotechnology 26, 483–489. doi:10.1016/j.tibtech.2008.05.004 (Sept. 2008).

15. Wintermute, E. H. & Silver, P. A. Emergent cooperation in microbial metabolism. Molecular Systems Biology 6, 1–7. doi:10.1038/msb.2010.66 (2010).

16. Co, A. D., van Vliet, S., Kiviet, D. J., Schlegel, S. & Ackermann, M. Short-range interactions govern the dynamics and functions of microbial communities. Nature Ecology and Evolution 4, 366–375. doi:10.1038/s41559-019-1080-2 (2020).

17. Aditya, C., Bertaux, F., Batt, G. & Ruess, J. A light tunable differentiation system for the creation and control of consortia in yeast. Nature Communications 12. doi:10.1038/s41467-021-26129-7 (2021).

18. Fiore, D., Della Rossa, F., Guarino, A. & Di Bernardo, M. Feedback ratiometric control of two microbial populations in a single chemostat. bioRxiv, 2021.03.05.434159 (2021).

19. Treloar, N. J., Fedorec, A. J., Ingalls, B. & Barnes, C. P. Deep reinforcement learning for the control of microbial co-cultures in bioreactors. PLoS Computational Biology 16, 1–18. doi:10.1371/journal.pcbi.1007783 (2020).

20. Bernstein, H. C., Paulson, S. D. & Carlson, R. P. Synthetic Escherichia coli consortia engineered for syntrophy demonstrate enhanced biomass productivity. Journal of Biotechnology 157, 159–166. doi:10.1016/j.jbiotec.2011.10.001 (Jan. 2012).

21. Morris, B. E., Henneberger, R., Huber, H. & Moissl-Eichinger, C. Microbial syntrophy: Interaction for the common good. FEMS Microbiology Reviews 37, 384–406. doi:10.1111/1574-6976.12019 (2013).

22. Rosenzweig, R. F., Sharp, R. R., Treves, D. S. & Adams, J. Microbial evolution in a simple unstructured environment: Genetic differentiation in Escherichia coli. Genetics 137, 903–917 (1994).

23. Rozen, D. E. & Lenski, R. E. Long-Term Experimental Evolution in Escherichia coli. VIII. Dynamics of a Balanced Polymorphism. The American Naturalist 155, 24–35. doi:10.1086/303299 (2000).

24. Mauri, M., Gouzé, J.-L., de Jong, H. & Cinquemani, E. Enhanced production of heterologous proteins by a synthetic microbial community: Conditions and trade-offs. PLOS Computational Biology 16, 1–30. doi:10.1371/journal.pcbi.1007795 (2020).

25. Lotka, A. J. Elements of Physical Biology. Nature 115. doi:https://doi.org/10.1038/116461b0 (1925).

26. Volterra, V. Fluctuations in the Abundance of a Species Considered Mathematically. Nature 118, 558–560. doi:https://doi.org/10.1038/118558a0 (1926).

27. Momeni, B., Xie, L. & Shou, W. Lotka-Volterra pairwise modeling fails to capture diverse pairwise microbial interactions. eLife 6, 1–34. doi:10.7554/elife.25051 (2017).

28. MacArthur, R. Species packing and competitive equilibrium for many species. Theoretical Population Biology 1, 1–11. doi:10.1016/0040-5809(70)90039-0 (1970).

29. Niehaus, L. *et al.* Microbial coexistence through chemical-mediated interactions. Nature Communications 10. doi:10.1038/s41467-019-10062-x (2019).

30. George, A. B., Wang, T. & Maslov, S. Functional universality in slow-growing microbial communities arises from thermodynamic constraints. arXiv: 2203.06128 (2022).

31. Marsland, R. *et al.* Available energy fluxes drive a transition in the diversity, stability, and functional structure of microbial communities. PLoS Computational Biology 15, 1–18. doi:10.1371/journal.pcbi.1006793. arXiv: 1805.12516 (2019).

32. Klipp, E., Liebermeister, W., Wierling, C. & Kowald, A. Systems Biology Second. ISBN: 9783527336364 (Wiley, Weinheim, 2016).

33. Mahadevan, R., Edwards, J. S. & Doyle, F. J. Dynamic flux balance analysis of diauxic growth. Biophysical Journal 83, 1331–1340 (2002).

34. Mori, M., Hwa, T., Martin, O. C., De Martino, A. & Marinari, E. Constrained Allocation Flux Balance Analysis. PLoS Computational Biology 12, 1–24. doi:10.1371/journal.pcbi.1004913. arXiv: 1607.00128 (2016).

35. Bulović, A. *et al.* Automated generation of bacterial resource allocation models. Metabolic Engineering 55, 12–22. doi:10.1016/j.ymben.2019.06.001 (2019).

36. Hanemaaijer, M. *et al.* Systems modeling approaches for microbial community studies: From metagenomics to inference of the community structure. Frontiers in Microbiology 6, 1–12. doi:10.3389/fmicb.2015.00213 (2015).

37. Gottstein, W., Olivier, B. G., Bruggeman, F. J. & Teusink, B. Constraint-based stoichiometric modelling from single organisms to microbial communities. Journal of the Royal Society Interface 13. doi:10.1098/rsif.2016.0627 (2016).

38. Koch, S. *et al.* Redcom: A strategy for reduced metabolic modeling of complex microbial communities and its application for analyzing experimental datasets from anaerobic digestion. **2.** ISBN: 1111111111. doi:10.1371/journal.pcbi.1006759 (2019).

39. Frioux, C., Singh, D., Korcsmaros, T. & Hildebrand, F. From bag-of-genes to bag-of-genomes: metabolic modelling of communities in the era of metagenome-assembled genomes. Computational and Structural Biotechnology Journal 18, 1722–1734. doi:10.1016/j.csbj.2020.06.028 (2020).

40. Deutscher, J., Francke, C. & Postma, P. W. How Phosphotransferase System-Related Protein Phosphorylation Regulates Carbohydrate Metabolism in Bacteria. Microbiology and Molecular Biology Reviews 70, 939–1031. doi:10.1128/mmbr.00024-06 (2006).

41. Postma, P. W., Lengeler, J. W. & Jacobson, G. R. Phosphoenolpyruvate:carbohydrate phosphotransferase systems of bacteria. eng. Microbiological reviews 57, 543–594. doi:10.1128/mr.57.3.543-594.1993 (Sept. 1993).

42. Death, A. & Ferenci, T. The importance of the binding-protein-dependent Mgl system to the transport of glucose in Escherichia coli growing on low sugar concentrations. Research in Microbiology 144, 529–537. doi:10.1016/0923-2508(93)90002-J (1993).

43. Hunter, I. S. & Kornberg, H. L. Glucose transport of Escherichia coli growing in glucose-limited continuous culture. Biochemical Journal 178, 97–101. doi:10.1042/bj1780097 (1979).

44. García-Alles, L. F., Zahn, A. & Erni, B. Sugar recognition by the glucose and mannose permeases of Escherichia coli. Steady-state kinetics and inhibition studies. Biochemistry 41, 10077–10086. doi:10.1021/bi025928d (2002).

45. Steinsiek, S. & Bettenbrock, K. Glucose transport in Escherichia coli mutant strains with defects in sugar transport systems. Journal of Bacteriology 194, 5897–5908. doi:10.1128/JB.01502-12 (2012).

46. Hua, Q., Yang, C., Oshima, T., Mori, H. & Shimizu, K. Analysis of Gene Expression in Escherichia coli in Response to Changes of Growth-Limiting Nutrient in Chemostat Cultures. Applied and Environmental Microbiology 70, 2354–2366. doi:10.1128/AEM.70.4.2354-2366.2004 (2004).

47. Crabtree, H. G. Observations on the carbohydrate metabolism of tumours. eng. The Biochemical journal 23, 536–545. doi:10.1042/bj0230536 (1929).

48. Warburg, O., Wind, F. & Negelein, E. Über den Stoffwechsel von Tumoren im Körper. Klinische Wochenschrift 5, 829–832. doi:10.1007/BF01726240 (1926).

49. Flickinger, M. C., Thierie, J. & Penninckx, M. Crabtree Effect. Encyclopedia of Industrial Biotechnology. doi:10.1002/9780470054581.eib243 (2010).

50. Niebel, B., Leupold, S. & Heinemann, M. An upper limit on Gibbs energy dissipation governs cellular metabolism. Nature Metabolism 1, 125–132. doi:10.1038/s42255-018-0006-7 (2019).

51. Basan, M. *et al.* Overflow metabolism in Escherichia coli results from efficient proteome allocation. Nature 528, 99–104. doi:10.1038/nature15765 (2015).

52. Valgepea, K. *et al.* Systems biology approach reveals that overflow metabolism of acetate in Escherichia coli is triggered by carbon catabolite repression of acetyl-CoA synthetase. BMC Systems Biology 4, 166. doi:10.1186/1752-0509-4-166 (2010).

53. Renilla, S. *et al.* Acetate scavenging activity in Escherichia coli: Interplay of acetyl-CoA synthetase and the PEP-glyoxylate cycle in chemostat cultures. Applied Microbiology and Biotechnology 93, 2109–2124. doi:10.1007/s00253-011-3536-4 (2012).

54. Wolfe, A. J. The Acetate Switch. Microbiology and Molecular Biology Reviews 69, 12–50. doi:10.1128/mmbr.69.1.12-50.2005 (2005).

55. Dittrich, C. R., Vadali, R. V., Bennett, G. N. & San, K. Y. Redistribution of metabolic fluxes in the central aerobic metabolic pathway of E. coli mutant strains with deletion of the ackA-pta and poxB pathways for the synthesis of isoamyl acetate. Biotechnology Progress 21, 627–631. doi:10.1021/bp049730r (2005).

56. Enjalbert, B., Millard, P., Dinclaux, M., Portais, J. C. & Létisse, F. Acetate fluxes in Escherichia coli are determined by the thermodynamic control of the Pta-AckA pathway. Scientific Reports 7. doi:10.1038/srep42135 (Feb. 2017).

57. Kakuda, H., Hosono, K., Shiroishi, K. & Ichihara, S. Identification and characterization of the ackA (acetate kinase A)-pta (phosphotransacetylase) operon and complementation analysis of acetate utilization by an ackA-pta deletion mutant of Escherichia coli. eng. Journal of biochemistry 116, 916–922. doi:10.1093/oxfordjournals.jbchem.a124616 (Oct. 1994).

58. Kumari, S. *et al.* Regulation of acetyl coenzyme A synthetase in Escherichia coli. eng. Journal of bacteriology 182, 4173–4179. doi:10.1128/JB.182.15.4173-4179.2000 (Aug. 2000).

59. Peebo, K. *et al.* Proteome reallocation in Escherichia coli with increasing specific growth rate. Molecular BioSystems 11, 1184–1193. doi:10.1039/c4mb00721b (2015).

60. Novak, K. *et al.* Characterizing the effect of expression of an acetyl-CoA synthetase insensitive to acetylation on co-utilization of glucose and acetate in batch and continuous cultures of E. coli W. Microbial Cell Factories 17. doi:10.1186/s12934-018-0955-2 (July 2018).

61. Anane, E., López C, D. C., Neubauer, P. & Cruz Bournazou, M. N. Modelling overflow metabolism in Escherichia coli by acetate cycling. Biochemical Engineering Journal 125, 23–30. doi:10.1016/j.bej.2017.05.013 (2017).

62. Millard, P., Uttenweiler-joseph, S. & Enjalbert, B. From toxic waste to beneficial nutrient : acetate boosts Escherichia coli growth at low glycolytic flux . bioRxivxiv. doi:https://doi.org/10.1101/2022.09.20.506926 (2022).

63. Waegeman, H. & Soetaert, W. Increasing recombinant protein production in Escherichia coli through metabolic and genetic engineering. Journal of Industrial Microbiology and Biotechnology 38, 1891–1910. doi:10.1007/s10295-011-1034-4 (2011).

64. Hong, S. & Lee, S. Metabolic Flux Analysis for Succinic Acid Production by Recombinant Escherichia coli. Biotechnology and bioengineering 74, 89–95 (2001).

65. De Mey, M., De Maeseneire, S., Soetaert, W. & Vandamme, E. Minimizing acetate formation in E. coli fermentations. Journal of Industrial Microbiology and Biotechnology 34, 689–700. doi:10.1007/s10295-007-0244-2 (2007).

66. Contiero, J. *et al.* Effects of mutations in acetate metabolism on high-cell-density growth of Escherichia coli. Journal of Industrial Microbiology and Biotechnology 24, 421–430. doi:10.1038/sj.jim.7000014 (2000).

67. Diaz-Ricci, J. C., Hitzmann, B., Rinas, U. & Bailey, J. E. Comparative Studies of Glucose Catabolism by Escherichia coli Grown in a Complex Medium under Aerobic and Anaerobic Conditions. Biotechnology Progress 6, 326–332. doi:10.1021/bp00005a003 (1990).

68. Pinhal, S., Ropers, D., Geiselmann, J. & De Jong, H. Acetate metabolism and the inhibition of bacterial growth by acetate. Journal of Bacteriology 201. doi:10.1128/JB.00147-19 (2019).

69. Sharan, S. K., Thomason, L. C., Kuznetsov, S. G. & Court, D. L. Recombineering: A Homologous Recombination-Based Method of Genetic Engineering. Nature protocols 4, 206–223. doi:10.1038/nprot.2008.227.Recombineering (2010).

70. Zhang, Y., Buchholz, F., Muyrers, J. P. P. & Stewart, A. F. A new logic for DNA engineering using recombination in Escherichia coli. Nature Genetics 20, 123–128. doi:10.1038/2417 (1998).

71. Datta, S., Costantino, N. & Court, D. L. A set of recombineering plasmids for gram-negative bacteria. eng. Gene 379, 109–115. doi:10.1016/j.gene.2006.04.018 (Sept. 2006).

72. Baba, T. *et al.* Construction of Escherichia coli K-12 in-frame, single-gene knockout mutants: The Keio collection. Molecular Systems Biology 2. doi:10.1038/msb4100050 (2006).

73. Cherepanov, P. P. & Wackernagel, W. Gene disruption in Escherichia coli: TcR and KmR cassettes with the option of Flp-catalyzed excision of the antibiotic-resistance determinant. Gene 158, 9–14. doi:https://doi.org/10.1016/0378-1119(95)00193-A (1995).

74. Gibson, D., Young, L. & Chuang, R. Enzymatic assembly of DNA molecules up to several hundred kilobases. Nature Methods 6, 343–345. doi:https://doi.org/10.1038/nmeth.1318 (2009).

75. Stevenson, K., McVey, A. F., Clark, I. B., Swain, P. S. & Pilizota, T. General calibration of microbial growth in microplate readers. Scientific Reports 6, 4–10. doi:10.1038/srep38828 (2016).

76. Koch, A. L. Turbidity measurements of bacterial cultures in some available commercial instruments. eng. Analytical biochemistry 38, 252–259. doi:10.1016/0003-2697(70)90174-0 (Nov. 1970).

77. Galbusera, L., Bellement-Theroue, G., Urchueguia, A., Julou, T. & van Nimwegen, E. Using fluorescence flow cytometry data for single-cell gene expression analysis in bacteria. PLoS ONE 15, 1–23. doi:10.1371/journal.pone.0240233 (2020).

78. Davey, H. M. & Kell, D. B. Flow cytometry and cell sorting of heterogeneous microbial populations: the importance of single-cell analyses. eng. Microbiological reviews 60, 641–696. doi:10.1128/mr.60.4.641-696.1996 (Dec. 1996).

79. Van de Velde, C. C. *et al.* Fast quantification of gut bacterial species in cocultures using flow cytometry and supervised classification. ISME Communications 2, 1–11. doi:10.1038/s43705-022-00123-6 (2022).

80. Abcam. Introduction to flow cytometry. Jan. 2023.

81. Egli, T. Microbial growth and physiology: A call for better craftsmanship. Frontiers in Microbiology 6, 1–12. doi:10.3389/fmicb.2015.00287 (2015).

82. Martin, Y., Page, M., Blanchet, C. & De Jong, H. WellInverter: A web application for the analysis of fluorescent reporter gene data. BMC Bioinformatics 20, 1–18. doi:10.1186/s12859-019-2920-4 (2019).

83. Novick, A. & Szilard, L. Experiments with the Chemostat on spontaneous mutations of bacteria. Proceedings of the National Academy of Sciences of the United States of America 36, 708–719. doi:10.1073/pnas.36.12.708 (1950).

84. Monod, J. The Growth of Bacterial Cultures. Annual Reviews in Microbiology 3, 371–394. doi:https://doi.org/10.1146/annurev.mi.03.100149.002103 (1949).

85. Wides, A. & Milo, R. Understanding the Dynamics and Optimizing the Performance of Chemostat Selection Experiments. 2018. doi:10.48550/ARXIV.1806.00272.

86. Nanchen, A., Schicker, A. & Sauer, U. Nonlinear dependency of intracellular fluxes on growth rate in miniaturized continuous cultures of Escherichia coli. Applied and Environmental Microbiology 72, 1164–1172. doi:10.1128/AEM.72.2.1164-1172.2006 (2006).

87. Klein, T., Schneider, K. & Heinzle, E. A system of miniaturized stirred bioreactors for parallel continuous cultivation of yeast with online measurement of dissolved oxygen and off-gas. Biotechnology and Bioengineering 110, 535–542. doi:10.1002/bit.24633 (2013).

88. Steel, H., Habgood, R., Kelly, C. & Papachristodoulou, A. In situ characterisation and manipulation of biological systems with Chi.Bio. PLoS Biology 18, 1–12. doi:10.1371/journal.pbio.3000794 (2020).

89. Takahashi, C. N., Miller, A. W., Ekness, F., Dunham, M. J. & Klavins, E. A low cost, customizable turbidostat for use in synthetic circuit characterization. ACS Synthetic Biology 4, 32–38. doi:10.1021/sb500165g (2015).

90. Miller, A. W., Befort, C., Kerr, E. O. & Dunham, M. J. Design and use of multiplexed chemostat arrays. Journal of Visualized Experiments, 2–7. doi:10.3791/50262 (2013).

91. Bertaux, F. *et al.* Enhancing bioreactor arrays for automated measurements and reactive control with ReacSight. Nature Communications 13, 1–12. doi:10.1038/s41467-022-31033-9 (2022).

92. Balleza, E., Kim, J. M. & Cluzel, P. Systematic characterization of maturation time of fluorescent proteins in living cells. Nature Methods 15, 47–51. doi:10.1038/nmeth.4509 (2018).

93. Pavlou, A., Cinquemani, E., Geiselmann, J. & de Jong, H. Maturation models of fluorescent proteins are necessary for unbiased estimates of promoter activity. Biophysical journal 121, 4179–4188. doi:10.1016/j.bpj.2022.09.021 (Nov. 2022).

94. Manen, D. & Caro, L. The replication of plasmid pSC101. Molecular Microbiology 5, 233–237. doi:10.1111/j.1365-2958.1991.tb02103.x (1991).

95. German, G. J., Misra, R. & Kropinski, A. M. in *The bacteriophages* (ed Calendar, R.) 211–224 (Oxford University Press, New York, NY, 2006).

96. Ljung, G. M. & Box, G. E. P. On a measure of lack of fit in time series models. Biometrika 65, 297–303. doi:10.1093/biomet/65.2.297. eprint: https://academic.oup.com/biomet/article-pdf/65/2/297/649058/65-2-297.pdf (Aug. 1978).

97. Rai, N., Huynh, L., Kim, M. & Tagkopoulos, I. Population collapse and adaptive rescue during long-term chemostat fermentation. Biotechnology and Bioengineering 116, 693–703. doi:10.1002/bit.26898 (2019).

98. Keseler, I. M. *et al.* EcoCyc: a comprehensive database of Escherichia coli biology. Nucleic Acids Research 39, D583–D590. doi:10.1093/nar/gkq1143 (Nov. 2010).

99. Newville, M. lmfit/lmfit-py 1.0.0. doi:10.5281/zenodo.3588521 (2019).

100. Folsom, J. P., Parker, A. E. & Carlson, R. P. Physiological and proteomic analysis of Escherichia coli iron-limited chemostat growth. Journal of Bacteriology 196, 2748–2761. doi:10.1128/JB.01606-14 (2014).

101. Lis, A. V. *et al.* Exploring small-scale chemostats to scale up microbial processes: 3-hydroxypropionic acid production in S. cerevisiae. Microbial Cell Factories 18, 1–11. doi:10.1186/s12934-019-1101-5 (2019).

102. Farmer, I. S. & Jones, C. W. The Energetics of Escherichia coli during Aerobic Growth in Continuous Culture. European Journal of Biochemistry 67, 115–122. doi:10.1111/j.1432-1033.1976.tb10639.x (1976).

103. Sá-Pessoa, J. *et al.* SATP (YaaH), a succinate–acetate transporter protein in Escherichia coli. Biochemical Journal 454, 585–595. doi:10.1042/BJ20130412. eprint: https://portlandpress.com/biochemj/article-pdf/454/3/585/677130/bj4540585.pdf (Aug. 2013).

104. Mihalcescu, I., Van-Melle Gateau, M., Chelli, B., Pinel, C. & Ravanat, J. L. Green autofluorescence, a double edged monitoring tool for bacterial growth and activity in micro-plates. Physical Biology 12, 66016. doi:10.1088/1478-3975/12/6/066016 (2015).

105. Kell, D. B. *et al.* Metabolic footprinting and systems biology: The medium is the message. Nature Reviews Microbiology 3, 557–565. doi:10.1038/nrmicro1177 (2005).

106. Enjalbert, B., Letisse, F. & Portais, J.-C. Physiological and Molecular Timing of the Glucose to Acetate Transition in Escherichia coli. Metabolites 3, 820–837. doi:10.3390/metabo3030820 (2013).

107. Senn, H., Lendenmann, U., Snozzi, M., Hamer, G. & Egli, T. The growth of Escherichia coli in glucose-limited chemostat cultures: a re-examination of the kinetics. Biochimica et Biophysica Acta 1201, 424–436 (1994).

108. Rocabert, C., Knibbe, C., Consuegra, J., Schneider, D. & Beslon, G. Beware batch culture: Seasonality and niche construction predicted to favor bacterial adaptive diversification. **3,** 1–32. ISBN: 1111111111. doi:10.1371/journal.pcbi.1005459 (2017).

109. Jansen, M. L. *et al.* Prolonged selection in aerobic, glucose-limited chemostat cultures of Saccharomyces cerevisiae causes a partial loss of glycolytic capacity. Microbiology 151, 1657–1669. doi:10.1099/mic.0.27577-0 (2005).

110. Adamberg, K., Valgepea, K. & Vilu, R. Advanced continuous cultivation methods for systems microbiology. Microbiology (United Kingdom) 161, 1707–1719. doi:10.1099/mic.0.000146 (2015).

111. Dykhuizen, D. & Hartl, D. Evolution of Competitive Ability in Escherichia coli. Evolution 35, 581. doi:10.2307/2408204 (1981).

112. Wick, L. M., Weilenmann, H. & Egli, T. The apparent clock-like evolution of Escherichia coli in glucose-limited chemostats is reproducible at large but not at small population sizes and can be explained with Monod kinetics. Microbiology 148, 2889–2902. doi:10.1099/00221287-148-9-2889 (2002).

113. Ingalls, B. Mathematical modeling in systems biology: An Introduction, 396. ISBN: 9783319577104. doi:10.1007/978-3-319-57711-1_14 (2012).

114. Bequette, B. W. Process Control: Modeling, Design and Simulation. ISBN: 9780133536409 (Prentice Hall, Upper Sadlle River, NJ (2003), 2003).

115. Salzano, D., Fiore, D. & Di Bernardo, M. Ratiometric control of cell phenotypes in monostrain microbial consortia. Journal of the Royal Society Interface 19. doi:10.1098/rsif.2022.0335 (2022).

116. Martinez, C., Cinquemani, E., de Jong, H. & Gouze, J.-L. Optimal protein production by a synthetic microbial consortium: Coexistence, distribution of labor, and syntrophy. bioRxiv, 2022.01.12.476046 (2022).

117. Milias-Argeitis, A., Rullan, M., Aoki, S. K., Buchmann, P. & Khammash, M. Automated optogenetic feedback control for precise and robust regulation of gene expression and cell growth. Nature Communications 7. doi:10.1038/ncomms12546 (Aug. 2016).

118. Cinquemani, E., Laroute, V., Cocaign-Bousquet, M., De Jong, H. & Ropers, D. Estimation of time-varying growth, uptake and excretion rates from dynamic metabolomics data. Bioinformatics 33, i301–i310. doi:10.1093/bioinformatics/btx250 (2017).

119. Levskaya, A. *et al.* Engineering Escherichia coli to see light. Nature 438, 441–442. doi:10.1038/nature04405 (Nov. 2005).

120. Anderson Promoter Collection. http://parts.igem.org/Promoters/Catalog/Anderson.

121. Davis, J. H., Rubin, A. J. & Sauer, R. T. Design, construction and characterization of a set of insulated bacterial promoters. Nucleic Acids Research 39, 1131–1141. doi:10.1093/nar/gkq810 (2011).

122. Papa, L. J. & Shoulders, M. D. Genetic Engineering by DNA Recombineering. Current protocols in chemical biology 11, e70. doi:10.1002/cpch.70 (2019).

123. Millard, P., Enjalbert, B., Uttenweiler-Joseph, S., Portais, J.-C. & Létisse, F. Control and regulation of acetate overflow in Escherichia coli. bioRxiv. doi:10.1101/2020.08.18.255356 (2020).

124. Teague, B. Cytoflow 1.0: Python tools for quantitative, reproducible flow cytometry analysis (2019).